A Numerical Study of Micro Flow and Its Applications on Thermal Energy Conversion and Water Desalination

ZHANG, Peng

A Thesis Submitted in Partial Fulfillment

of the Requirements for the Degree of

Doctor of Philosophy

in

Automation and Computer-Aided Engineering

The Chinese University of Hong Kong

June 2010

ProQuest LLC
789 East Eisenhower Parkway
P.O. Box 1346
Ann Arbor, MI 48106-1346

Thesis Assessment Committee

Professor Li, Wenjung (Chair)
Professor Ng, Hangleung Dickon (Committee member)
Professor Zhou, Lixing (External Examiner)
Professor Du, Ruxu (Thesis Supervisor)

Abstract

Energy and water are two of the most important issues in the world today. The social and economic health of the world depends on sustainable supply of both energy and water. Especially, these two critical resources are always inextricably linked. To solve the emerging crisis of energy and water, renewable energy technologies is the key. On the other hand, recent advances in Micro-Electro-Mechanical Systems (MEMS) technology have opened new ways for us to use micro / nano scale physical and chemical effects. It is no doubted that the combination of the renewable energy technologies and micro / nano technologies will have great potential and there are plenty of room to explore.

The research presented in this thesis focuses on extending the micro scale effect to the macroscopic applications. Based on this idea, a new energy harvesting method and two new water desalination technologies are proposed, with computer simulations and experiment validations. These include:

(1) A new model for the mass transfer in Direct Contact Membrane Distillation (DCMD) process is developed. The model is based on Direct Simulation Monte Carlo (DSMC) method. It avoids the over simplification of the resistance mechanisms and hence, give more accurate prediction. The model is validated by means of experiments. The influences of the main parameters in DCMD are also studied, including temperature difference between the feed side and the permeate side, the membrane's thickness and the pore size. Moreover, it is proposed to use aerogel as the membrane material. It is shown that the aerogel's hydrophobic property, low thermal conductivity and high porosity offer a much improved performance over the commonly used membrane material PTFE. The fresh water productivity can reach 10.0 kg/m^2 per day.

(2) A new energy harvesting method for converting thermal energy to kinetic energy is proposed. This method is based on the rarefied gas phenomenon called Knudsen effect. By Knudsen effect, a gas flow can be generated from temperature difference. In order to generate Knudsen effect, a special material, aerogel, is used. It is a porous material full of holes of dozens of nanometers. Using Direct Simulation Monte Carlo (DSMC) simulation, it is shown that Knudsen effect

still works under atmosphere pressure with aerogel material. Accordingly, a device is designed. Based on the numerical simulation, the device can generate about 70 W kinetic energy when driven by a solar panel with intensity of 1 kW/m^2.

(3) A solar desalination system is designed. This system is based on a combination of Knudsen compressor and simple solar still. The Knudsen effect is generated from the aerogel driven by solar radiation. As a result, the system operates at lower pressure resulting in enhanced water evaporation process. Based on the simulation, the evaporation rate is significantly increased. It is found that in a typical summer day in tropic region like Hong Kong, such a system can generate about 5 kg fresh water per 1 m^2 solar still per day. This number is about 30% higher than the simple direct solar still. Moreover, the proposed technology can be readily combined with other technologies such as condensation heat recovery to further improve the fresh water productivity. The optimal working condition is also studied.

論文摘要

能源和水資源是世界環境與發展日程中最重要的兩個議題。社會和經濟的健康發展都依賴著能源和淡水的充足供應。特別要指出的是，這兩種緊要的資源還常常緊密的相互關聯在一起。爲了應對日漸緊迫的能源危機和淡水危機，利用好可再生能源是關鍵。另一方面，微機電系統（MEMS）在近年來發展迅猛，他爲我們提供了一些新的方法和思路來利用微/納尺度的物理和化學效應。可再生能源技術與微納米技術的結合必將有巨大的潛力和充足的可探索空間。

本論文中的研究著眼於將微尺度效應擴展到常規尺度的應用中去。基於這一想法，本論文提出了一種新的能量採集方法和兩種水處理技術，進行了相應的數值模擬研究和實驗研究。具體來說，本研究包含了以下幾個課題：

（1）發展了描述膜蒸餾過程中物質疏運的新模型。這一模型基於 DSMC 方法，它避免了對流動阻力機制的過分簡化，可給出更爲準確的預測。進行的實驗研究驗證了本模型的正確性。本文還用這一模型研究了直接接觸式膜蒸餾過程中各主要參數的影響，例如冷熱兩側溫度差，膜的厚度和孔徑。此外，氣凝膠作爲一種新的膜材料被提出並進行了研究，結果表明氣凝膠的疏水性，低導熱率和高孔隙率都十分有利於提升膜蒸餾過程的表現，它大大優於目前應用較廣的聚四氟乙烯膜（PTFE）。它的淨水產能可達 10.0 公斤/平方米.天。

（2）提出了一種可用於將热能轉換爲動能的新的能量採集方式。它是基於在稀薄氣體中發現的努森效應，即利用溫度差來驅動氣體流動。爲了在大氣壓力下產生努森效應，我們使用了一種充滿納米尺度小孔的材料—氣凝膠材料。蒙特卡羅直接模擬方法被用於研究氣凝膠材料中的努森效應，模擬結果表明了在大氣壓力下，努森效應在氣凝膠材料中仍然較爲高效的起作用。基於這一效應，本文設計了一個結構簡單的裝置，並建立了數學模型來研究本裝置的性能。模擬結果表明，這一裝置在強度爲 1 千瓦/平方米的太陽能驅動下可產生 70 瓦的動能。

（3）設計了一套太陽能淨水系統。這一系統是努森壓縮機與現有太陽能蒸餾裝置的結合。通過陽光驅動的努森效應,可使得系統中的蒸發過程在低壓環境進行。數值模擬表明這一措施可使低溫下的蒸發速率大爲提高。計算得到了在有陽光的夏日，對應每方米太陽能集熱面積的日淨水產量約爲5公斤。這一數值比簡單的太陽能直接蒸餾方式高約百分之三十。此外，這一技術可容易的和其他技術（如冷凝熱回收）相結合以進一步提高淨水產能。本文對系統的最優工作參數也進行了研究。

Acknowledgement

I would like to express my sincere appreciation to those who help the completion of this thesis. First of all, I would like to thank my supervisor, Professor *Ruxu Du*, for his enthusiastic encouragement, help and guidance on my work and life. During the past three years, I have learnt a lot from him, not only including the methodology and skills to do the research, but also including the attitude and spirit to be a researcher. Without the supervision and urge from Prof. *Du*, it is impossible for me to finish my thesis. What I learnt from him will be very helpful for my future study and career. I would also like to thank Professor *WenJung Li*, Professor *Dickon HangLeung Ng,* and Professor *LiXing Zhou* for serving in my thesis committee, and for their valuable suggestions and advices.

Moreover, I should also thank Professor *Shiming Xu*, as an expert in this field, gave me valuable advices and help. I would also like to thank Dr. *Ya Liu* for her help and cooperation to make the research smoothly.

Thanks to all the colleges working in the Institute of Precision Engineering, I enjoy the work and life here together with them, and will cherish our friendship forever.

Finally, with great love and respect, I would like to express my heartful appreciation to my parents, for their love, patience and encouragement in my life.

Zhang Peng

March 2010

Table of Contents

List of the Tables

List of the Figures

Nomenclature

A	Area (m^2)
C,c	specific heat (kJ/kg)
d_i, d_s, d_m	heat conductivity coefficient ($Wm^{-1}K^{-1}$)
D	radiuses
E, e	energy (W)
ΔH_v	latent heat (kJ/kg)
H	enthalpy (kJ/kg)
h	Heat transfer coefficient ($Wm^{-2}K^{-1}$)
L	length (m)
m	mass of the molecules or
n	number density of gas
k_B	Boltzman's constant, 1.38×10^{-23} (JK^{-1})
Kn	Knudsen number
M	mass flux
N	molecule flux or vapor flux
N_c	number of collection
P,p	pressure (Pa), or pressure ratio
Q	heat transfer rate (W)
Q_T	temperature driven follow coefficient
Q_P	pressure driven follow coefficient
R	gas constant ,8.31 ($JK^{-1}mol^{-1}$), 287($JK^{-1}kg^{-1}$)
T	temperature (°C or K)
t	time (s)
Δt	time interval
U,u,v	speed (ms^{-1})

Greeks

α	reflection coefficient
λ	mean free path (m)
ρ	density (kg m^{-3})
σ	collision diameter (m)
$\wp$	total pressure ratio
κ	coefficient of pressure increase in one stage Knudsen compressor
ε	porosity
Ω , μ	viscosity
v	probability of collision
ζ	freedom of internal energy
φ	relative humidity

Subscript

AVG	average
DES	design
EFF	effective
evap	evaporation
cond	condensation
bf	bulk at the feed side
mf	membrane surface at the feed side
mp	membrane surface at the permeate side
bp	bulk at the permeate side
ref	refence
rot	rotation
e	exit
in	inlet
out	outlet
i	i^{th} stage
max	maximum
S	Saturated
V	vapor
w	water

Chapter 1
Introduction

1.1 Motivation

Energy and water are two of the most important issues in the world today. The social and economic health of the modern world depends greatly on sustainable supply of both energy and water.

For energy, international economic and political crises and conflicts can be initiated by shortages of fossil fuels. Moreover, burning fossil fuels release harmful emissions such as carbon dioxide, nitrogen oxides, aerosols, and etc. which could have a devastative effect on the local, regional and global environment. Therefore, in recent decades, much research has been carried out on the clean and renewable energy. There are many forms of renewable energy, such as solar energy, geothermal, ocean energy and wind energy. They are almost inexhaustible and offer many environmental benefits compared to the fossil fuels. Each form of renewable energy also has its own special advantages that make it uniquely suited to certain applications. Almost none of them release gaseous or liquid pollutants during operation. However, it is still a long way to replace fossil fuels by renewable energies, both technologically and economically.

Among various forms of renewable energy, thermal energy is perhaps the most common. For example, The Sun emits energy at a rate of 3.8×10^{23} kW and about 1.08×10^{14} kW of the energy reaches the surface of the earth. About 0.1% of this energy, when converted at an efficiency of 10% would generate four times the current world's total generation about 3000 GW. The high temperature gases from heating and air conditioning systems of buildings and industries are also significant. In the past decades, many methods were proposed for harvesting the thermal energy. Solar power plants, geothermal power plants have already been used in industrial scales, but they are ineluctably complex, expensive and large. Some technologies for small scale application are also studied. An example is the thermoelectric method which uses thermoelectric material to convert heat to electricity. But it is still being researched in laboratory, as the low conversion efficiency got only little

improvement in the past thirty years. In addition, it requires a large temperature gradient. These problems are rooted at the basic thermoelectric principle and the improvement is restricted by the fundamental physics. Some newly proposed devices for harvesting thermal energy are using Micro-Electro-Mechanical Systems (MEMS) fabricated micro-generators such as micro-turbine engines, micro-rotary engines, and micro-free piston knocks engines. However, these miniature devices are far from mature for practical applications. In short, the study on the energy conversion of thermal energy is still in its infancy.

For water, its scarcity is becoming a critical problem to the world. It has been reported that by 2020, 50% of the world population will face fresh water shortage. To solve this problem, desalination is the key. According to literatures, distillation is the most widely used process for desalination. Currently, Multi-Stage-Flash (MSF) and Multi-effect distillation (MED) technology produces 56% of the total fresh water produced by desalination. However, it is an energy thirsty process. It has been estimated by Kalogirou [2005] that the production of 1000 m^3 per day of freshwater requires 10,000 tons of oil per year. The Reverse Osmosis (RO) produces about another half of desalinated water. Its energy consumption is lower than MSF and MED, but the complex process needs experienced worker and the membranes and equipments are high cost. Moreover, for generating high operation pressure about 8 Mpa (80 Atm), the high quality electricity energy is required. The emerging concerns of energy and environment have consequently increased the interest for the use of renewable energy for desalination. Recently, much effort has been put into the R&D of renewable energy driven desalination system, but it only represents about 0.02% of the total desalination capacity. This is mainly because of the low efficiency. The low efficiency of the existing thermal solar desalination systems is largely attributed to the lower quality of the thermal energy and the heat loss during the condensation process. Recent advances on the thermal solar desalination are using solar energy to drive the conventional thermal desalination plants, like MSF and MED. But these systems are complex and expensive. Many researchers try to increase the efficiency by recovering latent heat of condensation. Others try to increase feeding water temperature by using various techniques, such as integration of solar cell with multi-source and multi-use system. Though, the success is limited.

It shall be pointed out that in the last twenty years, the rapid advances of MEMS technology has made a significant impact to the energy and environment.

Many new physical and chemical phenomena and effects in micro / nano scale were founded and utilized. The aforementioned thermoelectric material is an example. These effects offer new ways of generation, storage and usage of renewable energy and water treatment.

This thesis first studies the membrane distillation (MD) for desalination by numerical simulation and experiment. Direct Simulation Monte Carlo (DSMC) method is used to describe the mass transfer in MD process, new candidate membrane material is proposed and studied to get higher fresh water productivity. Then the Knudsen effect, which is a thermal driven flow in micro scale, is studied by computer simulation. The simulation is also conducted by DSMC and is aimed at finding the heat and mass transfer properties of Knudsen effect. Based on the computer simulation, two new methods are proposed. The first one is an energy harvesting device which can effectively convert thermal energy to kinetic energy. The second one is to improve the efficiency of water desalination using the negative pressure generated by the Knudsen effect. Accordingly, a solar energy driven desalination system is designed. Based on computer simulation, the new system can improve the efficiency of desalination by as much as 30%. These studies open new ways for solving the energy and water problem.

1.2 Organization of the Thesis

The rest of the thesis is organized as follows. Chapter 2 consists of literature survey related to micro flow simulation, membrane distillation, thermal energy harvesting and solar still desalination. In Chapter 3, Direct Simulation Monte Carlo (DSMC) is introduced and discussed. In Chapter 4, the Direct Contact Membrane Distillation (DCMD) is studied. A new model is proposed for describing the mass transfer process in DCMD. Compared with conventional methods, it avoids the over simplification of the resistance mechanism and offers a better understanding of the vapor transportation process. With the new model, the influences of some key membrane characters are analyzed. Furthermore, the performance of aerogel as the membrane material, which is highly hydrophobic, thermal isolate and highly porosity, is investigated. It is shown that the aerogel outperforms the commonly used PTFE material. In Chapter 5, a new energy harvest method based on Knudsen effect is

investigated. A mathematical model of Knudsen compressor working near atmosphere pressure is derived. The micro flow in Knudsen compressor is studied by DSMC method. Based on this method a device is designed. The simulation results show that the device can achieve acceptable performance on solar energy collecting. In Chapter 6, a new system for solar desalination is proposed. By using the Knudsen effect to reduce the vapor pressure, it improves the efficiency of desalination. A comprehensive mathematical model including mass balance and heat balance of the system is established. It is estimated that the system has a significant improvement on efficiency over the traditional solar desalination method. Finally, Chapter 7 contains conclusions and future research topics.

Chapter 2

Literature Survey

2.1 History of Micro Scale Flow

In his famous speech in 1959, 'There is Plenty Room at the Bottom', Richard P. Feynman [1961] predicted the atomic scale fabrication would change the world. During the past half a century, the success of MEMS has proved his prophesy. Micro-Electro-Mechanical System (MEMS) refer to devices that have characteristic length of less than 1 mm but more than 1 μm, that combine electrical and mechanical components and that are fabricated using various advanced processing technologies. Current MEMS manufacturing techniques include surface micromachining; bulk micromachining; lithography, electro deposition, plastic molding (or, in its original German term, lithographic galvanoformung abformung, LIGA), as well as Electro-Discharge Machining (EDM). MEMS devices have several unique features. First, it is small; which can be one or more orders of magnitude smaller than traditional devices. Second, it can be made by batch processing, which is a characteristics of IC fabrication, and hence, large quantities can be made consistently. Third, it has a high level of integration. MEMS manufacturing technology is derived from, although not completely compatible with, IC manufacturing technology, so mechanical components can be easily integrated to electronic circuits [Ho and Tai, 1998].

With the benefits of low cost, small volume, small weight, and small power consumption, reliable batch-processing, fast corresponding, and etc., MEMS devices are playing increasingly important role on many disciplines (e.g., biology, medicine, optics, aerospace, as well as mechanical and electrical engineering). Presently, a large number of MEMS devices have been made, such as accelerometers for automobile airbags, keyless entry systems, dense arrays of micro mirrors for high-definition optical displays, micro-heat-exchangers for cooling of electronic circuits, reactors for separating biological cells, micropumps for ink jet printing, environmental testing and electronic cooling. More applications can be found in Gad-el-Hak's paper [1999].

2.1.1 Fluid flow in micro/nano scale

Many MEMS devices involve the flow of liquids and gases. Its scientific principle is as the foundation for design and manufacturing of MEMS devices. However, as pointed out by Gad-el-Hak [1999], "The rapid progress in fabricating and utilizing micro-electro-mechanical systems during the last decade has not been matched by corresponding advances in our understanding of the unconventional physics involved in the operation and manufacture of small devices." Many questions have been raised when the results of experiments with microdevices could not be explained via the traditional flow models [Guo and Li, 2003]. For example, whether the resistance of gas flow is increase or decrease in a micro channel is a disputed problem for a long time. Another example is the propulsion systems for attitude control of spacecraft. Fig. 2.1 is Bayt's [1999] Laval nozzle with a 20 micron throat width. Because of the increase in viscous losses as the size is reduced, it was feared that high Mach number supersonic flows could not be generated in such kind of nozzle. Bayt's experiment demonstrates that supersonic flows can be generated at this scale, and in fact, the thrust/weight ratio is much higher than the conventional nozzle. Up to today, researchers know little about the flow mechanism in micro nozzle, the simulation seems always over predicting the thrust efficiency of this nozzle.

Owing to its importance, recently micro scale fluid flow and heat transfer becomes a hot research topic. Publications about micro flow increase year by year, for example, since 2003, ASME organize an annual conference on "Microchannels and Minichannels" for discussing the fluid flow and heat transfer in micro channels. In *Journal of Micromechanics and MicroEngineering,* the proportion of papers about micro flow is increasing. The impact factor of a specialized journal *Microscope Thermophysical Engineering* is rising. Another journal focus on the micro and nano fludics, *Microfluidics and Nanofluidics*, is launched in 2004.

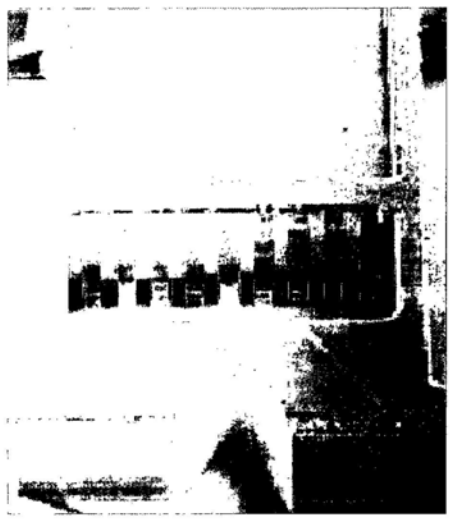

Figure 2.1: Bayt's Laval nozzle[Bayt, 1999]

2.1.2 Current research status of micro flow

Since early 1990s, many experiments on micro flow were carried out [Pong et al., 1994; Arkilic, 1997]. However, two major problems are found. The first one is the repeatability. The highly accurate micro fabrication techniques could not guarantee the repeatability of the experiments. The second problem is the precision measurement. The measured pressure distribution and heat flux are not accurate enough for analyzing the flow and the heat transfer at the micro / nano scale. As a result, various models and hypotheses were proposed to interpolate the experiment results.

Though, theoretical study is also challenge as traditional fluid flow and heat transfer models are not applicable at micro / nano scales. Micro scale flow is characterized by the Knudsen number. It is a dimensionless number which represents the degree of rarefied gas. It is defined as the ratio of the mean free path, λ, over the characteristic geometric length, L_c:

$$Kn = \frac{\lambda}{L_c} = \frac{\lambda}{\rho / (d\rho / dx)} \tag{2-1}$$

where, ρ is gas density. The mechanics of fluid flow and heat transfer depend on the range of the Knudsen number. A classification of the different flow regimes is given below [Schaaf and Chambre, 1961]:

$Kn < 10^{-3}$ – continuum

$10^{-3} < Kn < 0.1$ – slip flow

$0.1 < Kn < 10$ – transition flow

$Kn > 10$ – free-molecular flow

As the Knudsen number increases, rarefaction effects become more important and thus pressure drop, shear stress, heat flux, and corresponding mass flowrate cannot be predicted from the fluid flow and heat transfer models based on the *continuum hypothesis*. On the other hand, the models based on kinetic gas theory are not appropriate either, except in the very high Knudsen number regime corresponding to near vacuum conditions.

For micro / nano flow, the characteristic geometry length is very small, even though the fluid is not really dilute gases, the Knudsen number is still big. Most of the micro / nano flow belongs to this regime. In this case, Boltzmann equation is the only governing equation. Define a velocity function $f(t,x,v)$, where x is the position and v is the velocity of the molecules. The distribution function represents the number of particles in the six-dimensional phase space *dx*, *dy* at time *t*. This distribution function obeys the Boltzmann equation [Cercignani, 1988; Bird, 1994]:

$$\frac{\partial f}{\partial t} + v \cdot \frac{\partial f}{\partial x} + F \cdot \frac{\partial f}{\partial v} = Q(f, f_*) \qquad (2\text{-}2)$$

where, F is an external force, and the term on the right-hand-side, $Q(f, f_*)$, represents molecule collisions. Since $Q(f, f_*)$ is very complex, there is no general expression. For a simple monoatomic gases, it is given by

$$Q(f, f_*) = \int_{R^3} \int_{S^+} |V.n| [f(x, v_*') f(x, v') - f(x, v_*) f(x, v)] dn dv_* \qquad (2\text{-}3)$$

This represents collisions of two molecules with post velocity v and v_*. We define $V = v - v_*$, $v' = v - n(n \cdot V)$ and $v_*' = v + n(v \cdot V)$. n is the unit vector along $(v - v')$.

It should be pointed that the analytical solution of the Boltzmann equation has not been found even for the simple monoatomic condition. Thus, numerical solutions become necessary. For example, **B**hatnagar, **G**ross and **K**rook proposed a BGK model to approximate the collision integral as $Q(f, f_*) = v_*(f_{loc} - f)$

[Bhatnagar et al., 1954]. It is an accurate method for isothermal flow with large Knudsen number, but does not fit for non-isothermal flow or any other flow regimes.

Fluid flows in small devices differ from those in macroscopic machines. The operation of MEMS-based ducts, nozzles, valves, bearings, turbo machines, etc., cannot always be predicted from conventional flow models such as the Navier-Stokes equations with no-slip boundary condition at a fluid-solid interface, as routinely and successfully applied for larger flow devices. In this section, we give a brief introduction to the continuum as well as molecular based flow models, and the choices to be made.

Gad-el-Hak [1999] in his review paper gave a classification of the simulation methods for fluid flow. Fig. 2.2 contains almost all the methods that could use for micro flow's simulation. There are basically two ways of modeling a flow field. Either as the fluid really is, a collection of molecules, or as a continuum where the matter is assumed continuous and indefinitely divisible. The choice of proper method is depend on the flow regime.

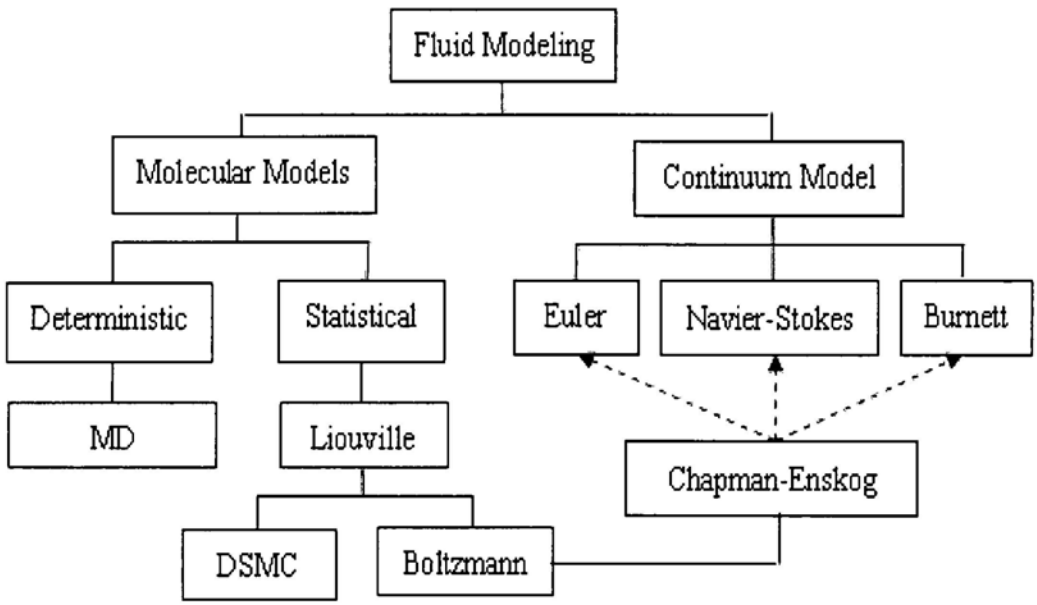

Figure 2.2: Molecular and Continuum Flow Model[Gad-el-Hak, 1999]

For gas flow in slip flow regime, the continuum hypothesis breaks down, but the *Kn* is not big (*Kn*<0.1), the rarefaction is not so important, Navier-Stokes equations with slip boundary conditions is sill valid [Beskok, 1996, Beskok et al., 1996]. N-S equation with slip boundary conditions is the most widely used method, Maxwell analyzed the velocity and temperature near the wall boundary, and proposed the Maxwell-Smoluchowski slip model [Maxwell, 1878]; Kennard simplified Maxwell's model and got the most widely used first order slip model [Kennard, 1938]. This first-order model is only fit for $Kn < 0.1$, Beskok developed high-order slip model based on the first-order model, and proposed the famous μ-Flow model [Beskok, 1996]. The new model's application scope is extended to *Kn*<0.3. Burnett equations are derived from Boltzmann equation using Chapman-Enskog's second-order approximation. Qian [1946] pointed out that with not very low *Kn* and high *Ma*, the Burnett equation is more accuracy than the N-S equation, but it required more complex boundary condition. The advantages of N-S equation and Burnett equation is the computational efficiency, especially for gas flow and heat transfer of single specie, non multi-flow regime, and simple geometry. The disadvantage is their accuracy is not good when the case is multi-species, with chemical reaction or multi-regime flow, for high *Ma* and complicate geometry, both continuum hypothesis and slip boundary faces some problems.

For the transitional flow, the slip boundary is not enough to predict the gas flow, the gas flow is described by Boltzmann equation. So direct discrete and solve the Boltzmann equation is available method for simulating high *Kn* gas flow, Finite Discrete Method and Finite Element Analysis are all potential discretizations. And a big problem of the direct solution is the required element number is huge. For example, a one-dimension steady-state problem, the velocity distribution function is axisymmetric, a three dimension array is needed in phase spaces. If the velocity distribution function is two or three dimension, a five-dimension array is need. If we divide 100 grids in one dimension, a three-dimension steady Boltzmann dimension ask 10^{14} mesh point. If consider of multi-spices and unsteady or even chemical reaction and radiation, it is almost impossible to solve the Boltzmann equation. For simple cases, some solution of Boltzmann is got by Nordsieck and Hicks [1967] and Yen [1970].

Lattice Boltzmann Method (LBM) is another method for solving the Boltzmann equation, it is developed from Lattice Gas Cellular Automata (LGCA) [Frisch et al., 1986]. Essentially the LBM is between macroscopic and microscopic, it use the distribution function of the molecules to represents the molecules' movement in lattice, mass or density could only transport along the lattice's line [Sauro, 2001; Wolf-Gladrow, 2000]; LBM replace the Boolean occupation number in LGCA by a float-digital distribution function as the ensemble average, thus the statistical noise is successfully removed [McNamara and Zanetti, 1988]. Since the LBM is more close to microscopic compared with the N-S equation, it could show more details about the mechanism of fluid flow. Recently, LBM is used for simulate the gas flow in MEMS [Nie et al., 2002; Lim et al., 2003; Tang et al., 2003; Shen et al., 2003]. Limit of using LBM for simulating gas flow of micro/nano scale is: because of LBM do not solve the complete Boltzmann equation, but is the simplified model—BGK equation, so it is only fit for $Kn<1$ [Chen and Doolen, 1998].

Particle based method is developed for avoiding the problem of Boltzmann equation. Molecular Dynamic is based on quantum mechanics and deterministic principle [Koplik and Banavar, 1995; Allen and Tildesley, 1987]. The simulation begins with a set of molecules in a region of space, each assigned a random velocity corresponding to a Boltzmann distribution at the temperature of interest. The interaction between the particles is prescribed typically in the form of a two-body potential energy and the time evolution of the molecular positions is determined by integrating Newton's equations of motion. The required CPU time is proportion to the square of molecule number. For given molecular dimension, flow domain and gas density, the simulation molecular is not tunable. The required molecular number is proportion to the cubic of mean free path. For a gas with the molecule diameter is 4×10^{-10} m, the required molecule number is:

$$N_\lambda \equiv n\lambda^3 = 3856(n_0/n)^2 \qquad (2\text{-}4)$$

where n_0 is the number density under standard condition. Extend 30λ in all the six directions, there will be 10^8 simulated molecules. However, for the number density increases to $100n_0$, only 10^4 is required. So the Molecular Dynamics simulations are highly inefficient for dilute gases where the molecular interactions are infrequent. The simulations are more suited for dense gases and liquids [Allen and Tildesley, 1987]. For an extreme situation, the gas is dilute which the density is 10^{-6} of the

standard situation. From Eq. (2-4) about 10^{20} molecules are required.

Unlike molecular dynamics simulations, Direct Simulation Monte Carlo (DSMC) which first proposed by Bird [1970] is a statistical computational approach. The Monte Carlo method is, like its name sake, a random number strategy based directly on the physics of the individual molecular interactions. The idea is to track a large number of randomly selected, statistically representative particles, and to use their motions and interactions to modify their positions and states. A significant advantage of the DSMC is that the amount of computation required is proportional to N, in contrast to N^2 for molecular dynamics simulations. In essence, particle motions are modeled deterministically while collisions are treated probabilistically, each simulated molecule representing a large number of actual molecules. The DSMC method is valid for all ranges of Knudsen number, although it becomes quite expensive for $Kn < 0.1$. Fortunately, this is the continuum regime where the Navier-Stokes equations can be used analytically or computationally. DSMC is therefore ideal for the transition regime ($0.1 < Kn < 10$), where the Boltzmann equation is difficult to solve. DSMC is succeed applied in the aerospace and aviation field, and becomes a criteria to evaluate new method in transitional regime [Shen, 1996]. Recently DSMC is used for simulating flow and heat transfer in micro scale [Shen, 2003; Alexander and Garcia, 1997; Liou and Fang, 2001; Hadjiconstantinou and Simek, 2002; Fan and Shen, 2001; Sun and Boyd, 2002]. In this thesis, I choose the DSMC method to simulate the flow and heat transfer of micro / nano scale, the detail factors of DSMC will be introduced in chapter 3.

2.2 Review of Membrane Distillation

It has been reported that by 2020, 50% of the world population will face fresh water shortage. To solve this problem, desalination is the key. Membrane distillation (MD) is a thermal driven membrane separation process. It has potential applications in many areas of scientific and industrial interest, yielding highly purified permeate and separating contaminants from liquid solutions. MD has been applied for separation of non-volatile components from water like ions, colloids, macromolecules, for the removal of trace volatile organic compounds from water such as benzene, chloroform, trichloroethylene or the extraction of other organic

compounds such as alcohols from dilute aqueous solutions [Lawson, 1997; Mengual and L. Pena, 1997; Duan et al., 2001]. MD is suited for both distilled water production or for the concentration of aqueous solutions. MD has been applied for water desalination, environmental waste clean up, water reuse and food processing among others like milk and juice concentration, biomedical applications such as water removal from blood and treatment of protein solutions [Banat and Simandl, 1994]. Separation of azeotropic aqueous mixtures such as alcohol–water mixtures, concentration of radioactive solutions and application for nuclear desalination, waste water treatment in which a less hazardous waste can be discharged to the environment specially in textile waste treatment that is contaminated with dyes, concentration of coolant (glycol) aqueous solutions, treatment of humic acid solutions, pharmaceutical waste water treatment and in areas where high temperature applications lead to degradation of process fluids, can be attractive. It must be pointed out that desalination is the most known MD application as near 100% rejection of non-volatile ionic solutes is easily achieved [Khayet et al., 2003].

MD process involves transport of vapor through micro porous hydrophobic membranes and operates on the principle of vapor–liquid equilibrium as a basis for molecular separation. The liquid feed to be treated by MD must be in direct contact with one side of the membrane and does not penetrate inside the dry pores of the membranes. The hydrophobic nature of the membrane prevents liquid solutions from entering its pores due to the surface tension forces. As a result, liquid/vapor interfaces are formed at the entrances of the membrane pores. The MD driving force is the transmembrane vapor pressure difference that may be maintained with one of the four following possibilities (see Fig. 2.3) applied in the permeate side [Lawson, 1997]:

(a) An aqueous solution colder than the feed solution is maintained in direct contact with the permeate side of the membrane giving rise to the configuration known as direct contact membrane distillation (DCMD). The transmembrane temperature difference induces a vapor pressure difference. Consequently, volatile molecules evaporate at the hot liquid/ vapor interface, cross the membrane in vapor phase and condense in the cold liquid/vapor interface inside the membrane module.

(b) A stagnant air gap is interposed between the membrane and a

condensation surface. In this case, the evaporated volatile molecules cross both the membrane pores and the air gap to finally condense over a cold surface inside the membrane module. This MD configuration is called air gap membrane distillation (AGMD).

(c) A cold inert gas sweeps the permeate side of the membrane carrying the vapor molecules and condensation takes place outside the membrane module. This type of con-figuration is termed sweeping gas membrane distillation (SGMD).

(d) Vacuum is applied in the permeate side of the membrane module by means of a vacuum pump. The applied vacuum pressure is lower than the saturation pressure of volatile molecules to be separated from the feed solution. In this case, condensation occurs outside of the membrane module. This MD configuration is termed vacuum membrane distillation (VMD).

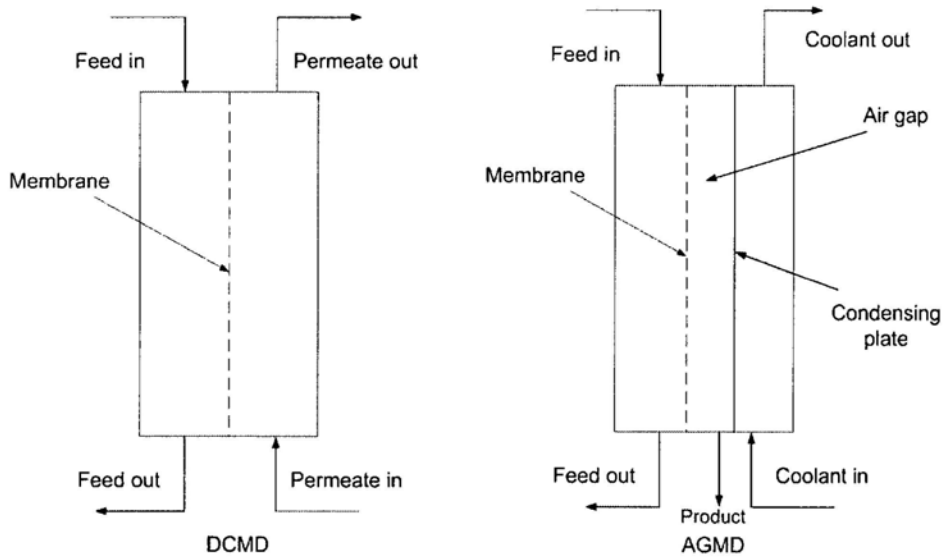

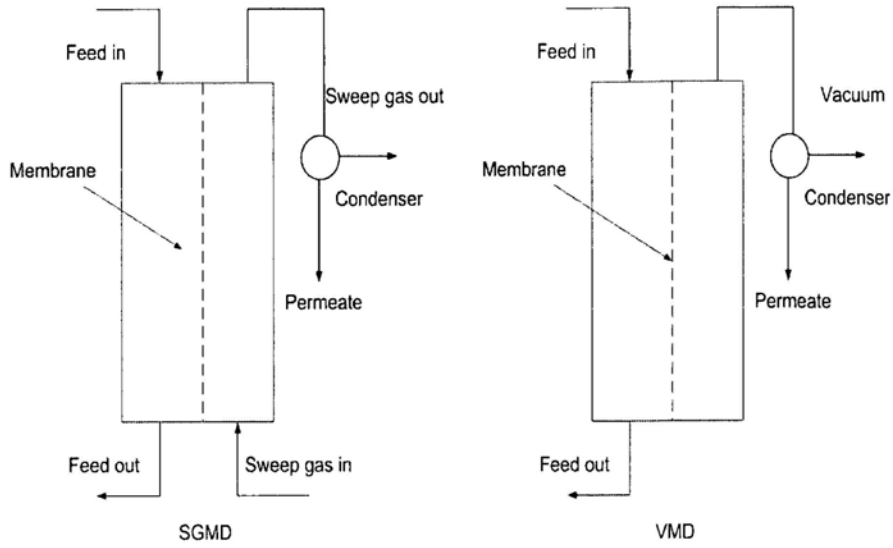

Figure 2.3: Different types of MD configurations

Each one of the above possibilities has its advantages and inconveniencies for a given application. The potential advantages of MD process in comparison to the conventional separation processes rely on the lower operating temperature and hydrostatic pressure. Feed solutions having temperatures much lower than its boiling point under pressures near atmosphere can be used.

The first MD paper is published by Findley [1967]. At that time, interest in this process has been faded quickly loosing its brightness due partly to the observed lower MD production compared to the reverse osmosis technique. MD process has recovered interest within the academic communities in the early of 1980s when novel membranes and modules with better characteristics became available [Gore, 1982; Anderson et al., 1985]. This alongside with the actual merits of MD capability to utilize low-grade waste and/or alternative energy sources, such as solar and geothermal energy, made it becomes more promising separation technique [Bier and Plantikow, 1995; Koschikowski et al., 2003].

Recently, many theoretical presented for improvements of MD process. Schofield and Fane [1987] first analyzed the heat and mass transfer in MD simultaneously, they stated that the resistance for mass transfer mainly comes from the membrane structure and the air in the pores. They also pointed out that both temperature and concentration polarization effects should be taken into consideration. After that many literatures try to predict the values of the permeate flux and its

dependence on the membrane module design, membrane parameters and operating variables like the temperature and velocity of feed water and cooling water, the width of the air gap, the pressure difference and temperature difference. [Banat and Simandl, 1998; Khayet et al., 2000]. On the other hand, many experimental works have been done to validate the theoretical models, or to find the proper operating variables and membranes. Banat and Simandl [1994] investigated the performance characteristics of an air gap membrane distillation (AGMD) process for water desalination by conducting two long-run experiments. They compared a PVDF membrane of 0.45 μm pore diameter and a PTFE membrane of 0.5 μm pore diameter. Furthermore, the effect of hot side temperature, cold side flow rate and feed concentration were investigated. The experimental results obtained showed that the mass flux was steady over time and that it was affected only slightly by an increase in salt concentration. Permeate quality was dramatically affected when membrane wetting occurred, the cold side flow rate had a negligible effect on the permeate flux and the flux exponentially increased with an increase in hot side temperature. Zhang et al. [2010] studied the performances of various membranes that assessed in Direct Contact Membrane Distillation (DCMD) under different feed velocities and inlet temperatures. The membranes studied included a polyvinylidenefluoride (PVDF) microfiltration membrane with a non-woven support layer, a polytetrafluoroethylene (PTFE) microfiltration membrane with a non-woven support layer, and three MD membranes made from PTFE of different pore size and all with a structured scrim support layer. The results showed that distillation using PTFE membranes produced much higher flux than that of the PVDF microfiltration membrane at the same operational conditions, and the support layer affected not only the flux, but also the energy efficiency (0.51–0.24). The results also show that increasing the velocity of the feed and its inlet temperature increased the flux, but the rate of flux increase diminishes at high velocities. The mass transfer coefficient improved for thinner support and active layer membranes, leading to fluxes as high as 46 Lm^{-2} h^{-1} at 80 °C.

However, despite the numerous mathematical models that has been developed by MD investigators and regardless of their precision in predicting the MD permeates flux. This may caused by the inaccurate description of the mass transfer process, empirical relation between heat transfer coefficient and velocity is not exactly for porous surface or the uneven distribution of temperature and

concentration in bulk water is not considered, etc. In experiment aspect, there are number of issues which are still need to be fully understood, such like membrane fouling, the long-term performance, the energy consumption and cost evaluation. One major obstacle for the MD process finally reaches industry is the membrane material. Current used membranes in MD process are mainly from other membrane applications, such like Reverse Osmosis (RO) membrane or filtering, etc. If some membranes can be specific designed for MD process, the performance could be greatly improved.

In this thesis, a new model for describing the mass transfer process of DCMD is proposed, this may brings a better understanding of the whole membrane distillation process and improve the precision in predicting the water flux of MD. A DCMD experiment system is setup to validate the new developed model and for further investigated of new membrane materials. Moreover, a new material—aerogel is proposed to be used as the membrane, the performance of the aerogel membrane is also investigated.

2.3 Review of Renewable Thermal Energy Harvesting

There are many forms of renewable energy, such as solar energy, geothermal, ocean energy, wind energy and biomass. They have many environment benefits compared to conventional energy source. Each type of renewable energy also has its own special characteristic that make it requires certain technology and suited to certain applications.

Among various forms of renewable energy, thermal energy is perhaps the most common. For example, there exists a temperature difference between the two surfaces of a wall with one surface facing toward the sun and the other surface facing backward from the sun; there also exists a temperature difference between the hot air generated by an air conditioning system and the environment; and the geothermal is also abundant. For harvesting these energies, many technologies are presented. Solar water heat, solar cooker, solar drier and solar ponds are the direct simple way for utilizing solar energy [Thirugnanasambandam et al., 2010]. Solar power plant is a kind of large scale technology to drive steam cycle by solar thermal. Zarza et al.

[2006] presented a parabolic-trough solar field producing 410 °C and 70 bar superheated steam delivering a power output of 5 MW. Hong et al. [2005] proposed a new solar thermal power cycle in which the solar energy is used to decompose methanol into syngas and combusting it with air resulting in an efficiency of 35 % at a collector temperature of 220 °C. Yamada et al. [2009] conducted numerous theoretical and experimental studies on the combination of Ocean thermal energy conversion (OTEC) generation method and solar collector. By a closed Rankine cycle, they convert the heat energy associated with the temperature difference between the warm surface water and cold deep water of the ocean into electricity. However, due to a small temperature difference (approximately 15–25 K) between the surface water and deep water of the ocean, the Rankine-cycle efficiency is limited to be only 7%. Geothermal is also used for heating working fluid to higher temperature and higher pressure, and then driving a thermodynamic cycle. Sometimes it is also combined with solar heating. However, these conventional technologies usually require large and complex system, experienced worker and high cost.

Besides the above conventional technologies, many new methods have been proposed recently for harvesting thermal energy in temperature difference form. Solar chimney is recent studied [Zhou et al., 2007;], it use solar energy to heat a large amount of air, and the hot air is force by buoyancy to move up the chimney as a hot wind, driving the turbine generator to generate electricity. But conversion is quite inefficiency. Woo and Lee [2003] examined the thermoelectric generation which is a direct energy conversion method from heat to electricity. It could use the thermal energy below 423 K. Sebald et al. [2008] proposed a micro generator which harvests energy from the temperature difference using ferroelectric materials. It has higher efficiency than that of the thermoelectric generation. Generally speaking, most thermal-electric conversion methods are based on thermoelectric materials. The conversion efficiency is rather low. According to Yamashta et al. [2007], the latest thermoelectric generator's conversion efficiency is only 0.27%. Another problem is the necessity of a large temperature gradient [Minaev and Fursenko, 2007]. These problems are rooted at the fundamental thermoelectric principle, and the improvement is restricted by the properties of the materials.

To find a better way for thermal energy harvesting, this thesis propose a new method for solar thermal energy collection. Numerical analysis is conducted to

investigate the performance of this method. A device is designed and optimized [Zhang and Du, 2009[a,b]].

2.4 Review of Desalination by Solar Thermal Energy

According to literatures, distillation is the most widely used process for desalination. Currently, Multi-Stage-Flash (MSF) technology produces 56% of the total fresh water produced by desalination [Hussan, 2003]. However, it is an energy thirsty process. It has been estimated by Kalogirou [2005] that the production of 1000 m^3 per day of freshwater requires 10,000 tons of oil per year.

The emerging concerns of energy and environment have consequently increased the interest for the use of renewable energy source, especially in remote areas and islands, because of the high costs of fossil fuels, difficulties in obtaining it, attempts to conserve fossil fuels, interest in reducing air pollution, and the lack of electrical power in remote areas. Fig. 2.4 shows the possible combinations of renewable energy technologies and desalination plants technologies. Renewable energy-driven desalination systems fall into two main categories: thermal processes and electromechanical processes. As regards the energy source, a desalination plant powered by renewable energy is likely to be a stand-alone system at a location which has no electricity grid. Stand-alone systems are often hybrid systems, combining more than one type of renewable energy sources, for instance, wind and solar energy or including a diesel generator. In order to ensure continuous or semi-continuous operation independent of weather conditions, stand-alone systems usually include a storage device.

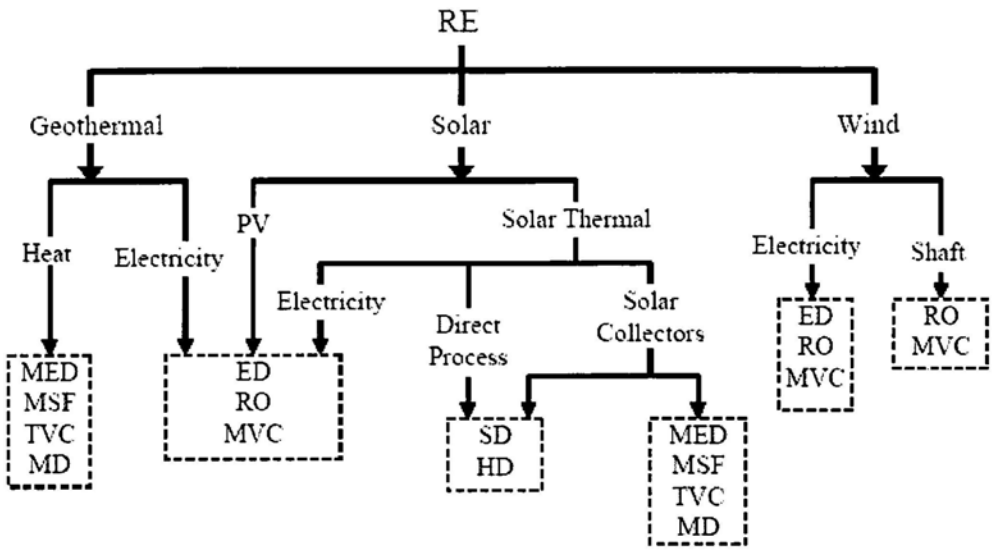

Figure 2.4: Possible technological combinations of the main renewable energies and desalination methods [Mathioulakis et al., 2007]

Thermal solar energy is considered to be one of the most promising applications of renewable energies to seawater desalination, especially for arid and sunny regions. Because of the common distributed of solar energy. A thermal solar distillation system usually consists of two main parts, the collecting device and the distiller. Solar thermal desalination processes are characterized as direct processes when all parts are integrated into one system, while the case of indirect processes refers to the heat coming from a separate solar collecting device, usually solar collectors or solar ponds.

The indirect-type stills are based on the fact that heat is provided only at the first stage of such multi-effect unit, thus the use of external heat source is possible. Conventional solar thermal collectors, corrosion-free collectors developed for the specific application [Rommel et al., 2000; Hermann et al., 2000] or even evacuated tube collectors [El-Nashar, 2000] have been used as the external heat source. Within the category of indirect processes installations based on conventional thermal desalination technology, as MED and MSF, are also included. For reasons related to the complexity and the cost of desalination units, these plants are usually of greater size. Even though during past years the development of such installations has been rather abandoned, several MED and MSF pilot plants have been designed and tested

during the past, especially in late 90s. These installations have been driven by a flat plate, parabolic trough or vacuum solar collectors [El-Nashar, 2000; Ajona, 1992; Garcia-Rodriguez, 2003]. The evaluation of these plants has shown that MED has greater potential than MSF for designs with high performance ratio and, moreover, the MED processes appear to be less sensitive to corrosion and scaling than the MSF processes. Solar thermal energy can be used, in principle, for the production of electricity or mechanical energy. Evidently, the process of thermal energy conversion is accompanied with a decreased efficiency. During the past, only single attempts are reported, as the case of a solar-assisted freezing plant powered by a point-focusing solar collector field [Luft, 1982], a cogeneration hybrid MSF–RO system driven by a dual-purpose solar plant [Delyannis, 1987], and an RO plant powered by flat-plate collectors with freon as the working fluid [Rodriguez et al., 1996].

Solar stills belong to the case of direct processes, and due to the interest they present, they will be discussed thoroughly below. The main problem of the solar still is the low efficiency. For solving this problem, many bibliographies have been published. The most common is finding new design concepts that would decrease the loss of latent heat of condensation at the glass cover or furthermore would partly recover this energy. Thus, the idea of utilizing latent heat of condensation via multi-effect solar stills has come out. The basic principle imposes the use of condensation heat of the vapor from the n-th effect, for the evaporation of water at the $n + 1^{st}$ effect. Actually, one should talk of direct processes utilizing humidification–dehumidification techniques through a broad area of design solutions [Fath, 1998; Mink et al., 1998; Graeter et al., 2001; Rheinlaender and Graeter, 2001], leading eventually to significantly improved performance, compared to a simple solar still.

However, all the above mentioned technologies have to add other components to the solar still, this increases the cost and complexity of the solar still and decreases the stability. It is therefore the purpose of chapter 6 in this thesis, a new method for increasing the efficiency of solar sill is proposed. By utilizing Knudsen effect also driven by solar energy, the desalination system can operate under low pressure condition. This will increase the efficiency of evaporation under low temperature. It is thermodynamic efficient and also the daily fresh water productivity is enhanced.

Chapter 3

Numerical Method

As discussed in chapter 2, it is hard to predict the gas flow and heat transfer in micro / nano scale with traditional continue based model and hence, the molecular based model have to be used. For high Knudsen number flow, Direct Simulation Monte Carlo (DSMC) method has the most widely application range. This chapter introduces the basic principle and the process of DSMC. The influences of the model parameters are also discussed.

3.1 Direct Simulation Monte Carlo (DSMC)

DSMC is first proposed by Bird [1970], it is a molecular based statistical method original used for simulating supersonic dilute gas [Oran et al, 1998]. Recently, DSMC achieved more and more successes in simulating micro scale gas flow and heat transfer [Hadjiconstantinou and Simek, 2001; Liou and Fang, 2002].

3.1.1 Basic principle of DSMC

For high Knudsen number flow, the collision term in Boltzmann equation is hard to describe accurately, so both theoretical and numerical solution is hard to get [Cercignani, 1988]. DSMC method is based on the mechanism of molecular movement and collision, by statistically calculate the molecular movement and collision, the gas flow problem could be solved. During the simulation, one simulate particle represents a large amount of real particles. Subject to the dilute gas and molecular chaos assumptions, the DSMC method is to uncouple the molecular motions and the intermolecular collisions over small time intervals. It is proved that the DSMC is theoretically consistent to with Boltzmann method [Bird, 1970; Wagner, 1992].

3.1.2 Standard procedure of DSMC

The standard program flow of DSMC is shown in Fig.3.1: at the beginning, distribute the particles with random initial position and velocity; in each time step, move the particles and compute interactions with boundaries and index particles; in each cell, select the collision pair and perform intermolecular collision, get the velocity and internal energy after collision; finally sample flow properties. Repeat the above procedures until the residual error is satisfy.

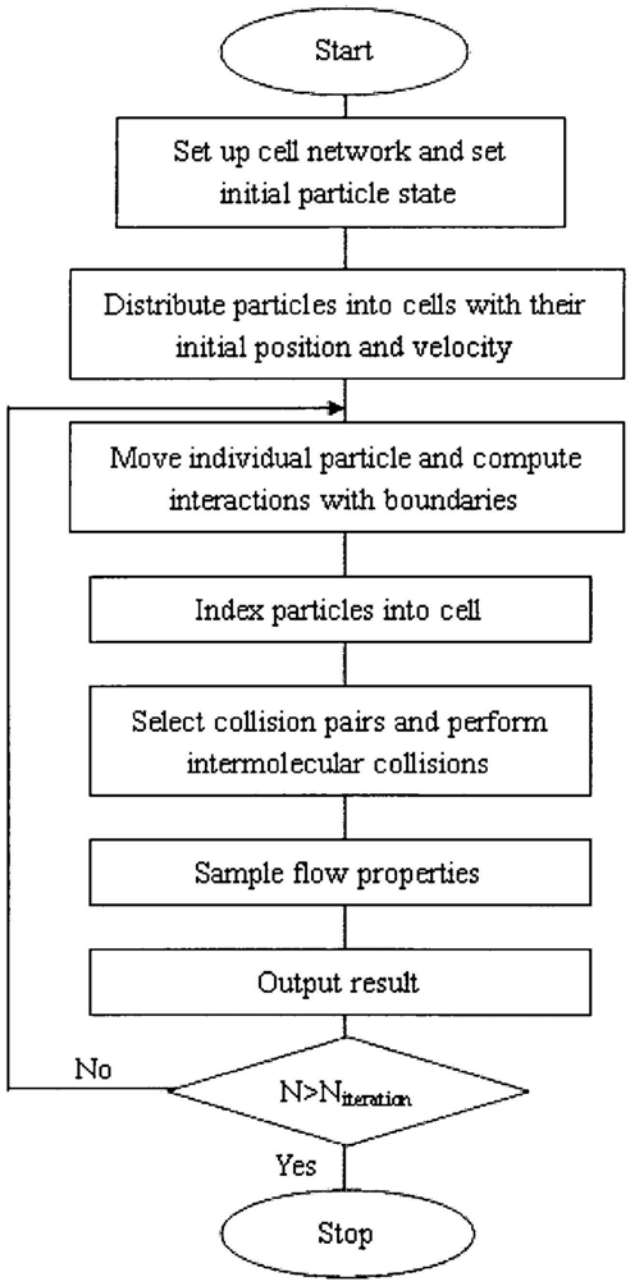

Figure 3.1: Standard Flowchart of DSMC

3.1.3 Collision model

The accuracy of DSMC is dependant `on the selection of a proper collision mode. Bird [1994] had introduced many molecular collision models, such as hard sphere model, variable hard sphere (VHS) and variable soft sphere (VSS), etc. Generally speaking, simple model has limited application area, and complicate model has low computational efficiency. In this section, I will introduce some simple collision model and the model I used in this thesis.

Hard Sphere (HS) model is the simplest molecular collision model as shown if Fig. 3.2. When the center distance between two molecules is smaller than the sum of the two molecule's radiuses, the collision happens, the collision cross section is

$$\sigma_T = \pi D_{12}^2 \tag{3-1}$$

where D_{12} is the su`m of the two molecule's radiuses.

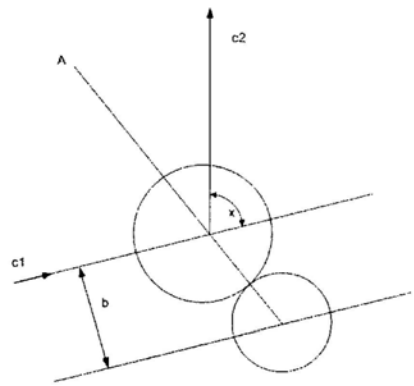

Figure 3.2: Collision geometry of hard sphere molecules

The deflection angle after collision is:

$$x = 2\arccos(b/d) \tag{3-2}$$

For the hard sphere model, the viscosity cross-section and momentum or diffusion coefficients are:

$$\sigma_\mu = \frac{2}{3}\sigma_T \tag{3-3}$$

$$\sigma_M = \sigma_T \tag{3-4}$$

The molecular diameter in hard sphere is not real molecular diameter, it is calculated

from the molecular viscosity:

$$D_{12} = [\frac{5}{16}(mk_B T_{ref} / \pi)^{1/2} / \mu_{ref}]^{1/2} \qquad (3\text{-}5)$$

This approximation causes an invariable cross-section, and the relationship between gas viscosity μ and temperature T is not consist with real case. So Bird proposed a variable hard sphere (VHS) model to solve the problem.

In **Variable Hard Sphere** (VHS), the deflection angle is also uniform as HS model, but the cross-section is proportional to the reverse power of relative velocity. In this way, we can get a variable molecular diameter and a more accuracy relation between viscosity and temperature.

The uniform deflection angle induces the ratio of the momentum to the viscosity cross-section is a constant, this is different from the real gas. And this deficiency will cause big error when deal with the multi-species case. In response to this problem, Koura and Matsumotic [1991, 1992] introduced the **Variable Soft Sphere** (VSS) model. In VSS model, the deflection angle is:

$$x = 2\arccos[(b/d)^{1/\alpha}] \qquad (3\text{-}6)$$

The above models only include the repellant potential. The addition of long-range attractive potential to the inverse power law model leads to a better representation of the potential curve of real molecules. Moreover, Hassan et al. [1995] extended VHS and VSS to get **Generalized hard Sphere** (GHS) model. This model could get good result in cases with big temperature changes, but it is not easy to use.

In this thesis I use VSS model for collision.

3.1.4 Collision sampling techniques

The probability of a collision between two molecules in a homogeneous gas is proportional to the product of their relative speed u_r and total collision cross-section σ_T:

$$\nu = n\overline{\sigma_T u_r} \qquad (3\text{-}7)$$

The number of collision in each cell at each time step is:

$$N_c = \frac{1}{2}n\nu = \frac{1}{2}n^2\overline{\sigma_T u_r} \qquad (3\text{-}8)$$

In DSMC, it is important to represent the collision number at time interval Δt, the collision number in each cell during Δt is

$$N_t = \frac{N}{2} v \Delta t = \frac{nN}{2} \overline{\sigma_T c_r} \Delta t \tag{3-9}$$

N is the molecular number is the cell. In this thesis I use No Time Counter (NTC) method [Bird, 1994].

The collision pair number is:

$$N_{NTC} = \frac{N\overline{N}}{2} F_N \left(\sigma_T c_r\right)_{\max} \Delta t / V_c \tag{3-10}$$

For pairs selected from the cell at the time step, the collision is computed with probability

$$P_{NTC} = \frac{\sigma_T c_r}{(\sigma_T c_r)_{\max}} \tag{3-11}$$

3.1.5 Macroscopic properties

The macroscopic properties of flow could be got from the statically equation:

$$U_j = \frac{1}{N_j} \sum u \tag{3-12}$$

where U_j is the macroscopic mean velocity in j cell, N_j is the particle number in j cell.

$$\rho = nm \tag{3-13}$$

$$T = (3T_{tr} + \zeta T_{rot}) / (3 + \zeta) \tag{3-14}$$

where T_{tr} is translation temperature, T_{rot} is the rotation temperature, ζ is the freedom of internal energy. Translation temperature and rotation temperature is calculated from:

$$T_{tr} = 2(\overline{mv^2} - \overline{mv}^2) / 3k_B \tag{3-15}$$

$$T_{rot} = \frac{2}{k_B} (\overline{\varepsilon_{rot}} / \varsigma) \tag{3-16}$$

where v is molecular velocity, ε_{rot} is the rotation energy of single molecule.

For thermal absolute gas, the pressure is given by:

$$P = \rho RT = nk_B T \tag{3-17}$$

3.1.6 Boundary condition

Boundary conditions include the gas-solid wall interaction and inlet and outlet boundary.

When the simulated molecules strike a surface boundary, some reflect off the surface without transferring any of their streamwise momentum and others transfer all of their momentum. To simulate the energy exchange between molecules and surface, several gas-surface interaction models such as diffuse, specular, and Cercignani-Lampis-Lord (CLL) have been utilized in the past [Lord, 1991; Weast et al., 1984]. For most of the gas flow in MEMS / NEMS, the velocity is not high, vacuum degree is low, wall temperature is near the atmosphere temperature, diffuse reflection model is fit for most of the common surface. Many results got good agreement with experiment [Alexander and Garcia, 1997; Liou and Fang, 2001; Hadjiconstantinou and Simek, 2002; Fan and Shen, 2001; Sun and Boyd, 2002]. I also choose the diffused reflection model to deal with the gas-solid wall interaction in my simulation. The diffused reflection assumes the velocities of the reflected molecules are distributed in accordance with the Maxwell distribution.

In standard DSMC program, the characteristic values of inlet and outlet boundary are the number density n_∞, velocity u_∞ and temperature T_∞ of flow from infinite far. With this treatment, we can not set the inlet and outlet conditions separately and the inlet and outlet flow have the same direction. For supersonic flow, there is no problem of utilizing this boundary. But for the micro flow, the gas velocity is low and the measured quantities are pressure and temperature, it is not easy to convert them to the number density and velocity. Another problem is for un-straight channel this boundary treatment must be modified [Lee et al., 2001].

In the simulation of Knudsen compressor in this thesis I use a new boundary treatment method developed by Wang et al. [2004]. In case of low velocity flow in micro scale, we need to use pressure boundary to take place the number density in DSMC. In MEMS experiment, we usually measure the inlet pressure P_{in}, inlet temperature T_{in} and outlet pressure P_e, so we need to transfer these macroscopic quantities to the particles properties.

At the inlet boundary, we need to set the molecules' velocities based on the

pressure and temperature. Compared the boundary treatment in traditional CFD, the particles velocities are:

$$(u_{in})_j = u_j + \frac{P_{in} - P_j}{\rho_j a_j} \tag{3-18}$$

$$v_{in} = v_j \tag{3-19}$$

where a_j is the local sound velocity. For thermal absolute gas, the relationship between number density and pressure and temperature is

$$n_{in} = \frac{P_{in}}{k_B T_{in}} \tag{3-20}$$

At the outlet boundary, we use the similar treatment method:

$$(\rho_e)_j = \rho_j + \frac{P_e - P_j}{(a_j)^2} \tag{3-21}$$

$$(u_e)_j = u_j + \frac{P_j - P_e}{\rho_j a_j} \tag{3-22}$$

$$(v_e)_j = v_j \tag{3-23}$$

$$(T_e)_j = P_e / \left[(\rho_e)_j R\right] \tag{3-24}$$

$$(n_e)_j = (\rho_e)_j / M \tag{3-25}$$

where R is gas constant, M is molecular mass. Eq. (3-21)-(3-25) are about the x-direction, for y-direction, the velocities are:

$$(u_e)_j = u_j \tag{3-26}$$

$$(v_e)_j = v_j + \frac{p_j - p_e}{\rho_j a_j} \tag{3-27}$$

The macroscopic quantities in boundary cells have been discussed in section 3.1.5.

Eq. (3-18) ~ (3-27) are the boundary condition used in my simulation, correspondingly the standard DSMC program is modified to the pressure boundary condition.

3.2 Validation of the Program

Our program is developed from Bird's open source program DSMC2.FOR. Before using it for the study cases in the thesis, the code need to be validated. For validation, we simulate two classical flows—Couette flow and Poiseuille flow in micro channels, and compare the simulation results with theoretical solution in slip flow region. The channel is 5μm×1μm, the grid is 50×50.

3.2.1 Micro Couette flow

For the micro Couette flow in slip region, based on Beskok's [1996] second order slip boundary condition, the dimensionless velocity distribution on the channel's cross-section is:

$$\frac{u}{U}=\frac{\frac{y}{h}+\frac{2-\sigma_v}{\sigma_v}Kn}{2\left(\frac{2-\sigma_v}{\sigma_v}\right)Kn+1} \tag{3-28}$$

where U is the velocity of the moving wall, h is distance between walls, σ_v is the cooperation coefficient for momentum.

Based on slipping theory, the first order temperature distribution of micro Couette flow is:

$$\frac{T-T_w}{T_g-T_w}=\left(-\left(\frac{y}{h}\right)^2+\frac{y}{h}+\frac{2-\sigma_T}{\sigma_T}\frac{2\gamma}{\gamma+1}\frac{Kn}{\mathrm{Pr}}\right)\Big/\left(\frac{2-\sigma_T}{\sigma_T}\frac{2\gamma}{\gamma+1}\frac{Kn}{\mathrm{Pr}}\right) \tag{3-29}$$

where T_w is the wall temperature, T_g is the gas temperature beside the wall, σ_T is temperature cooperation coefficient.

I use the DSMC code to simulate a Couttee flow with U=200 m/s、T_w=273K and boundary pressure is 1 atm. Fig. 3.3 shows the comparison between simulation results and theoretical results, where σ_T、γ and Pr are 1.0, 1.4 and 0.72 [Weast et al., 1984], it is found the simulation results and theoretical results got good agreement, the relative error is less than 2.5%.

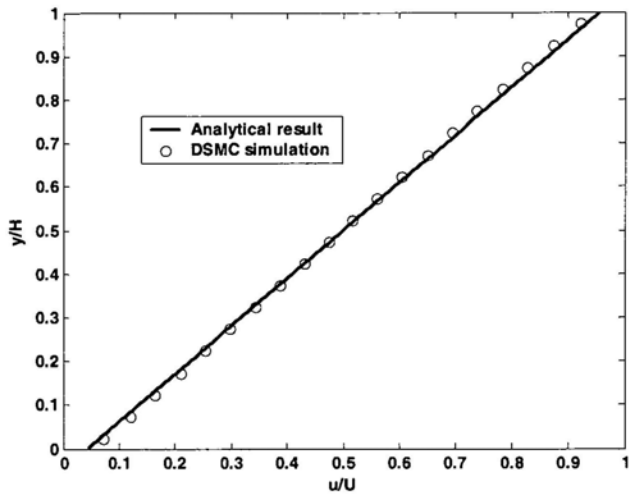

(a) Velocity Distribution

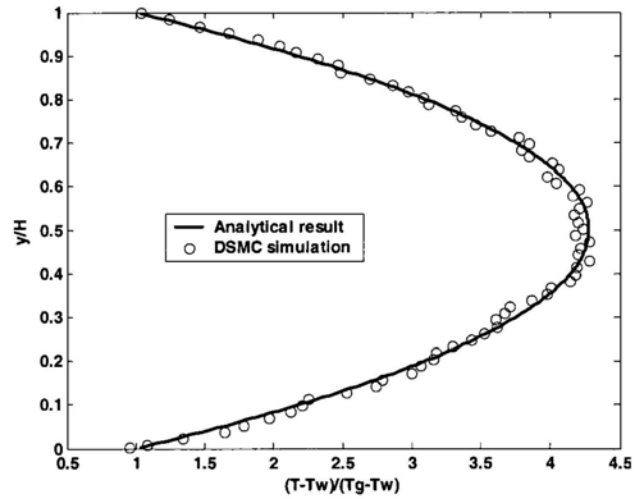

(b) Temperature Distribution

Figure 3.3: Comparison between DSMC simulation and theoretical solution for micro Couette flow

3.2.2 Micro Poiseuille flow

For Poiseuille flow, based on slipping theory, the first and second order velocity distributions are [Beskok, 1996]:

$$\frac{u}{u_c} = \left[-\left(\frac{y}{h}\right)^2 + \frac{y}{h} + Kn \right] \Big/ \left(\frac{1}{4} + Kn \right) \tag{3-30}$$

$$\frac{u}{u_c}=\left[-\left(\frac{y}{h}\right)^2+\frac{y}{h}+\frac{Kn}{1+Kn}\right]\Big/\left(\frac{1}{4}+\frac{Kn}{1+Kn}\right) \tag{3-31}$$

where u_c is the velocity at the center line.

The micro Poiseuille flow for two different Knudsen number is simulated. The wall temperature is 300 K. Fig. 3.4 shows the velocity distributions at the middle cross-section in the channel, and compares the DSMC results with first and second order theoretical solution. For small Knudsen number (Kn=0.18), the DSMC results, first and second order results agree well; for larger Knudsen number (Kn=0.53), the first order solution and second order solution has some difference, and DSMC result is closer to the second order result.

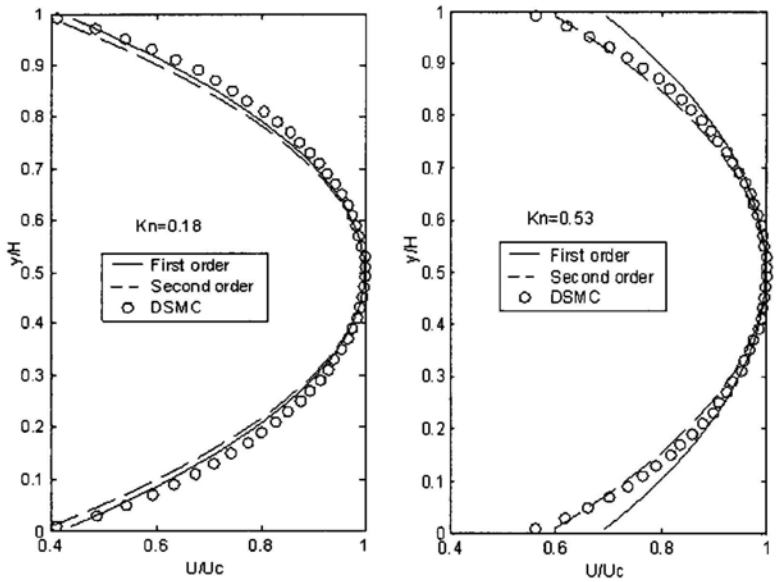

Figure 3.4: Comparison between DSMC simulation and theoretical solution for micro Poiseuille flow

By the above simulations and comparisons about micro Couette flow and micro Poiseuille flow, the DSMC program used in this thesis is validated.

3.3 Influence of the Simulation Parameters

There are some important parameters for DSMC, such cell size, time interval, particle number and etc. For example, Bird [1970] suggested the particle number in

each cell should not less than 20. An improper chosen of these parameters will affect the validity and accuracy of the simulation. Therefore, this section will discuss the influences of cell size and time interval.

3.3.1 Influence of cell size

Bird [1994] stated that the maximum cell size of DSMC simulation should smaller than the local mean free path. Alexander et al. [1998] proved this criterion theoretically. But recently some researchers [Ilgaz and Celenligil, 2003] pointed that the cell size could be enlarged to 100 times of the mean free path at the flow direction. In this case, it is necessary to numerically study the influence of cell size.

A micro Couette flow is simulated under different cell size. The distance between the two plates is 10 μm, low plate is stay, up plate moves at 200 m/s. Time interval is half of the mean collision time. No sub-grid, the total particle number are the same, the sample number is also the same as 8×10^5.

Fig. 3.5 shows the comparison between DSMC results and theoretical solution under different cell size. For velocity distribution, there is no big difference, but for temperature distribution, it is clear that when the cell is larger than mean free path, the DSMC results are far away from theoretical solution.

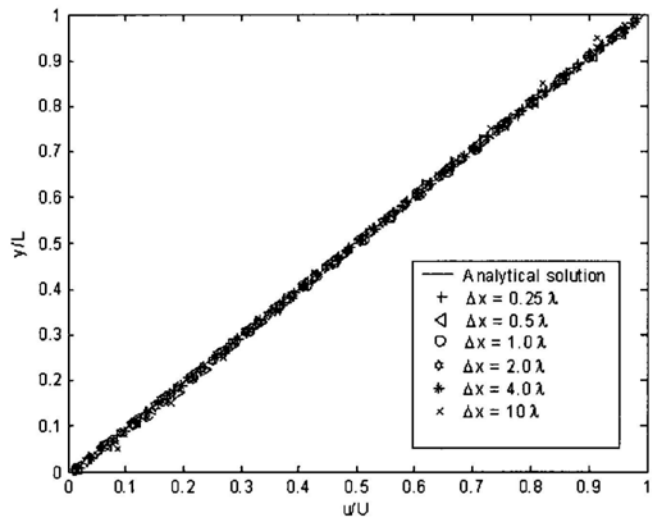

(a) Velocity distribution

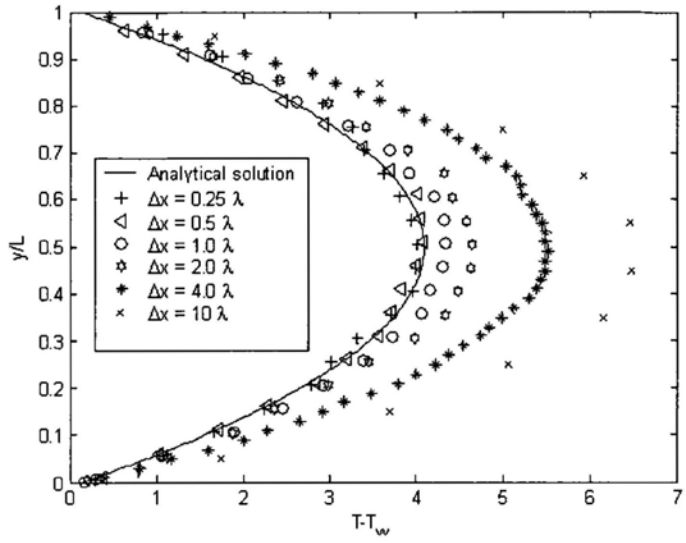

(b) Temperature distribution

Figure 3.5: Simulation results for different cell size

In Bird's code, we can also set the sub-cell, and that is equal to a second grid. We try the cases for same cell size but different sub-cell size, and the sub-cell size is smaller than mean free path. As show in Fig. 3.6, as the sub-cell size fulfills the requirement, the result is right.

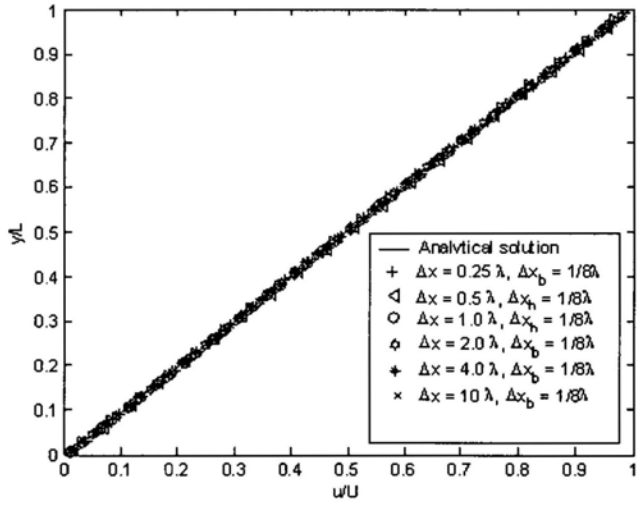

(a) Velocity distribution

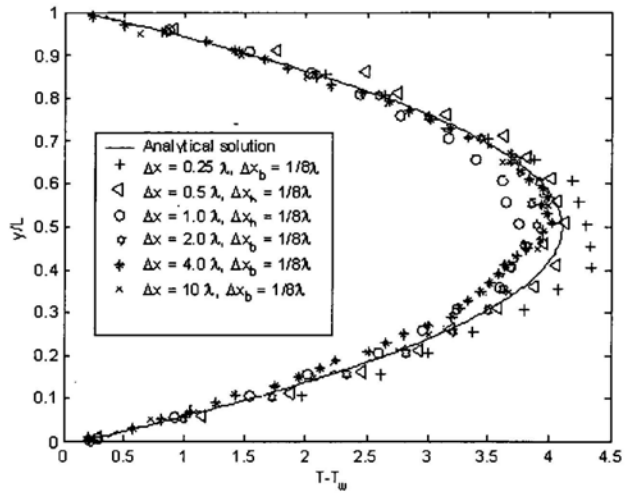

(b) Temperature distribution

Figure 3.6: Simulation results for different cell size but same sub-cell size

The above results indicated that, in DSMC the size of sub-cell should smaller than mean free path. When this criterion is satisfied, the simulation results will not affect by grid.

3.3.2 Influence of time interval

Garcia and Wagner [2000] gave the relationship between gas coefficients and time interval as below:

$$\mu = \mu_0 \left(1 + \frac{32}{150\pi} \left(\frac{c_0 \Delta t}{\lambda} \right)^2 \right) = \mu_0 \left(1 + 0.068 \left(\frac{\Delta t}{\Delta t_0} \right)^2 \right) \qquad (3\text{-}32)$$

$$D = D_0 \left(1 + \frac{4}{27\pi} \left(\frac{c_0 \Delta t}{\lambda} \right)^2 \right) = D_0 \left(1 + 0.0472 \left(\frac{\Delta t}{\Delta t_0} \right)^2 \right) \qquad (3\text{-}33)$$

where D is the diffusion coefficient of gas, c_0 gas molecular speed, Δt_0 is the mean collision time. The errors of gas coefficients between DSMC results and theoretical results are increase with time interval.

For the micro Couette flow in section 3.3.1, some simulations are carried out under different time interval. The cell size fulfills the requirement. The results are shown in Fig. 3.7.

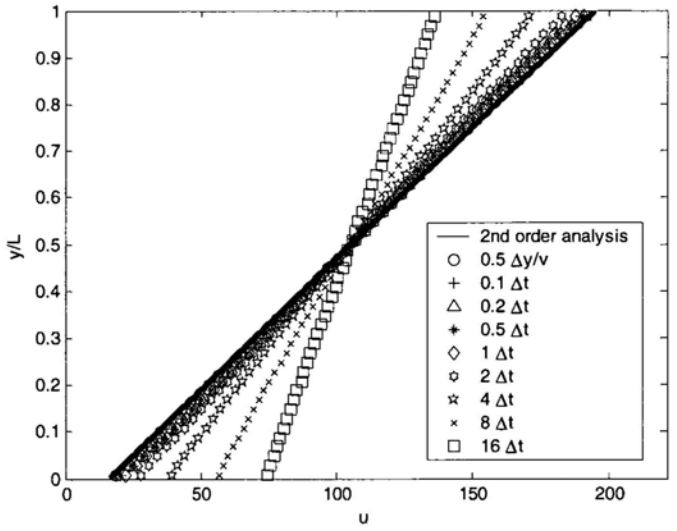

(a) Velocity distribution

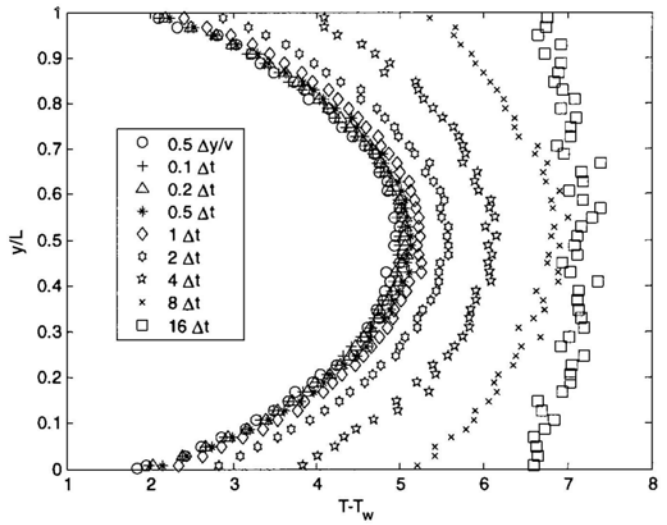

(b) Temperature distribution

Figure 3.7: Simulation results for different time interval

From Fig. 3.7 we found when time interval is smaller than mean collision time, the simulation results get good agreement with theoretical results, and results are independent with the time interval; as time interval is larger than mean collision time, the computational error is significant in both velocity distribution and temperature distribution.

Chapter 4

Direct Contact Membrane Distillation System

4.1 Introduction

In this chapter, a Direct Contact Membrane Distillation system driven by solar energy for seawater desalination is proposed and investigated. It is reported in membrane literature [Lawson and Lloyd, 1997] that DCMD is the most studied MD configuration as stated in the previous section. This is due to the fact that condensation step is carried out inside the membrane module leading in this way to a simple operation mode without the need of external condensers like in SGMD and VMD configurations.

Direct Contact Membrane Distillation (DCMD) is a thermally driven process in which a hydrophobic microporous membrane is used. The hydrophobic nature of the membrane prevents the passage of liquid water through the pores of the membrane while allowing the passage of water vapor (Fig. 4.1). In the DCMD process, the driving force is the vapor pressure gradient generated by temperature difference imposed between the two membrane sides. The water vapor passes through the membrane by diffusion and/or convection, and the result is distillate of high purity [Lawson and Lloyd, 1997; El-Bourawi et al., 2006; Khayet and Matsuura, 2004].

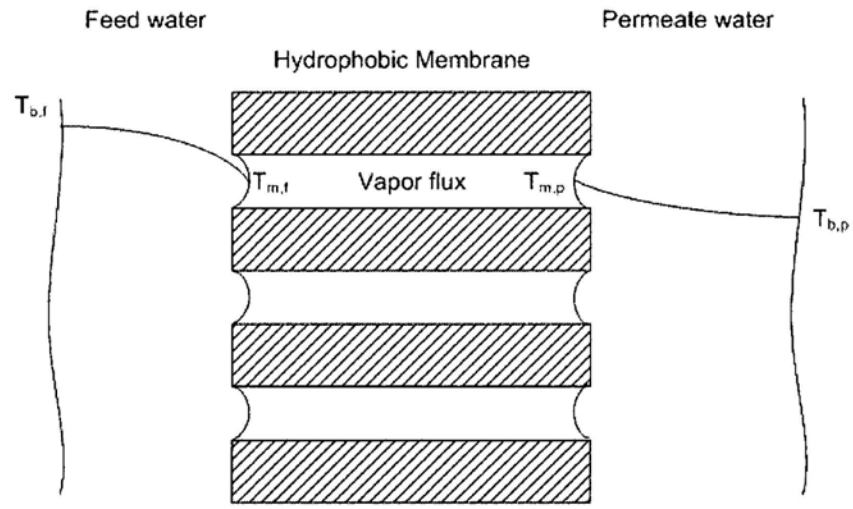

Figure 4.1: Illustration of DCMD

DCMD separation process should be characterized by both simultaneous heat and mass transfer, since mass (vapor) transport through membrane pores occurs as a result of the difference in temperature and composition between the feed and the permeate. Vapor flux across the DCMD membrane was described in the literature by the kinetic theory of gas [Lawson and Lloyd, 1997; Schofield, 1990]. In the application of DCMD, the total resistance (due to the sum of two momentum transfer processes); one is Knudson resistance which is due to direct collisions with a capillary wall, while the other is viscous resistance (due to indirect contact with capillary walls via molecule–molecule collisions terminating at molecule-wall collisions) [Imdakm and Matsuura, 2004]. In the literatures about mass transfer model in DCMD, they either make a linear combination of these two mechanisms [Schofield, 1990[b]] or simply consider the two mechanisms work separately (i.e. for viscous flow region, Knudsen resistance is neglected; for Knudsen flow region, viscous resistance is neglected) [Khayet et al., 2010]. The flow region is classified by the value of Kn which defined as follow

$$Kn = \frac{\lambda}{D_{pore}} \tag{4-1}$$

where λ is the mean free path length and D_{pore} is the average size of the membrane pores. The value of λ, defined as the average distance the molecule of diffusing species travels between two successive collisions, can be calculated from the kinetic theory of gases by the following equation:

$$\lambda = \frac{k_B T}{P\sqrt{2}\pi\sigma^2} \tag{4-2}$$

where k_{B} is the Boltzmann constant, T the absolute temperature (K), P the total pressure (Pa) and σ the collision diameter (m). The mean free path length therefore is proportional to temperature and inversely proportional to pressure.

The above mass transfer model achieved satisfied result for simulating the DCMD process. But from the viewpoint of micro flow simulation, it is too simple to consider the two resistance mechanism separately, neglecting of anther mechanism must brings some error. Linear combination is also not accurate.

As reviewed in chapter 2, the classification of different flow regimes is given below:

$Kn < 10^{-3}$ – continuum

$10^{-3} < Kn < 0.1$ – slip flow

$0.1 < Kn < 10$ – transition flow

$Kn > 10$ – free-molecular flow

For the DCMD, Kn is about 0.1 ~ 1, in other words, it is in the transition flow regime. In this regime, the aforementioned conventional model could suffer from significant errors.

In comparison, the Direct Simulation Monte Carlo (DSMC) is a much more appropriate for the transition flow regime. In this chapter, we propose to use DSMC to study the mass transfer process of DCMD. It takes both mechanisms into consideration and avoids the over simplification in the transition flow regime. In addition, the simulation result offers the insight of the vapor transportation process and paves the road for optimizing DCMD. In order to validate the simulation result, a DCMD experiment with a commercial PTFE membrane is conducted. The experiment results match the simulation results well. Using the new method, the influences of some key characters of the membrane (the pore size and the membrane thickness) are analyzed. Furthermore a new candidate membrane material — aerogel, which is highly hydrophobic and thermal isolate, is investigated and believed to have better performance.

4.2 The Mass and Heat Transfer Models

As shown in Fig. 4.1, the overall membrane distillation process involves heat transfer in the feed side, heat and mass transfer in the membrane as well as the heat transfer in the permeate side; these models are as follows:

4.2.1 Heat transfer

In DCMD the heat transfer can be divided into three regions: (1) convectional heat transfer in the feed boundary layer, $Q_{f,conv}$; (2) a combination of both conductive heat transfer through the membrane, $Q_{m,cond}$, and heat transferred because of water vapor migration through the membrane pores, $Q_{m,M}$.; (3) convectional heat transfer in

the thermal permeate boundary layer, $Q_{p,conv}$.

- The heat transfer through feed side boundary layer is:

$$Q_{f,conv} = h_f (T_{bf} - T_{mf}) \tag{4-3}$$

where h_f is the heat transfer coefficient of the boundary layer at the feed side, T_{bf} and T_{mf} are the boundary temperature and the membrane temperature at the feed side respectively.

- Heat transport through the membrane is:

$$Q_{m,cond} + Q_{m,M} = h_m (T_{mf} - T_{mp}) + N\Delta H_v \tag{4-4}$$

where h_m is the heat transfer coefficient, which can be evaluated by $h_m = d_m / \delta_m$, and d_m the average thermal conductivity of the membrane, δ_m the membrane thickness. The calculation of d_m takes into account both thermal conductivity of the membrane and the thermal conductivity of the gas presented in the membrane pores: $d_m = \varepsilon d_s + (1-\varepsilon) d_g$, where ε is the membrane porosity, d_s and d_g are the thermal conductivities of the membrane material and the gas in the pores respectively. N is the water vapor flux and ΔH_v is the latent heat of vaporization; T_{mp} is the membrane temperature at the permeate side.

- Heat transfer in permeate side:

$$Q_{p,conv} = h_p (T_{mp} - T_{bp}) \tag{4-5}$$

where h_p is the heat transfer coefficient of the boundary layer at the permeate side and T_{bp} is the boundary temperature at the permeate side.

4.2.2 Mass transfer

As stated in Section 1, we use DSMC method to describe the mass transfer in membrane. DSMC is a statistical computational approach. Subject to the dilute gas and molecular chaos assumptions, DSMC is to uncouple the molecular motions and the intermolecular collisions over small time intervals. The Monte Carlo method is, like its name sake, a random number strategy based directly on the physics of the individual molecular interactions. The idea is to track a large number of randomly selected, statistically representative particles, and to use their motions and interactions to modify their positions and states. It has been proved that DSMC is

valid for all ranges of Knudsen number, especially for our DCMD case where $0.1 < Kn < 1$. DSMC is ideal, where the Boltzmann equation is difficult to solve and molecular dynamics requires too many computational resource.

4.2.3 Other models

At the entrance of membrane's pore, it is assumed the kinetic effect of the molecular can be neglected at the liquid-vapor interface. In other words, the vapor and liquid are assumed to be in the equilibrium state corresponding to the temperature at the membrane surface and the pressure within the membrane pores. This separation process will not affect the total vapor flux of the whole DCMD process. This implies that the vaporization process is in equilibrium state and does not affect the vapor transfer process. Moreover, the bottle neck is the vapor transfer through the membrane. With this equilibrium assumption, vapor liquid equilibrium equations can be applied to determine the partial vapor pressures of each component on each side of the membrane. This gives the boundary conditions for mass transfer within the membrane. For pure liquids (with dissolved air) the partial vapor pressure is equivalent to the component's saturation pressure, P^0, which can be determined with the Antoine equation [Reid et al., 1997]:

$$p_i = P^0 = \exp\left(a - \frac{b}{c+T}\right) \tag{4-6}$$

where p_i is the partial pressure of component i, p^0 is in Pa, T is the temperature in K, and a, b, and c are constants that have been determined for a variety of substances and are readily available (water: a = 23.1964, b = 3816.44, c = - 46.13; ethanol: a = 23.4170, b = 3578.91, c = - 50.50).

4.3 The Model Validation

The DSMC simulation domain is show in Fig. 4.2. Round circles represent vapor molecules. For each DSMC iteration flow properties are calculated and the thermal boundaries, T_{mf} and T_{mp}, are updated; the iterations continue until a convergence result incurs. Different channel length (L) and channel width (W) are simulated to investigate the influence of pore size and membrane thickness. Different

bulk feed temperatures in a range of 30 – 90 °C are considered, permeate temperature is kept at 20 °C.

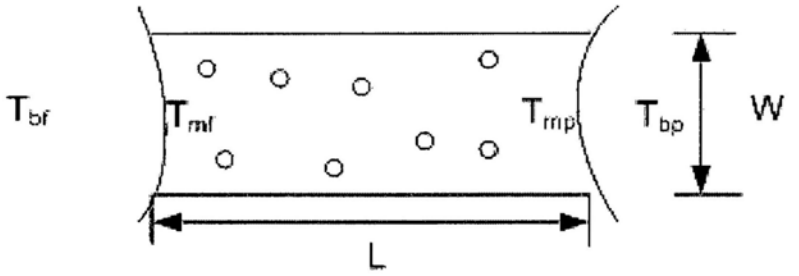

Figure 4.2: Simulation domain

The computational domain is divided by a 200 × 40 grid (i.e. 8000 cells), each cell contains 20 simulated molecules, and the total number of simulated molecules in the domain is about 160,000. In many cases, the ratio of thickness to pore size, L/W, is very large; but it is not very effective for DSMC to deal with very high L/W as the computation load will become unbearable. Thus, we assume there are few sections of such domain stacked along the longitude direction, which is consistent to the real case as the molecular do not move very fast. An additional flow resistance will be induced on the connection of sections, on which the total vapor flux will reduce 1% for each added section. For example, if the thickness of the membrane is 0.2 mm, and the section length is 2 μm, then there will be 100 sections and the flux is calculated by a factor of $(0.99)^{100} = 0.366$. It takes about 2 hours for one simulation.

The other key parameters used in the simulation include the thermal conductivity and the heat transfer coefficients. The value of water vapor's thermal conductivity d_g is 0.02 W/mK [Phattaranawik et al., 2003]. The two heat transfer coefficients h_f and h_p are 15,000 W/m^{2}K.

The common membrane material is PTFE. Fig. 4.3 is a commercial PTFE membrane used in our experiments. Its thermal conductivity is 0.23 W/mK. Its nominal thickness is 0.2 mm and the mean pore size is about 0.2 μm.

The schematic experiment setup is shown in Fig. 4.4 and Fig. 4.5 shows a photo of the experiment setup. It is a glass tank connected with an L shape glass tube, the two parts are divided by the PTFE membrane. The glass tank is filled with industrial grade $CuSO_4$ solution plus water (the ratio is 1:3) as the feed side. Pure

water is filled in the L shape glass tube as the permeate side. The tube is marked for measuring the flow rate. When the glass tank is heated by a hot plate, a temperature difference is generated between the two surfaces of the membrane, the DCMD process is then induced. The water vapor passes the PTFE membrane, the level in the tube rises. When the system reaches steady state, the temperatures of the liquid at the feed side will be stabilized. At this time, we measure the temperatures of the feed side and the permeate side, T_f and T_m, as well as the fresh water flux. The experiment results are shown in Table 4.1.

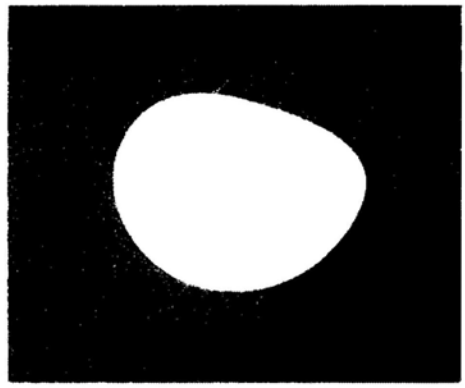

Figure 4.3: PTFE membrane

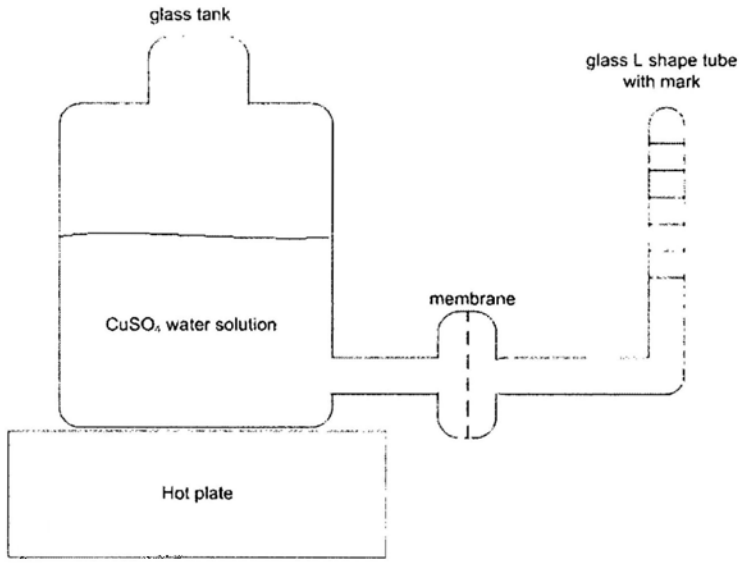

Figure 4.4: Schematic diagram of the experiment system

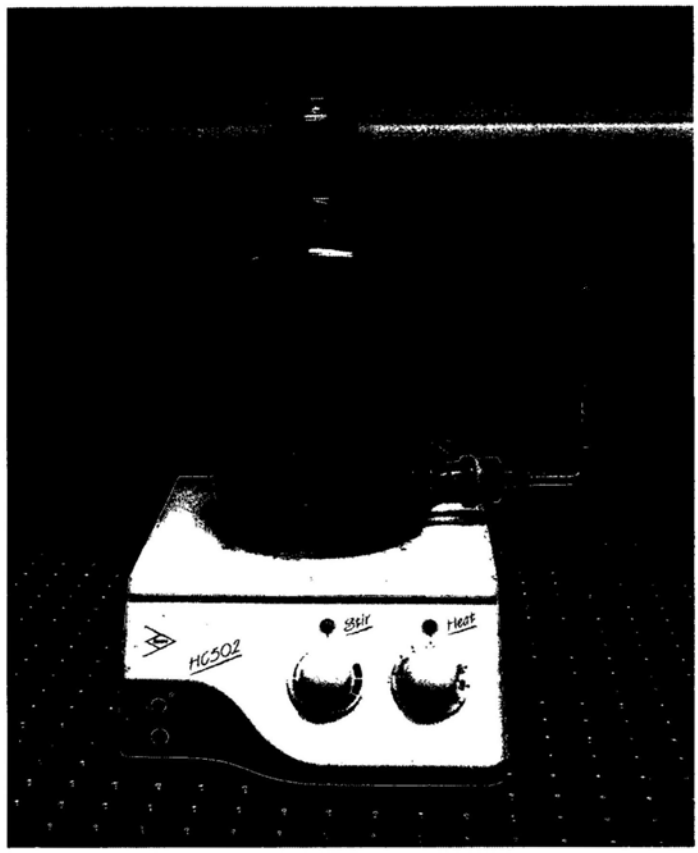

Figure 4.5: Experiment setup of the DCMD

Table 4.1: Water flux under different temperature

Temperature difference (°C)	*Water flux(kg/m^{2}h)*
10.2	4.2
20.3	5.7
30.1	10.5
40.4	16.5
50.1	23.4
60.3	35.6

Figures 4.6 to 4.8 show the simulation result. Fig. 4.6 shows the water vapor flow field in the micro channel of the membrane. As expected, the water vapor flows from the hot feed water side to the cold permeate water side. The color represents the value of the velocity; it is seen that the flow is not in non-slip condition at the wall,

and the velocity at the middle of the tube is higher than that of near the wall. Fig. 4.7 shows the temperature difference in the tube with a 40 °C temperature difference between the feed water and the permeate water. Because the length of the micro channel is only 0.5 μm, the heat resistant is very small. The induced temperature difference between the two sides of the tube is only about 4 °C. Fig. 4.8 shows the pressure distribution in the micro channel. Because the driven temperature difference is small, the pressure difference, which drives the vapor flow through the micro channel, is also small.

In Fig. 4.9, the comparison between the experiment results and simulation results is shown. It is seen that the simulation results and the experiment results have very good agreement. This proves the accuracy of the new model.

Examining the results, it is believed that the difference in temperature is the key factor that constrains the capability of membrane distillation. Therefore, we propose to use a special material, aerogel, to improve the capability.

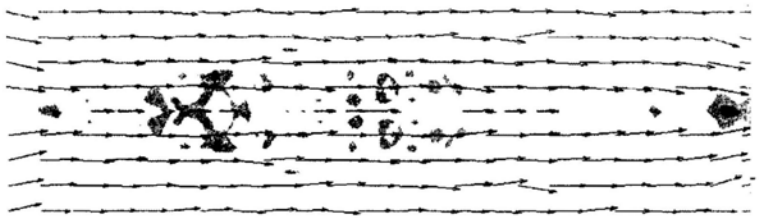

Figure 4.6: Flow field of water vapor

Figure 4.7: Temperature distribution in the micro channel

Figure 4.8: Pressure distribution in the micro channel

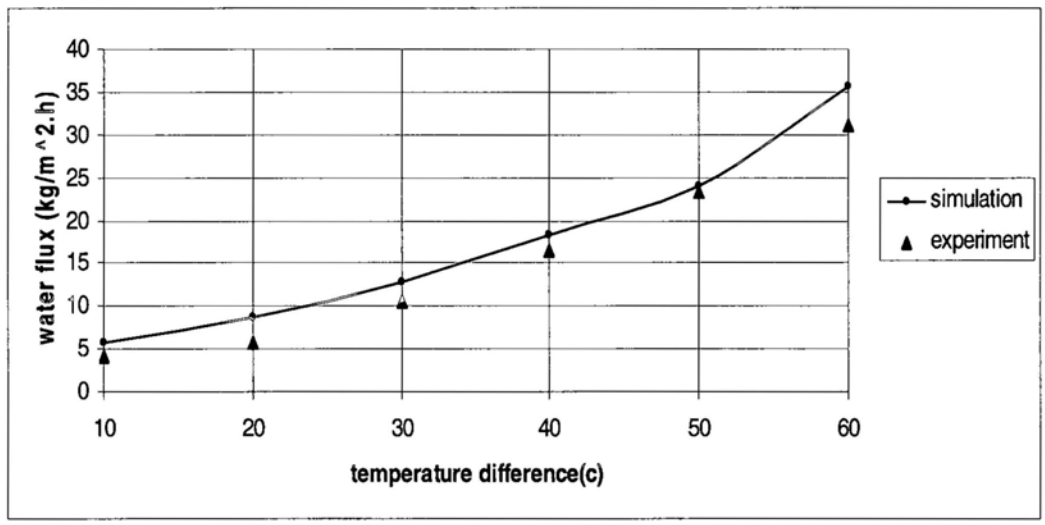

Figure 4.9: Comparison of experiment and simulation results about fresh water flux of PTFE membrane

4.4 Membrane Distillation Using Aerogel

As shown in the previous section, the PTFE membrane may result in significant heat lost and hence, reduce the efficiency of DCMD. Therefore, we propose to use a special material, aerogel, as shown in Fig. 4.10. Aerogel is a SiO_2 based porous material and has a mean pore size of dozens of nanometers. Its structure is rather empty (more than 95% void fraction). The solid phase thermal conductivity, ds, is 0.04 W/m.K, which is nearly six times smaller than that of PTFE. In this section, a comparison study on using aerogel and PTFE is given.

Figure 4.10: Aerogel

First, let us examine the case of PTFE. Fig. 4.11 shows the vapor flux against different membrane thickness. With the membrane thickness increase, the flow resistance is increased; meanwhile the temperature difference (T_{mf} -T_{mp}) is also increased. The first effect is negative to the vapor flux, while the second one is positive. From the figure it is seen that the vapor flux reaches a maximum value at the thickness of 220 μm. This is because before reaching this value the temperature difference increases a lot with the $(T_{m,f} - T_{m,p})/(T_{b,f} - T_{b,p})$ increase of the membrane thickness, after that the temperature polarization coefficient is almost equal to unity, so the vapor flux decreases with the increases of the thickness. It is also seen that higher temperature difference generates higher water flux. Fig. 4.12 shows that the temperature polarization coefficient increases as the membrane thickness increase from 0 to 300 μm and then keeps almost the same. It is also seen that lower feed temperature results in higher temperature polarization coefficient; this maybe because the thermal boundary layer of the two sides. Fig. 4.13 shows the water flux of PTFE membrane under different ΔT and pore size.

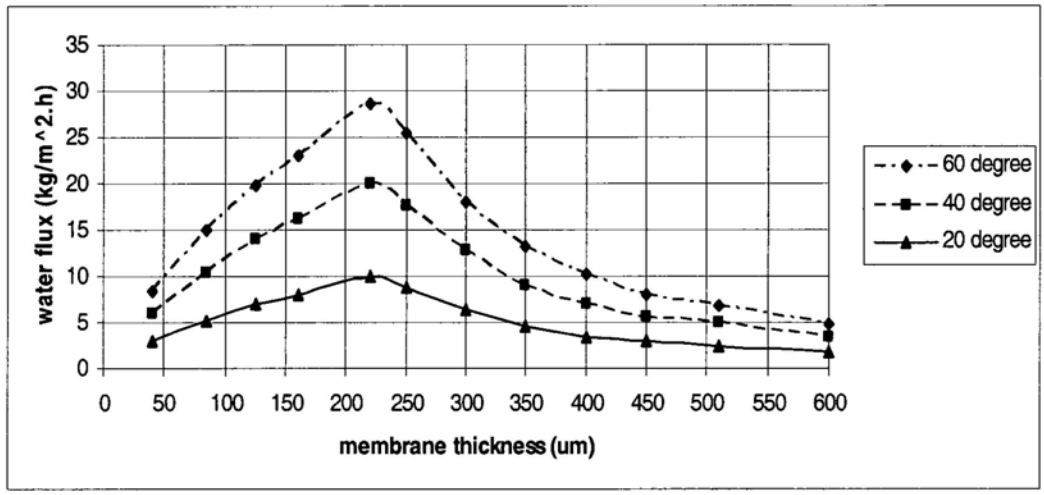

Figure 4.11: Water flux versus membrane thickness for PTFE membrane

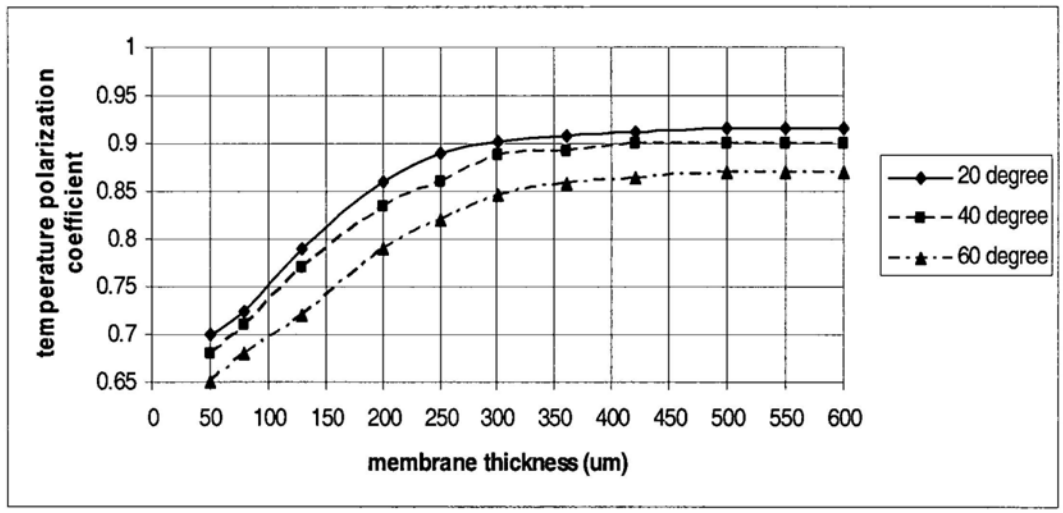

Figure 4.12: Temperature polarization coefficient versus membrane thickness for PTFE

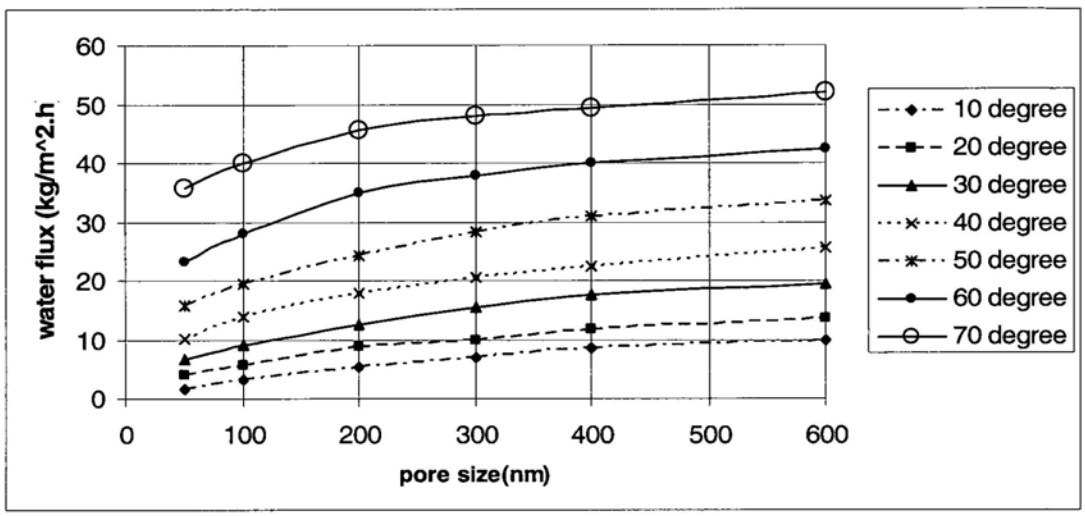

Figure 4.13: Water flux under different ΔT and pore size for PTFE membrane

Fig. 4.14 and Fig. 4.15 are the water flux and the temperature polarization coefficient when using aerogel membrane. Assume the pore size and porosity are the same with PTFE (0.2 μm and 0.75), the only difference is the thermal conductivity coefficient of solid membrane material, for aerogel it is 0.04W/m.K while for PTFE it is 0.23W/m.K. As shown in Fig. 4.14, the optimal thickness for reaching the peak water flux is now 180 μm. This is because areogel has very small thermal conductivity coefficient such that with even thinner membrane sufficient temperature difference between the feed side and the permeate side could be generated. The vapor flux is significantly higher as well.

Fig. 4.16 shows the vapor flux under different feed temperature with different pore size. Assume the porosity is 0.9 and the thickness is 200 μm. It is seen that larger channel width will result in larger vapor flux. This is because the Knudsen resistant for the flow is reduced with the channel width increase. The figure also shows that the vapor flux could be greatly increased by increasing the temperature difference. The peak value of 65 $kg/m^2 \cdot h$ is reached at 70 °C and 600 nm pore size.

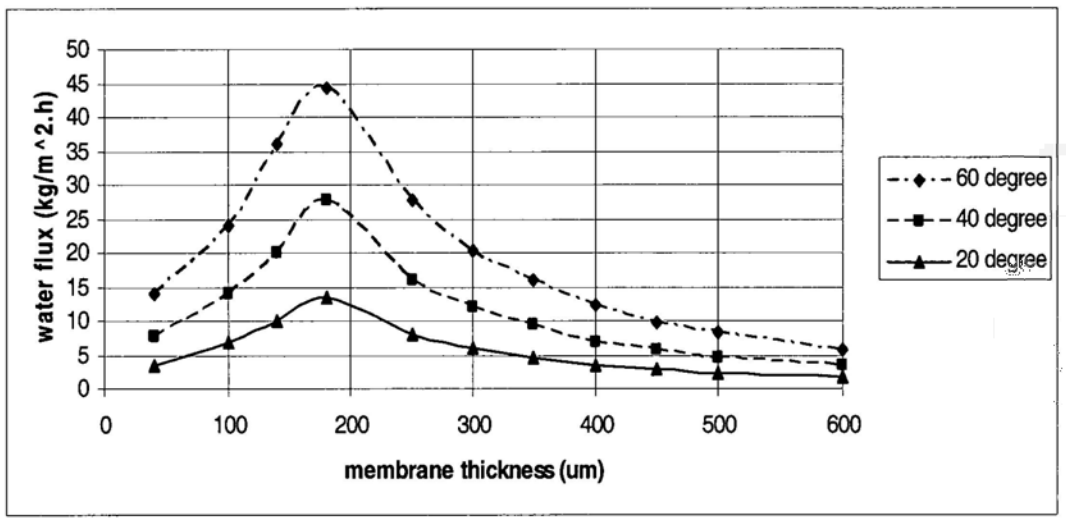

Figure 4.14: Water flux versus membrane thickness for aerogel membrane

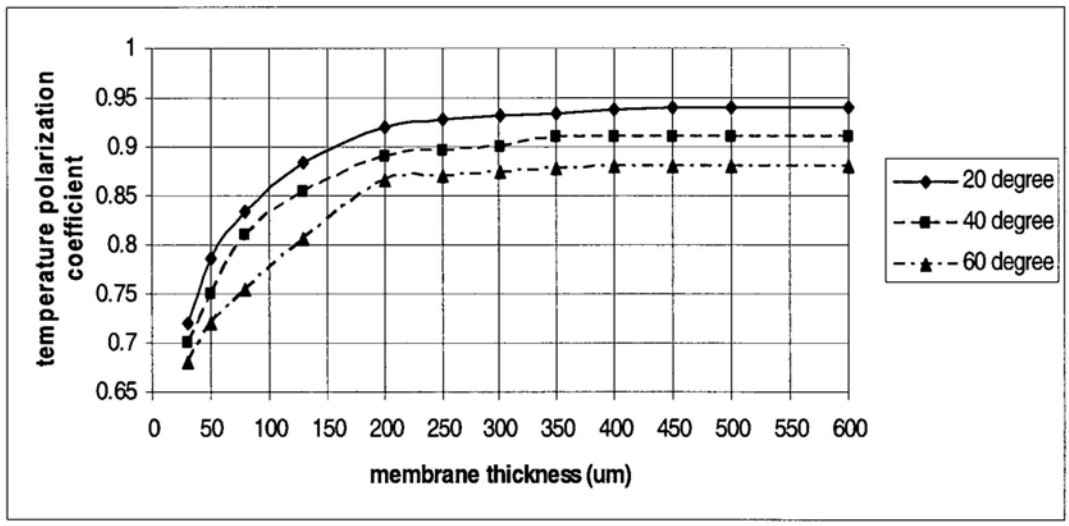

Figure 4.15: Temperature polarization coefficient versus membrane thickness for aerogel

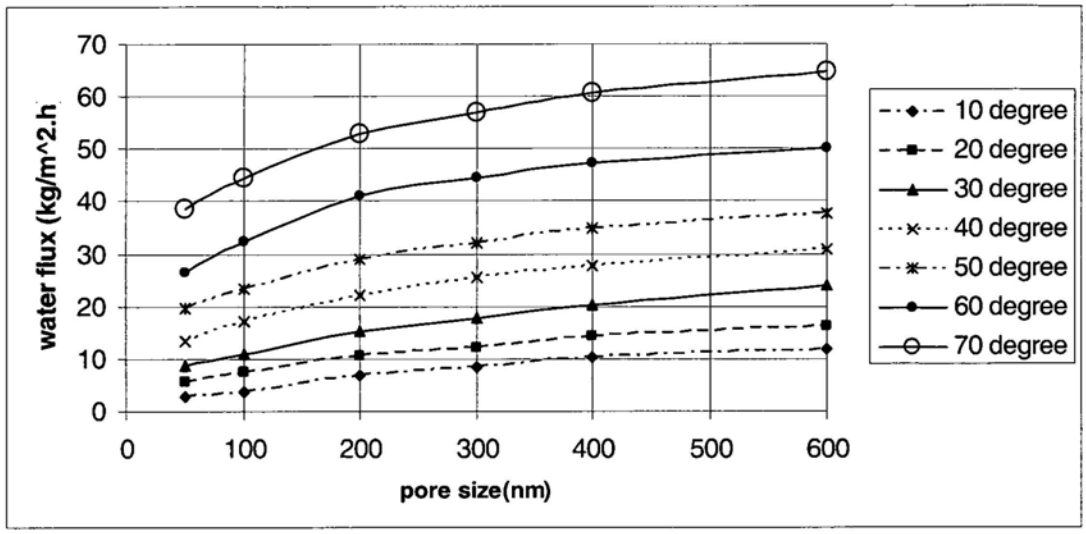

Fig. 4.16: water flux under different ΔT and pore size for aerogel

It should be mentioned that the channel width has an upper limit. The largest allowable pore size and operating conditions is governed by the Laplace (Cantor) equation:

$$P_{liquid} - P_{vapor} = \Delta P_{interface} < \Delta P_{interface} = \frac{-2E\gamma_L \cos\theta}{r_{max}} \quad (4\text{-}7)$$

where γ_L is the liquid surface tension, θ is the liquid-solid contact angle, r_{max}, is the largest pore radius, and E is a geometric factor determined by pore size. For water γ_L= 72 mN/m, θ=150 °C, the penetration pressure of a cylindrical (E = 1) pore of diameter 1 μm is only 124.7 kPa, which is just slightly greater than atmosphere pressure. To include a safety factor for long term performance, the membrane's pore size should lower than 500 nm to avoid of membrane wetting.

Fig. 4.17 and Fig. 4.18 concern the energy consumptions. When the DCMD process works at steady state, the three heat transfer should be equal (i.e. $Q_{f,conv}$ = $Q_{m,cond}$ + $Q_{m,M}$ = $Q_{p,conv}$). The total energy cost can then be calculated using Eq. (4-3). Fig. 4.17 shows the total energy cost of PTFE and aerogel at different water flux: it is obvious that higher water flux requires higher energy input. Additionally, it is seen that the aerogel's performance is much better than PTFE: for the same water flux, the

aerogel cost less total energy; in order words, for the same energy input, the aerogel produces more fresh water. Fig. 4.18 shows the energy efficiency, which is the ratio of the evaporation energy to the total energy cost, it is calculated using the following equation:

$$E = \frac{N\Delta H_v}{h_m(T_{mf} - T_{mp}) + N\Delta H_v} \tag{4-8}$$

From the figure, it is seen that higher operation temperature results in higher energy efficiency. This implies that the DCMD process shall be operated at higher temperature, say $\Delta T = 70°C$. Moreover, the advantages of aerogel is significant, it has much higher energy efficiency. This is due to its low thermal conductivity, because of which less energy is consumed.

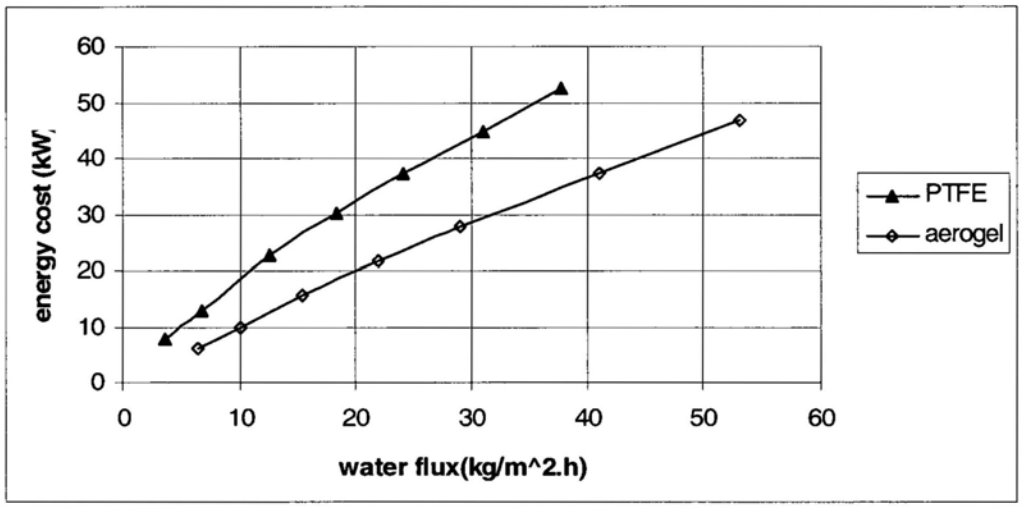

Fig. 4.17: Total energy cost versus water flux

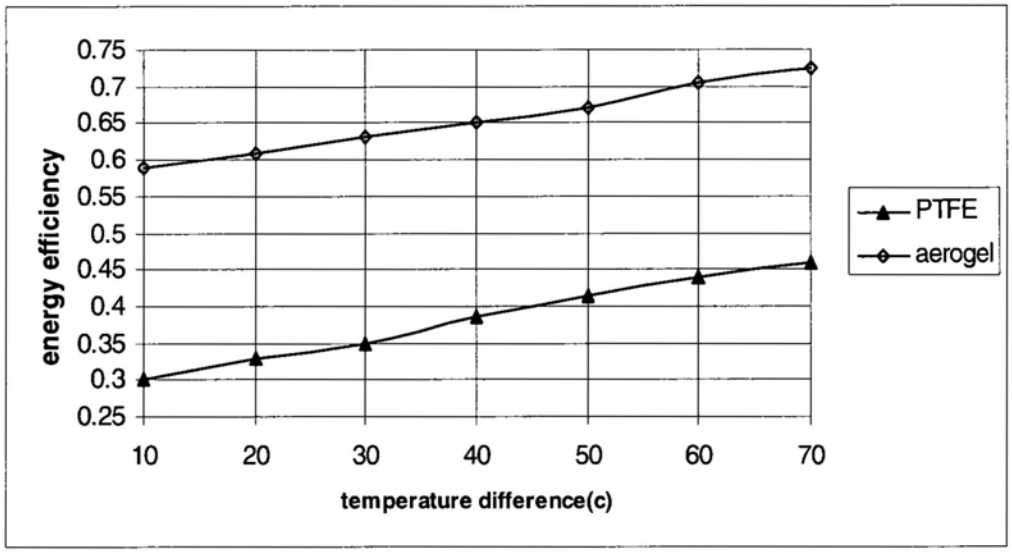

Fig. 4.18: Energy efficiency

Last but not the least, one may concern that 45 kW for 50 kg/h is still an energy thirsty process. This is because the thermal separation requires a large amount of latent heat. In fact, to evaporate 50 kg / h of water requires at least 30 kW alone. However, this process can be driven by low quality and renewable energy, say solar energy or waste heat. For a typical summer day, the average solar energy is 750W/m^2 for 12 hours. To get higher energy efficiency, we can control the system working at temperature difference of 70°C. For an aerogel membrane with 200 nm pore size and 200 μm thickness, the water flux is 53 kg/m^2h and total energy cost is 48 kW. In this condition, the required membrane area is 0.75kW/48kW*1m^2 = 0.0156 m^2, the productivity is 0.0156m^2*53 kg/m^2h =0.83 kg/h for 1m^2 solar collector area, the daily productivity is 10.0 kg.

4.5 Conclusions

This chapter presents a study on using DSMC for modeling the mass transfer process in DCMD process. The performance of using aerogel as DCMD's membrane is also investigated. Based on the discussions above, following conclusions can be drawn as follows:

(1) DSMC method is effective for modeling the mass transport process in DCMD. It avoids the oversimplification of the vapor transport

resistance mechanism, and gives good estimation. In addition, the model helps us to better understand the mechanisms of DCMD.

(2) Aerogel is a desirable material for DCMD process. It high hydrophobic property (contact angle is 150° for water), very low heat conductivity (0.04W/m.K) and high porosity (0.9) offer a much better performance over the conventional PTFE material.

(3) Based on the simulation, the water flux for 1 m^2 membrane area is about 53 kg/h. As a result, in a typical tropic day, the daily distillated water productivity is 10.0 kg/day for 1 m^2 solar collector area.

Chapter 5

A New Energy Harvesting Method Based on Knudsen Compressor

5.1 Introduction

As stated in chapter 2, for collecting renewable thermal energy such like solar energy and waste heat, various kinds of technologies are proposed and studied. Conventional technologies like solar power plants and solar-geothermal generator have achieved some success. But they are usually large scale, complex, requires experienced worker and high cost. Some new small scale new technologies are also proposed. Woo and Lee [2003] examined the thermoelectric generation which is a direct energy conversion method from heat to electricity. It could use the thermal energy below 423 K. Sebald et al. [2008] proposed a micro generator which harvests energy from the temperature difference using ferroelectric materials. Generally speaking, the conversion efficiency of this method is rather low. According to Yamashta et al. [2007], the latest thermoelectric generator's conversion efficiency is only 0.27%. Another problem is the necessity of a large temperature gradient [Minaev and Fursenko, 2007].

It is therefore the purpose of this chapter to investigate a new energy harvest method. It bases on the Knudsen effect which is first discovered by a Danish physicist Knudsen [1910]. The Knudsen effect describes the temperature difference between two chambers would generate a gas flow. This effect results in a micro-scale gas pump called Knudsen compressor. In this chapter, we first brief introduce the theory about Knudsen compressor. Then derive the mathematical model of Knudsen compressor working near atmosphere pressure in section 2. In section 3, we study the micro flow cases in Knudsen compressor by Direct Simulation Monte Carlo (DSMC) method, and then analyze the performance. Based on the simulation results, the integrate design is proposed in section 5.

5.2 Knudsen Compressor

The key component of our energy harvesting method is Knudsen Compressor. It is a solid state pump based on the gas kinetic phenomena of thermal creep, requires no moving parts or supplementary pumping fluids [Vargo, 2000]. About 100 years ago Knudsen [1910] demonstrated a compression ratio of ten using a series of alternately heated and cooled tubes which each contained a small diameter constriction. More recently a group from University of Southern California got several progresses on the analysis and fabrication of Knudsen compressor [Vargo et al.,1999; Vargo and Muntz, 2000; Muntz et al., 2002]. They want to use Knudsen compressor as a vacuum pump to cooperate with micro mass spectrometer system. So they want to demonstrate the Knudsen compressor's capability of efficiently operating at several Torr or even millitorr. Vargo et al. [1999] built a micro vacuum pump delivering 5×10^{14} molecules per second with a pump volume of 0.16mL at inlet pressure of 10mTorr and power input of 28.5mW.

5.2.1 Thermal creep

It is possible to start rarefied gas flows due to tangential temperature gradients along the channel wall, where the fluid starts creeping in the direction from cold towards hot. This is the so-called thermal creep or thermal transpiration. Thermal creep or thermal transpiration identifies the fundamental flow physics that governs the operation of Knudsen compressor. It was first explained by Reynolds [1879].

Thermal creep is illustrated in Fig. 5.1. As a simple physical example, consider two chambers divided by a thin aperture, they have the same pressure $P_1 = P_2$, but at different temperatures $T_1>T_2$. If the two chambers are connected with a relatively thick aperture area ($\lambda << \sqrt{A_a}$), where λ is the mean free path of the gas, equilibrium condition requires no-flow in the channel. If the aperture area A_a becomes comparable to the mean free path (λ), rarefied gas effects have to be taken into account. In such a case, the local equilibrium mechanism is very complex and interaction of the gas molecules with the walls must also be considered. Here we consider free-molecular flow (i.e. $\lambda >> \sqrt{A_a}$) to simplify the discussion. In this flow regime, the intermolecular collisions are negligible compared to the interaction of

molecules with the surfaces. If we assume that molecule-wall interactions are specular, then the following analysis is valid. Assuming that the density of the fluid is proportional to the number density n (n is defined as $p/(k_B T)$, k_B is the Boltzmann's constant, and T is the gas temperature, p is the gas pressure)

$$\rho \propto n,$$

and the temperature of the fluid is proportional to the square of average molecular speed

$$T \propto \overline{U}^2$$

($\overline{U}^2$ is given by $\sqrt{8k_B T/(\pi m)}$).

The mass fluxes at the hot and the cold end of the channel are $mn_1\overline{U_1}^2$ and $mn_2\overline{U_2}^2$ respectively; here m is the mass of the gas molecules. Then

$$\frac{mn_1\overline{U_1}^2}{mn_2\overline{U_2}^2} \approx \frac{\rho_1}{\rho_2}\left(\frac{T_1}{T_2}\right)^{0.5} = \frac{P_1}{P_2}\left(\frac{T_1}{T_2}\right)^{0.5} = \left(\frac{T_1}{T_2}\right)^{0.5} \leq 1 \quad (5\text{-}1)$$

where we have used the equation of state $P = \rho RT$ and $\frac{P_1}{P_2} = 1$.

The above analysis indicates a **flow creeping from cold to hot**.

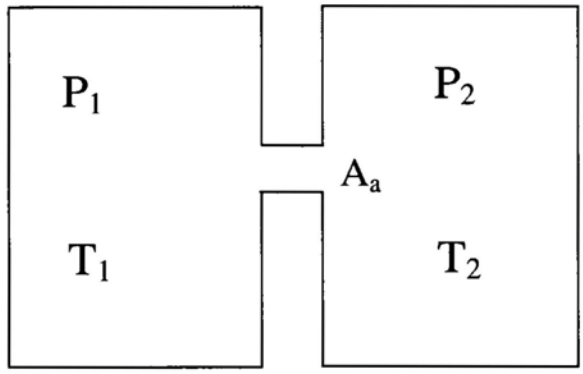

Figure 5.1: Elementary single stage of a thermal creep

At steady state, the number of molecules flow from cold to hot minus the flow from hot to cold is

$$n_1 \overline{U_1}^2 A_a - n_2 \overline{U_2}^2 A_a = N \tag{5-2}$$

For $N = 0$, the pressure ratio P_1/P_2 becomes

$$\frac{P_1}{P_2} = \sqrt{\frac{T_1}{T_2}} \tag{5-3}$$

For $P_1 = P_2$, the net flow of molecules from cold to hot is

$$N = A_a \frac{1}{\sqrt{2\pi m k_B}} P_2 [T_2 \sqrt{T_1} - T_1 \sqrt{T_2}]/(T_1 T_2) \tag{5-4}$$

Hence, for P_1 between P_2 and $P_2\sqrt{T_1/T_2}$, there will be both a pressure increase and a net flow, which are the requirements for a pump.

Real gas flow in channel is not collisionless, for the channel's characteristic dimension $\sqrt{A_a}$ is comparable to the mean free path λ, the flow is transitional rarefied flows, primarily along walls with a superimposed wall surface temperature gradient. Substantially diffuse and thermally accommodated reflections are required at the surface for thermal creep to be significant. The thermal creep effect is illustrated for transitional flow in Fig. 5.2.

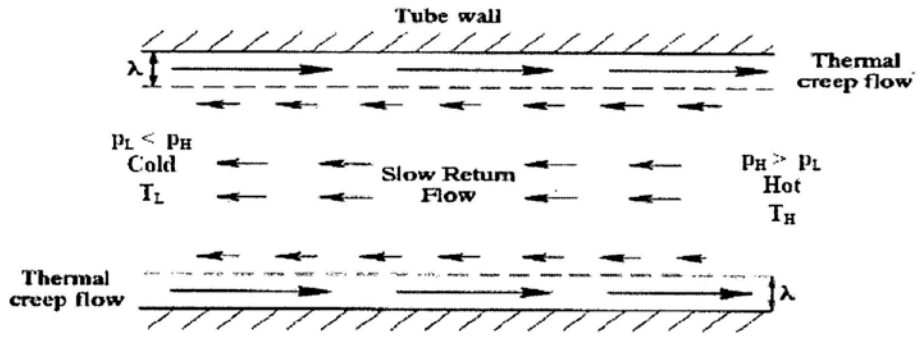

Figure 5.2: Illustration of transitional net flow Muntz and Vargo, 2002

As indicated in Fig. 5.2, thermal creep flow is driven from the cold end of a tube towards the hot end of the tube. For free molecular flow, thermal creep flow will fill the entire tube, becoming thermal transpiration. In the case of transitional flow, the thermal creep occurs closer to the tube's walls. As a pressure difference is established a pressure return flow will occur, partially or completely balancing the thermal creep flow. Thus, thermal creep can also produce a net gas flow and a pressure difference, which again are the requirements for a pump. Sone and Aoki [1996] used DSMC to carry out the numerical simulation of this phenomenon. The simulation demonstrates that there are two different transient processes before the flow reaches the steady state show in Fig. 5.2. Karniadiskis and Beskok [2002] proposed an experiment in his book to examine the importance of thermal creep effect in micro channel flows.

5.2.2 Theory of Knudsen compressor

A Knudsen compressor generates large changes in pressure by utilizing a cascade of multiple stages. A single stage of Knudsen compressor is illustrated in Fig. 5.3. Each stage consists of an array of capillaries and a connector section. The temperature increase imposed along the capillary pumps the gas from cold toward the hot direction, resulting in pressure increase in the capillary section. The gas is cooled in the connector section and thus the temperature drops to the value corresponding to the inlet of the capillary section.

Pham-Van-Diep et al. [1995] had assumed free molecule flow in both capillary section and connector section and got the formula of pressure ratio and mass flow rate. Parameters of the Knudsen compressor could be got based on the model, but it is not enough to analysis our application. Since the working pressure is about atmosphere pressure, the mean free path λ can be got by

$$\lambda = \frac{k_B T}{P\sqrt{2}\pi\sigma^2} \tag{5-5}$$

where T is the absolute temperature (K), P is the total pressure (Pa) and σ the collision diameter (m).

For atmosphere pressure, room temperature and air molecule, $\lambda \approx 6.5\times10^{-8} m$. Current membrane materials could give smaller capillary size at about 20nm, so the Kn is about 0.3, based on the classification of flow regime in the chapter 2, the flow

in the capillary section is transitional flow and in the connector section should be continuum flow. A stage analysis based on the transitional flow is necessary.

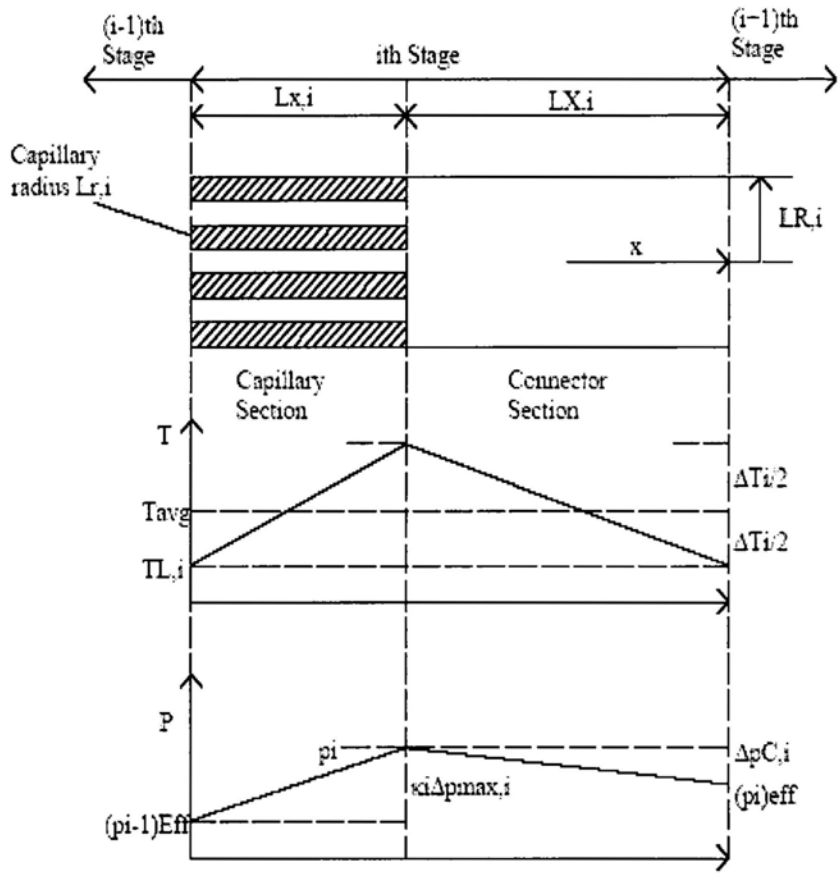

Figure 5.3: Illustrative one stage of a Knudsen Compressor[Vargo, 2000]

For transitional flow through infinite circular capillary tubes, Sone et al. [1989, 1990] had derived a model from linearized Boltzmann's. The model is capable for describe the capillary membrane section of the Knudsen compressor. Consider a stage "i" in a Knudsen compressor cascade show in Fig. 5.3. It connects to the next lower stage at the low-temperature ($T_{L,i}$) end of the capillary section where the pressure is the exit pressure of the $(i-1)^{th}$ stage, $(p_{i-1})_{EFF}$. The high-temperature ($T_{H,i}$) end of the capillary section connects to the $(i+1)^{th}$ stage through the i^{th} stage's connector, where the temperature adjusts from $T_{H,i}$ to $T_{L,i+1}$.

Following Sone and Itakura [1990], the mass flow through an infinite capillary channel subject to small gradients in temperature and pressure can be written as

$$M = P_{AVG}[2(k_B/m)T_{AVG}]^{-1/2} A \times (\frac{L_r}{T_{AVG}} \frac{dT}{dx} Q_T - \frac{L_r}{P_{AVG}} \frac{dp}{dx} Q_P) \quad (5\text{-}6)$$

where, Q_T and Q_P are thermal driven flow coefficient and pressure driven return flow coefficient respectively, they are functions of Kn based on a characteristic dimension L_r of the capillary,. The capillary's cross-sectional area is A.

For a finite capillary tube, rewrite Eq. (3-6) in terms of the temperature difference ΔT_i as

$$M_i = P_{AVG}[2(k_B/m)T_{AVG}]^{-1/2} F_i A_i \times (\frac{L_{r,i}}{L_{x,i}} \frac{\Delta T}{T_{AVG}} Q_{T,i} - \frac{L_{r,i}}{L_{x,i}} \frac{\Delta p_i}{P_{AVG}} Q_{P,i}) \quad (5\text{-}7)$$

where F_i is the fraction of the compressors inlet area A_i that is occupied by the capillaries. It is assumed that

$$T_{AVG} = T_{L,i} + \frac{\Delta T_i}{2} = T_{H,i} - \frac{\Delta T_i}{2} \quad (5\text{-}8)$$

where, ΔT_i is the temperature difference applied to the capillaries in the ith stage. Also,

$$p_{AVG} = (p_{i-1})_{EFF} + \frac{\Delta p_i}{2} \quad (5\text{-}9)$$

and,

$$\frac{\Delta p_i}{p_{AVG,i}} = \frac{[p_i - (p_{i-1})_{EFF}]}{p_{AVG,i}} = \frac{\kappa_i \Delta p_{\max,i}}{p_{AVG,\max,i}} \quad (5\text{-}10)$$

where, κ_i ranges between 0 (maximum upflow, which is when there is no pressure increase) and 1 (zero upflow with maximum pressure increase).

In order to find $\Delta p_{\max,i}$ it is necessary to set the mass flow equal to zero in Eq. (3-7). Assuming $T_{AVG,i} = T_{AVG}$, independent of stage,

$$\frac{\Delta p_{\max,i}}{p_{AVG,\max,i}} = \frac{\Delta T_i}{T_{AVG}} \frac{Q_{T,i}}{Q_{P,i}} \quad (5\text{-}11)$$

To give a quantitative feel for the two competing flows, a plot of Q_T / Q_P is presented in Fig. 5.4. The result is given Sone and Itakura [1990]. Note that for a circular tube the ratio Q_T / Q_P varies from close to 0.5 at large Kn (free-molecule ratio) to 0.006 at $Kn = 0.056$. It is evident that the operation of the Knudsen compressor will change dramatically in the transitional flow regime.

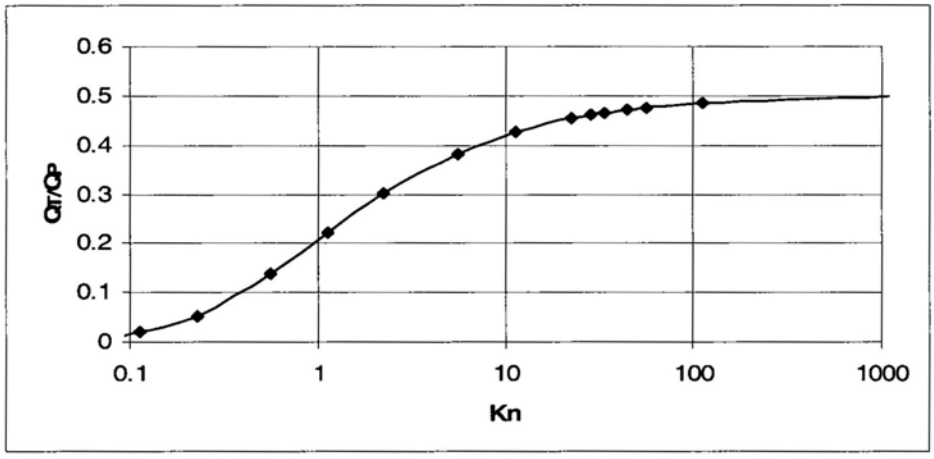

Figure 5.4: Q_T/Q_P as function of Kn given Sone and Itakura [1990].

For Knudsen compressor working under low pressure, the flow in connector segment is also transitional flow. So it is important to couple the connector section to the capillary section. But in our case, the gas flow in connector section is continuum flow $Kn_{C,i} << 1.$, it means there is no need to consider the thermal transpiration effect in this section. The gas temperature drops to the low temperature but no pressure drop induced by the temperature gradients. So for the entire stage, Eq. (5-7) to Eq. (5-11) are also available.

Based on the above Equations, detail analytical expression for the pressure increase, mass flow rate and energy consumption are developed

From Eq. (5-10) and Eq. (5-11), pressure ratio produced by ith stage is

$$P_i = \frac{(p_{i-1})_{EFF} + (\Delta p_i)_T}{(p_{i-1})_{EFF}} = 1 + \kappa_i \frac{|\Delta T_i|}{T_{AVG}} \frac{Q_{T,i}}{Q_{P,i}} \frac{p_{AVG,i}}{(p_{i-1})_{EFF}} \qquad (5\text{-}12)$$

$$\frac{p_{AVG,i}}{(p_{i-1})_{EFF}} = [1 + (\kappa_i / 2)(\frac{|\Delta T_i|}{T_{AVG}})(\frac{Q_{T,i}}{Q_{P,i}})] \tag{5-13}$$

Consider a block of N stages where $|\Delta T_i| = |\Delta T|_B$, the appropriate form of Eq. (5-12) is

$$P_i = 1 + \kappa_i \frac{|\Delta T|_B}{T_{AVG}} \frac{Q_{T,i}}{Q_{P,i}} \frac{p_{AVG,i}}{(p_{i-1})_{EFF}} \tag{5-14}$$

The pressure ratio obtained by a cascade of N stages is

$$\wp_N = \prod_{i=1}^{N} P_i = \prod_{i=1}^{N} \{1 + \kappa_i \frac{|\Delta T|_B}{T_{AVG}} \frac{Q_{T,i}}{Q_{P,i}})[1 + (\kappa_i / 2)(\frac{|\Delta T|_B}{T_{AVG}})(\frac{Q_{T,i}}{Q_{P,i}})]\} \tag{5-15}$$

Substituting Eq. (5-10) and Eq. (5-11) to Eq. (5-7), the mass flow rate $\dot{M}$ is then,

$$M_i = \frac{p_{AVG} F_B A_i [2(k_B / m) T_{AVG}]^{-1/2}}{(L_x / L_r)_i} \frac{\Delta T_B}{T_{AVG}} Q_{Ti}(1 - \kappa_i) \tag{5-16}$$

The energy consumption is an important. For the i[th] stage the heat transfer in the x direction through the capillary sections can be written as

$$E_i = \frac{|\Delta T|}{L_{x,i}} d_i A_i (1 - \varepsilon_i) \tag{5-17}$$

Here, d_i is the thermal conductivity of the material forming the capillaries and ε_i is the fractional area occupied by air.

The total energy use in a cascade block of N stages is thus

$$E_N = \sum_{i=1}^{N} \{\frac{|\Delta T|}{L_{x,i}} d_i A_i (1 - \varepsilon_i)\} \tag{5-18}$$

The capillary section's area A_i is

$$A_i = \frac{2\Omega (T_{AVG} / m k_B)^{1/2} Kn_i L_{ri}}{Q_{T,i}(\Delta T_B)\varepsilon_B (1 - \kappa_i)} M_{DES} \tag{5-19}$$

where Ω is a viscosity derived collision cross section for the gas that is being pumped. Choose $Kn_i = Kn_B$, this would be accomplished by reducing the characteristic capillary dimension $L_{r,i}$. With Eq. (5-18) and Eq. (5-19), the

relationship between energy consumption and mass flowrate is given as

$$\frac{E_N}{M_{DES}} = 2\Omega d_B \frac{1-\varepsilon_B}{\varepsilon_B}(T_{AVG}/mk_B)^{1/2}\frac{Kn_B}{Q_{T,B}}A_i \times \sum_{i=1}^{N}[(1-\kappa_i)^{-1}] \quad (5\text{-}20)$$

With the above developed model, the performance of a multi stages Knudsen compressor will be investigated in section 5.3.

5.3 Simulations & Discussions

To investigate the performance of the capillary section and verify our theoretical analysis, a series of simulation is carried out by using DSMC method. The simulation model is a 2D channel with 5μm length and 1μm height as shown in Fig. 5.5. The simulation domain contains only half of the channel because of symmetry, this will save the computational resources. The schematic grid was shown in Fig. 5.5, 110 grids are set in x direction and 20 grids are set in y direction, there are totally 2200 rectangular cells in the computation domain. The average number of simulated molecules per cell is 30. Then the total number of simulated molecules in the domain is about 66000. There is a temperature difference of 200K between the two ends and it is linear distributed on the channel wall. It is assumed the initial temperature of gas is thermal equilibrium with the wall temperature. Working pressure varies for different simulation case. One simulation case takes about 2 hour computational time on a 2.8GHz Pentium 4 PC with 1G ram.

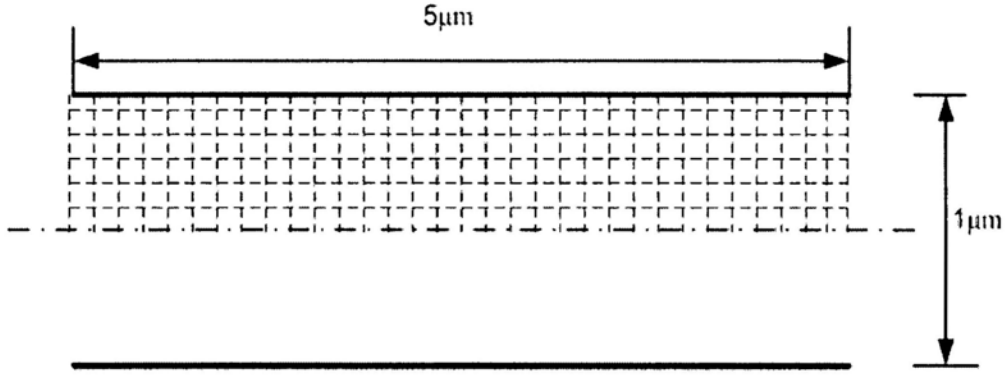

Figure 5.5: Micro channel of Capillary section

Fig. 5.6 and Fig. 5.7 show the temperature distribution and flow field in the channel of two typical cases. In Fig. 5.6, Kn = 0.05, we can see the gas at the middle of the channel flows from the hot end to the cold end. It is thermal transpiration with pressure driven back flow. In Fig. 5.7, Kn = 50, the gas flows for cold end to the hot end in the whole channel. This is because the whole channel is in free molecule flow regime. Compared these two Figures, we found the Knudsen number is very important to the flow pattern in micro channel. With low Knudsen number, the pressure driven flow is stronger than the thermal driven flow. When the Knudsen number increases, the thermal creep effect becomes more significant, so the thermal driven flow may dominates the flow in the channel. This reminds us there must be a critical Knudsen number which we can get a maximum mass flow. More simulations of different Knudsen numbers are presented in Fig. 5.8.

From Fig. 5.8, we found the maximum mass flow happens at Kn about 5, which corresponds to P = 0.01 atm with the 1 μm channel. This is because the mass flow rate relates to both gas velocity and density. In my simulation the channel's dimension is fixed, different Knudsen number is induced by different pressure. For high Knudsen number, the gas velocity is high but at the mean time the gas density is low caused by the low pressure. The trade-off between velocity and density makes the maximum mass flow happen. This is the optimal condition that balances the trade-off between flow velocity and gas density. This simulation result provides the foundation for us to design and choosing working parameters of a Knudsen compressor.

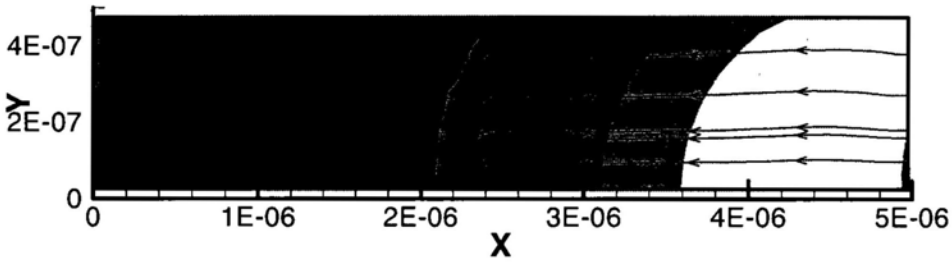

Figure 5.6: Temperature and Flow Field, Kn = 0.05

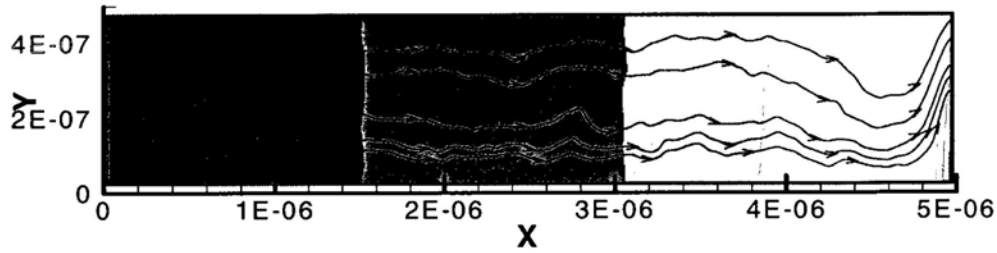

Figure 5.7: Temperature and Flow Field, Kn = 50

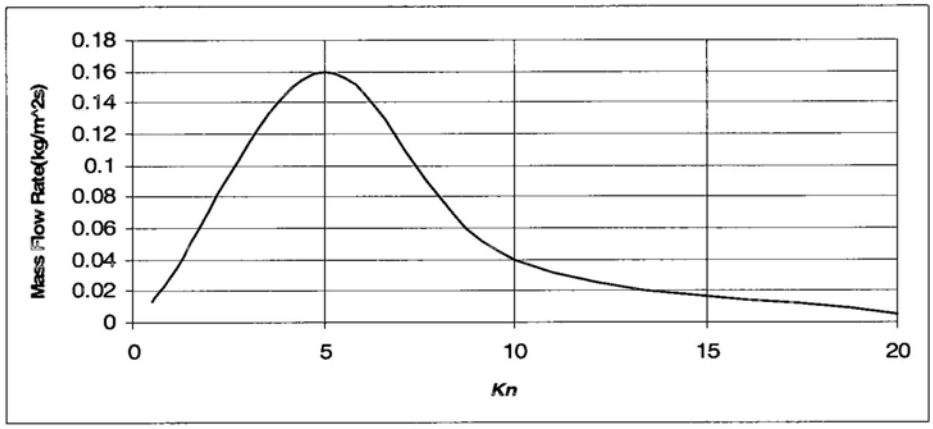

Figure 5.8: Mass flow rate against different Knudsen number

Temperature difference is the driven force of the Knudsen compressor, and the purpose of this method is harvesting the thermal energy. Therefore we need to study how the temperatures difference influence on pressure ratio. For one stage Knudsen compressor, in the model in section 5.2, we set $\kappa_i = 0.5$, inlet Knudsen number Kn_{in}=3.2, Q_T/Q_P is got from Fig. 5.4. Using Eq. (5-14), we got the plot of one stages pressure ratio. Fig. 5.9 shows that the pressure ratio increases fast with ΔT before ΔT = 300K, after that the increasing tendency is slow down. Consider of the difficulty to generate very high ΔT from solar radiation, we set the temperature ΔT = 200K in our design and following analysis.

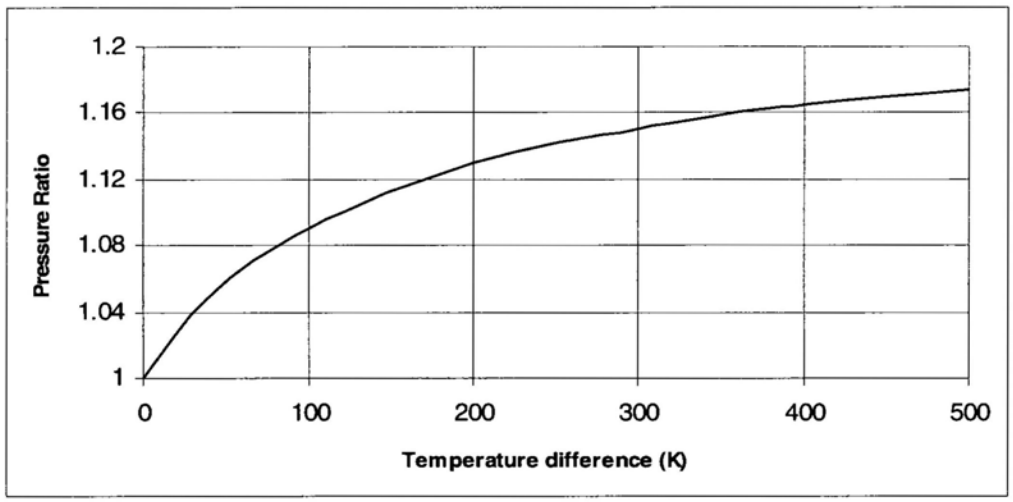

Figure 5.9: Pressure ratio against the temperature difference

With Eq. (5-14) and Fig. 5.4, we can also get the plot of one stage's pressure ratio against Kn. In Eq. (3-14), $\kappa_i = 0.5$, $\Delta T = 200\text{K}$ and $T_{\text{AVG}} = 400\text{K}$. In Fig. 5.10 we found that before $Kn \approx 5$, the pressure ratio increases dramatically with Kn. After $Kn \approx 10$ the pressure increases very little. For a given channel size, the Kn is corresponding with pressure, and the result in Fig. 5.10 means very high vacuum degree is useless for achieving high pressure ratio.

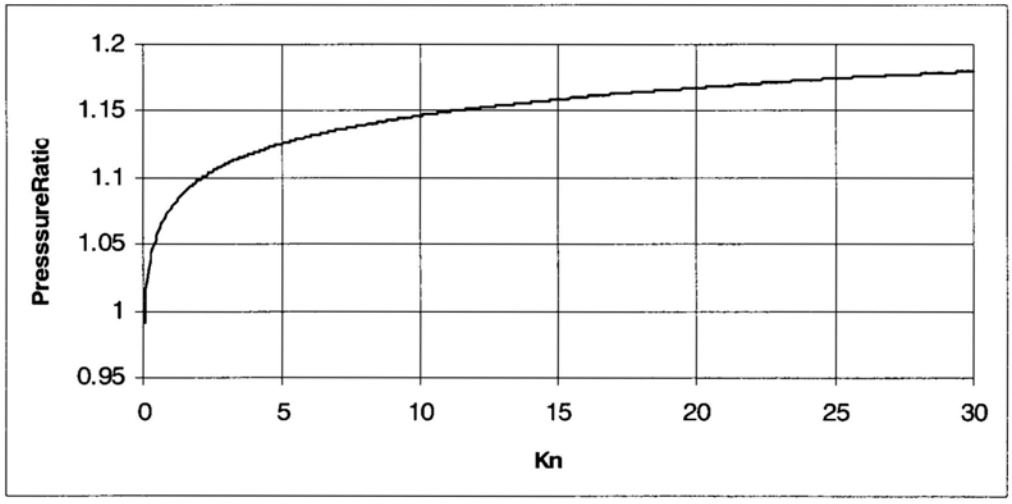

Figure 5.10: Pressure ratio of single stage against the Kn

For a multi-stages Knudsen compressor, the pressure ratio for each stage is different. The relationship between total pressure ratio and total number of stages, N, is important for design a Knudsen compressor. We set inlet Knudsen number Kn_{in} = 3.2, $\kappa_i = 0.5$, ΔT = 200K and T_{AVG} = 400 K, using Eq. (5-15), we got the plot of total pressure ratio against number of stages as shown in Fig. 5.11. It is seen that the pressure ratio increases fast with number of stages before N = 12, after that the trend of increasing slows down. This is because with the pressure increasing along with the multi-stages Knudsen compressor, the Kn is then decreasing, after several stages the Kn becomes quite small, the thermal driven effect is thus less significant in the capillary channel. Fig. 5.11 implies that with a constant capillary channel size of 20 nm and inlet pressure of 1 atm, the maximum total pressure ratio is about 12, which can be reached at stages number N = 20.

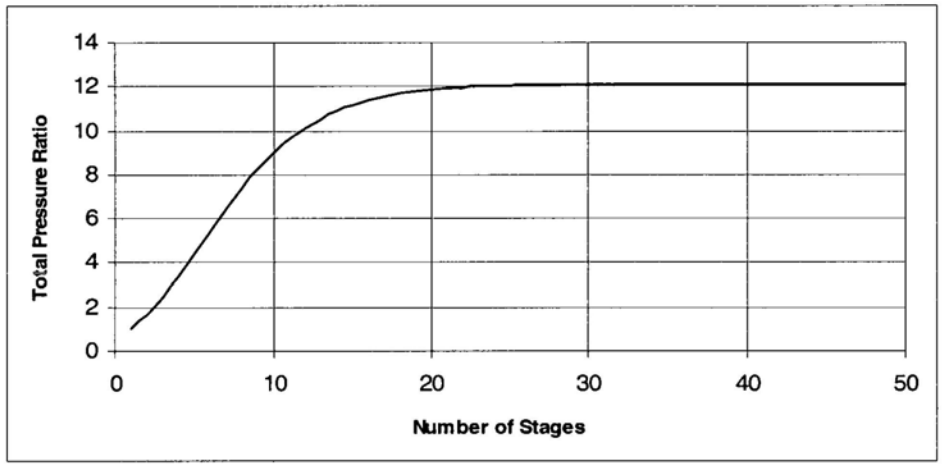

Figure 5.11: Pressure ratio against the Number of Stages

5.4 Design of Our Energy Harvesting Device

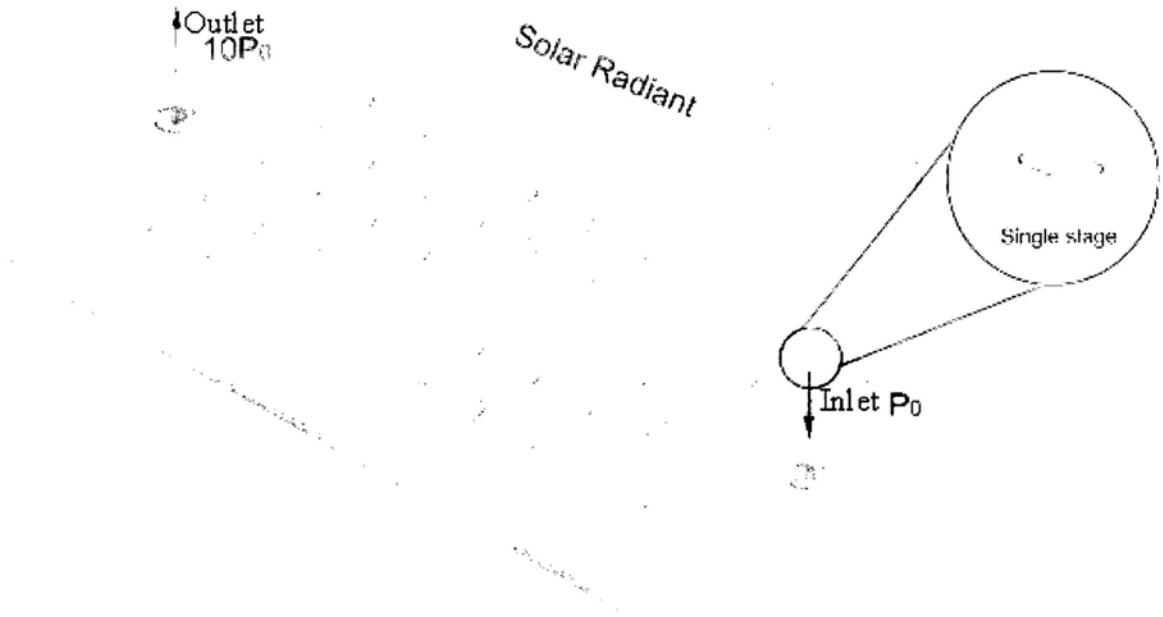

Figure 5.12: Design of the multi-stages energy harvesting device

With the analysis above, we can then design a device based on Knudsen compressor to harvest thermal energy. The design of our prototype energy harvesting device is shown in Fig. 5.12. The base compact device is multi stages structure. One side is heated by the solar radiant, and then the temperature gradient is generated. The inlet is open to the atmosphere, the thermal induced air exit at the outlet with a high pressure and velocity. The size of one unit is 46mm×22mm×28mm, so within a 1m×1m area, we can set about 1000 units. Based on the result in pervious section, here we arrange 16 units in series connection to generate pressure ratio while 42 series in parallel connection to achieve enough mass flow rate.

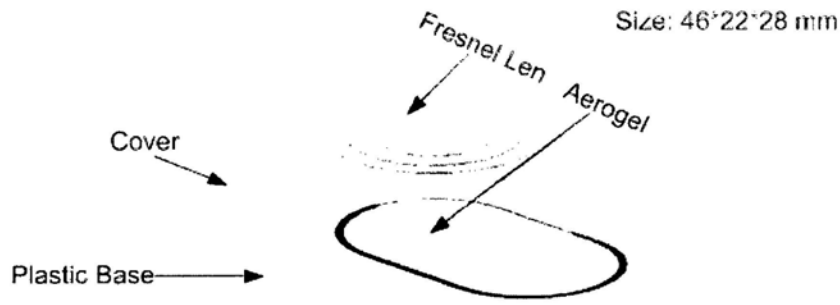

Figure 5.13: One Unit of the multi-stages device

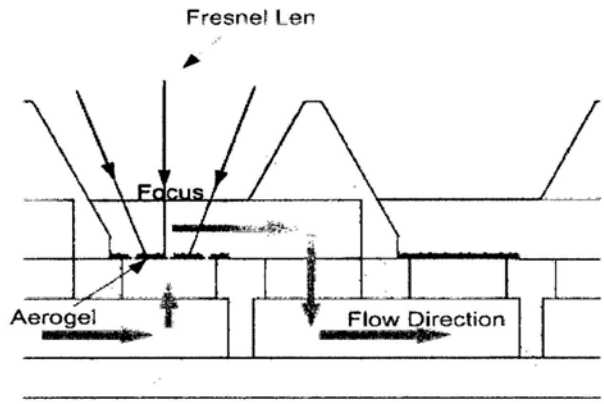

Figure 5.14: Cross-section of one unit

Fig. 5.13 and Fig. 5.14 show the single unit and the cross section. Aerogel is filled in the hole with 8 mm diameter, and 1mm thickness. Fresnel lens is integrated with the Plexiglas cover to focus the light source on the small area of aerogel. Torr Seal epoxy could be used to seal the sides of the aerogel and bond the aerogel transpiration membrane to an aluminum thermal guard. The thermal guard is kept in thermal contact with the pump body to maintain the low temperature side of the membrane and the stage inlet gas close to ambient temperature.

A Fresnel lens (see Fig. 5.15) is a type of lens invented by French physicist Augustin-Jean Fresnel. Originally developed for lighthouses, the design enables the construction of lenses of large aperture and short focal length without the weight and

volume of material which would be required in conventional lens design. Compared to earlier lenses, the Fresnel lens is much thinner, thus passing more light and allowing lighthouses to be visible over much longer distances.

The use of an aerogel membrane is great important to the performance of Knudsen compressor. Aerogels are a special class of continuously porous solid materials (see Fig. 5.16). characterized by nanometer size particles and pores. It's rather empty structure (see Fig. 5.17) results in a very low thermal conductivity (17mW/mK at 760 Torr). Particles of diameters 2-5nm and pores of diameters 10-100nm, produce a solid-gas matrix in which the volume fraction of the solid can be less than 5%. The pore size of the aerogel has a mean pore size of 20nm, and this gives $Kn = 6.4$ for air at 760 Torr.

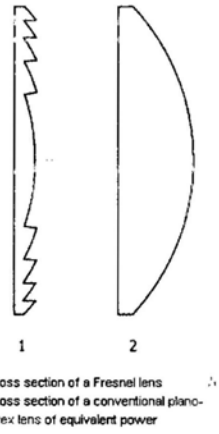

Figure 5.15: Cross-section of Fresnel lens and conventional lens

Figure 5.16: Aerogel material

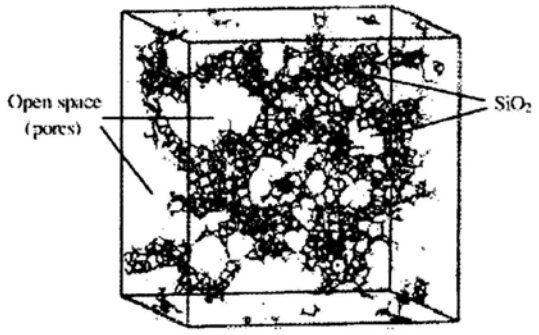

Figure 5.17: Schematic description of aerogel's structure[Hua et al. [1995]]

Finally, the performance the device is estimated based on the models in section 5.2 and results in section 5.4. The working gas is air. The temperature of focused solar light could reach high temperature as 150°C. So I assume the temperature difference $\Delta T = 150K$ of the capillary section. The aerogel gives $Kn_{in} = 6.4$ for air at 760 Torr. From Eq. (5-15), the total pressure ratio for 16 stages is 11 which means the output pressure is 11 atm. The mass flow can be calculated from Eq. (5-16), for 42 series the mass flow rate is 0.001 kg/s.

Then the condition of output gas is P_1 = 11 atm, T_1 = 300K, and mass flow $\dot{M} = 0.001kg/s$. The density $\rho = P/RT = 11\times101325/(287\times300) = 12.95kg/m^3$. The velocity is $v_1 = \dot{M}/\rho A = 1.5m/s$. Assuming such an amount of air pass through a turbine under an isentropic process, and the pressure changes to P_2 = 4 atm, the velocity changes to v_2 = 1 m/s, the output work can be calculated by

$$w = -\int_1^2 vdP - \Delta ke \tag{5-21}$$

where *ke* is kinetic energy. For is entropic process,

$$Pv^k = const \tag{5-22}$$

where $k=C_p/C_v$ (for air k = 1.4), then the output work is

$$w = -\frac{kRT_1}{k-1}[(\frac{P_2}{P_1})^{(k-1)/k} - 1] - (\frac{v_2^2 - v_1^2}{2})$$
$$= \frac{1.4*287*300}{0.4}[1 - (\frac{4}{11})^{0.286}] - \frac{1^2 - 1.5^2}{2}$$
$$= 75706.6\,J/kg$$

The final output work should be $\dot{M}w = 75.7\,W$

In a typical summer day, the solar radiant of 1m×1m area is 1 kW, the corresponding energy conversion efficiency is 7.57%.

5.5 Conclusions

This chapter presents the design, numerical analysis of a new method for harvesting solar thermal energy. The DSMC program with new developed pressure boundary condition has the ability to simulate the micro scale gas flow. Numerical analysis provides information for design, fabrication and choosing working parameters of such a device.

The designed device has a number of advantages:

(1) It can harvest energy directly from the renewable energy sources, such as solar radiation and hence no fuel is needed.

(2) The structure is simple, there is no moving parts in the system.

(3) Compare with the photovoltaic panel, no expensive materials is need.

It is estimated the device has a conversion efficiency of 7.57% from thermal to kinetic energy. Optimization remains to be studied with more comprehensive model and simulation, experiment work will be done for verification

Chapter 6

Water Desalination Based on Knudsen Compressor and Solar Energy

6.1 Introduction

As reviewed in chapter 2, solar energy is one of the most promising applications of renewable energies to seawater desalination, and solar still device is probably the simplest desalination device.

As shown in Fig. 6.1, solar radiation transport through the glass cover to increase the water temperature and accelerate the rate of evaporation. A wide, shallow black painted pan makes an ideal vessel for the water. It should probably be baked in the sun for a while before it is used in order to free the paint of any volatile toxicants, which might otherwise evaporate and condense along with the purified water. The pan is painted black (or some other dark color) to maximize the amount of solar energy absorbed. It should also be wide and shallow to increase the surface area, assuming the availability of a substance with good solar absorbing properties and durability in heated saline water. To capture and condense the evaporated water, we need some kind of surface close to the heated salt water, which is several degrees cooler than the water. The evaporating pan is usually covered by a sheet of clear glass or translucent plastic (to allow sunlight to reach the water) which is tilted to a slight angle to let the fresh water that condenses on its underside trickle down to a collecting trough. The glass cerates a cavity and also holds the heat inside.

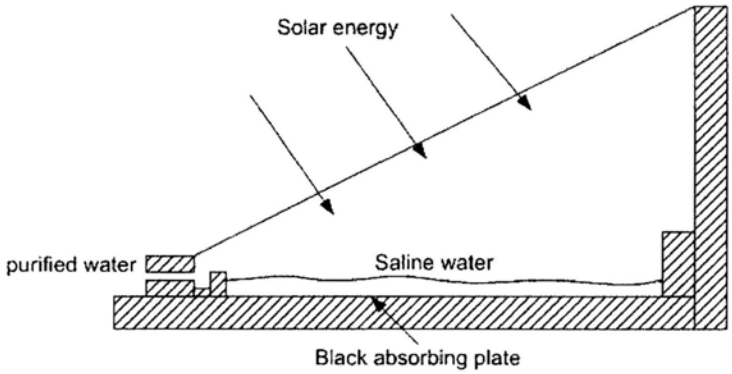

Figure 6.1: A simple solar still design

The solar still desalination device is simple, clean and using free energy source. However the application of such devices for industry or even pilot projects is very limited. It is mainly due to the low productivity and low energy efficiency of this technology. Zaki et al. [1993] built a simple basin type solar still, the fresh water productivity is approximately 2 L/m^2/day. Theoretically evaporate 1 kg of water at a temperature of 30°C about 2.3 × 10^6 J energy is required. Assuming a solar radiation of 300 W/m^2, averaged over 24 h, this energy could evaporate a maximum of 11.3 L/m^2/day. In practice heat losses will occur and the average daily yield which might be expected from a solar still is 4–5 L/m^2/day. Today's state-of-the-art single-effect solar stills have an efficiency of about 30–40% [Mink, 1998].

Many efforts have been made to improve the productivity and energy efficiency. For examples: 1. the wick still, the feed water flows slowly through a porous, radiation-absorbing pad (the wick). Tanaka et al. [1981] have proven the superiority of the tilted wick type solar still and confirmed an increase in productivity by 20-50%; 2. recover latent heat of condensation, the double-basin solar still [Al-Karaghouli and Alnaser, 2004] can produce 3.91 L/m^2/day at June; El-Sebaii [2005] reported a single-slop triple-basin solar still have the daily productivity 12.635 L/m^2/d with a daily average solar intensity of 651 W/m^2. Other attempts try to the increase the efficiency by separate evaporation and condensing zones [El-Bahi and Inan, 1999] or increase feeding water temperature by using various techniques, such as connection to solar collectors [Voropoulos et al., 2004], or integration of solar with multi-source and multi-use system [Jones, 1992].

All these technologies got some success, but they ineluctable increase the complexity and cost of the system. It is therefore the purpose of this research, to propose and investigate a new method for increasing the productivity of solar desalination. In this chapter, a comprehensive mathematical model including mass balance and energy balance was established, and computer simulation was performed to estimate and optimize the performance.

6.2 Proposed Method

With the use of solar energy, the saline water temperature usually does not reach boiling point. In this case, it is known that evaporation rate of saline water is a

function of temperature and pressure. According to the Hertz-Knudsen equation, the evaporation rate, n, can be expressed as [Jones, 1992]:

$$n = \frac{C}{(2\pi m k_B)^{1/2}} \left(\frac{P_S}{\sqrt{T_S}} - \frac{P_V}{\sqrt{T_V}} \right) \tag{6-1}$$

where, $m = 2.99 \times 10^{-23}$ g is the mass of the water molecule, k_B is the Boltzmann constant, T_S the surface temperature of the saline water, P_S the saturated vapor pressure at T_S, T_V is the temperature of water vapor, P_V the sub-pressure of the water vapor in the vapor region, and C the coefficient of evaporation (i.e., the ratio of the actual evaporation rate and the theoretical evaporation rate).

Equation (6-1) implies that $P_S / \sqrt{T_S}$ is the driving force of evaporation, and that is why people heating the water to higher temperature in order to get higher evaporation rate. On the other hand, $P_V / \sqrt{T_V}$ is the resistance of the evaporation. While the current research focus on increasing $P_S / \sqrt{T_S}$, our proposed method is trying to decrease $P_V / \sqrt{T_V}$. In this way, we may get a sufficient high evaporation rate under lower operating temperature. The advantages of evaporation under low temperature are analyzed below.

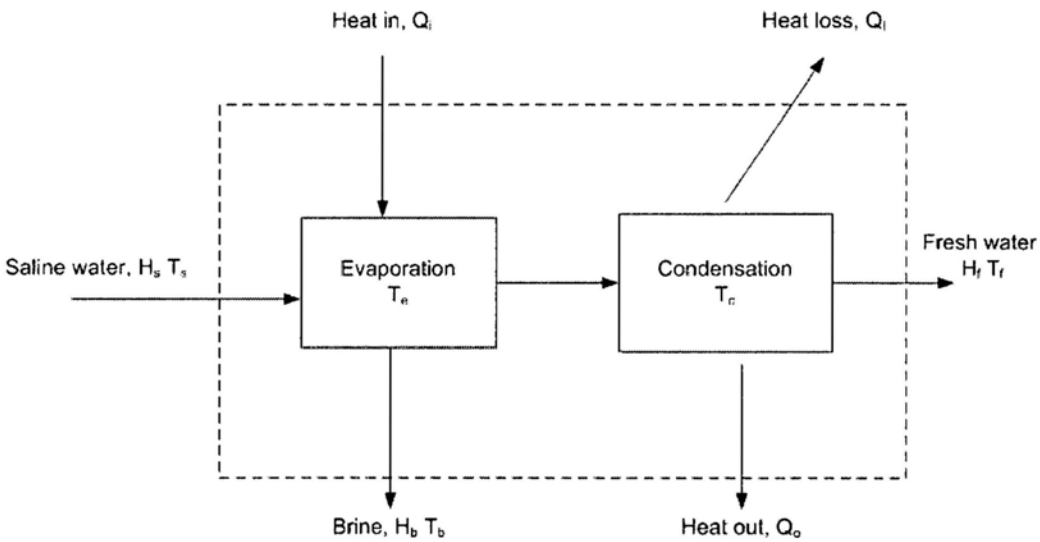

Figure 6.2: Generic phase-change desalination process

The generic phase-change desalination process is shown in Fig. 6.2 where H is the specific enthalpy, T is the temperature, and Q is the heat transfer rate. Here, Q_i

is the rate of heat input and $Q_o = m_f \Delta H_{(Te)}$ is the heat rejection rate, where m_f is the freshwater production rate and $\Delta H_{(Te)}$ is the latent heat of condensation at the temperature, T_e. The heat loss rate is $Q_l = h_A \Delta T$, where h is the heat transfer coefficient, A is the heat transfer area, and ΔT is the temperature difference between the evaporation chamber and the ambient. Based on first law of thermodynamics, the yield of this process, m_f / m_s, can be shown to be

$$\frac{m_f}{m_s} = \frac{(Q_i - Q_l)/m_s + (H_s - H_b)}{\Delta H_{(T_e)} + H_f - H_b} \tag{6-2}$$

Using the above result, contours of the freshwater production rate as a function of saline water feed rate and evaporation temperature can be generated for a given energy input. For a fixed rate of heat input, Q_i of 1,200 kJ/h and h_A = 1.0 J/s-K, the relationship between the process yield, m_f / m_s, and the specific energy consumption, Q_i / m_f [kJ/kg of freshwater produced] at various evaporation temperatures is shown in Fig. 6.3. This plot shows that the lower the evaporation temperature, the lower specific energy requirement for a desired yield.

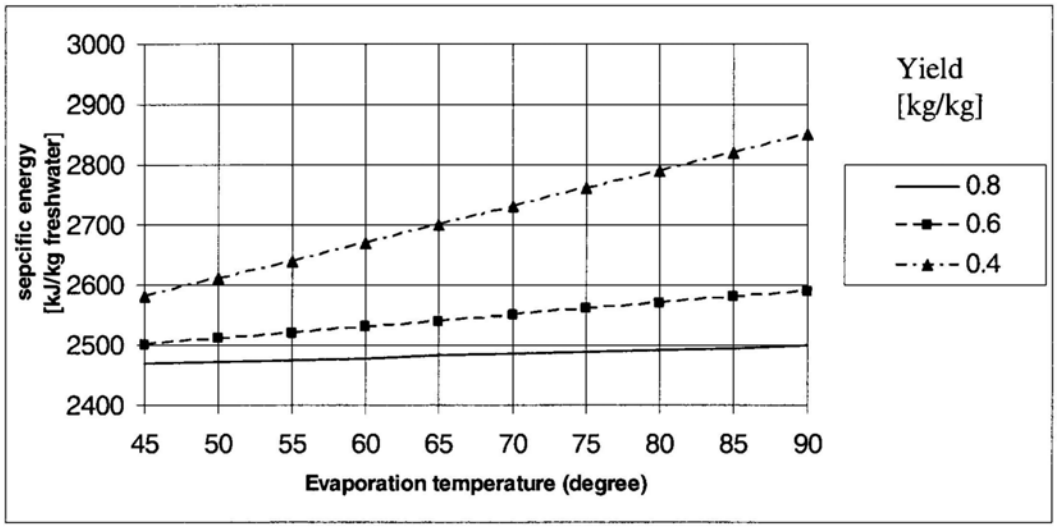

Figure 6.3: Relationship between yield and specific energy consumption

For rational technical comparisons of the different processes, and to improve existing processes or to develop new processes, quality of the energy utilized should be considered as well. A simple second law-based evaluation is presented below to illustrate how different qualities of heat energy used in phase-change desalination

processes can be compared. Consider, for example, the following two cases, each fed with saline water at 1 kg/h:

Case 1: a phase-change desalination process using moderate quality heat energy of 1,200 kJ/h at an evaporation temperature of 90 °C and ambient temperature of 25 °C.

Case 2: a phase-change desalination process using low quality heat energy of 1,200 kJ/h at an evaporation temperature of 50 °C and ambient temperature of 25 °C.

Based on first law analysis, freshwater production rates in Cases 1 and 2 can be found as 0.29 kg/h and 0.37 kg/h; and the corresponding specific energy requirements as 3,400 kJ/kg and 2,700 kJ/kg. Even though the quantities of energy input are the same in the two cases, their qualities are not. If, for instance, an ideal heat engine is operated across the respective temperature differences, their Carnot efficiencies will be 20% and 7.7% respectively. Thus, for the given heat energy input of 1,200 kW, the reversible work equivalence in Case 1 will be 240 kW and that in Case 2 will be 92 kW.

While the above analyses indicate that the phase-change process can be more energy efficient at low temperatures. In addition to the thermodynamic advantage, operation of phase-change processes at low temperatures can be beneficial in several other ways [Kronenberg and Lokiec, 2001]. Low corrosion rate at low temperatures allows low-cost materials to be used in construction and increases plant life. Scaling rate can be minimal as the operating temperatures are well below saturation limits for most scalants. Low temperature operation reduces fugitive heat losses and start-up periods. The motive energy for driving low temperature processes can be provided by low grade heat sources or waste heat rejections, so that overall efficiency can be achieved.

One approach is to maintain a low evaporation pressure whereby evaporation occurs at low temperature. Usually, additional mechanical energy has to be expended to maintain the required vacuum; since mechanical energy is a more valuable form of energy than heat energy, it is not a thermodynamically efficient approach. Our proposed method does not use a mechanical pump. Instead, we propose to use Knudsen compressor as the vacuum pump. Knudsen compressor has been reviewed and studied in pervious chapters. The multi stages Knudsen compressor working under atmosphere pressure to generate both gas flow and pressure difference has been investigate. In this chapter our research focuses on the one stage Knudsen

compressor's pumping effect and the integrated system's performance.

The proposed system, named as Lotus Water to signify the water purification process, is illustrated in Fig. 6.4. The system is driven by solar energy. As the sunlight shining on the system, the Fresnel lens focuses the sunlight on the upper surface of the aerogel. This will induce a temperature difference between the upper and lower surface of the aerogel layer. Aerogel, as mentioned in chapter 4, is a special class of continuously porous solid materials characterized by nanometer size particles and pores. Its extraordinary porous structure results in a very low thermal conductivity. Moreover, solid structures of diameters 2 ~ 5 nm and pores of diameters 10-100 nm produce a solid-gas matrix in which the volume fraction of the solid can be less than 5%. The pore size of the aerogel has a mean value of 20 nm, which gives $Kn \approx 3$ for air at atmosphere pressure of 760 Torr. The Knudsen effect is therefore generated and the gas especially the non-condensable gas in the evaporation chamber will flow out of the evaporation chamber. As a result, the vapor pressure in the evaporation chamber is decreased. In subsequent sections, the Knudsen effect is studied by DSMC method, followed by a comprehensive model of the whole system.

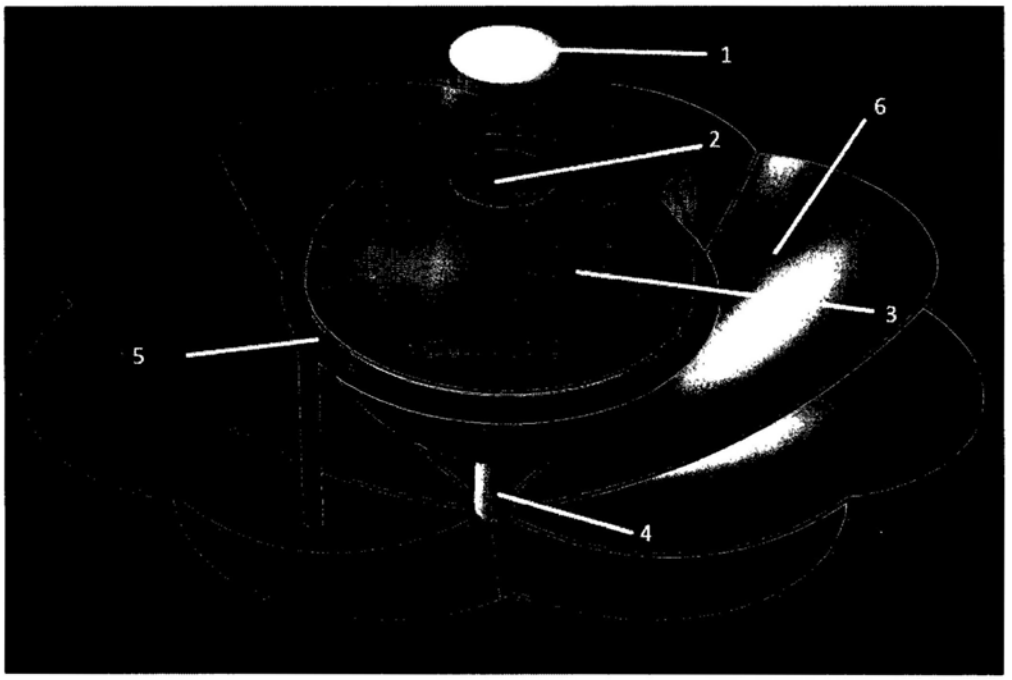

Figure 6.4: Lotus Water, our solar desalination system

1 – Fresnel lens, 2 – Aerogel material, 3 – Condensation cover, 4 –salt Water inlet tube, 5 – Fresh water outlet tube, 6 – Reflective mirror

6.3 Numerical Simulations

6.3.1 DSMC simulation of the Knudsen compressor

As discussed in chapter 5, for studying the performance of Knudsen effect in aerogel material, the particle based statistical method Direct Simulation Monte Carlo is used here again.

Our first simulation model is two chambers connect by a small channel as shown in Fig. 5.5. One chamber represents the evaporation chamber while the other represents the environment. The purpose of this simulation task is to investigate the pressure difference of the two sections at atmosphere operating pressures and temperature. For the nominal aerogel membrane, it is difficult to mimic the physical networking within the aerogel. As an initial and rough approach, the aerogel membrane section was modeled as a single representative flow channel to provide the most basic result from the DSMC simulations. .

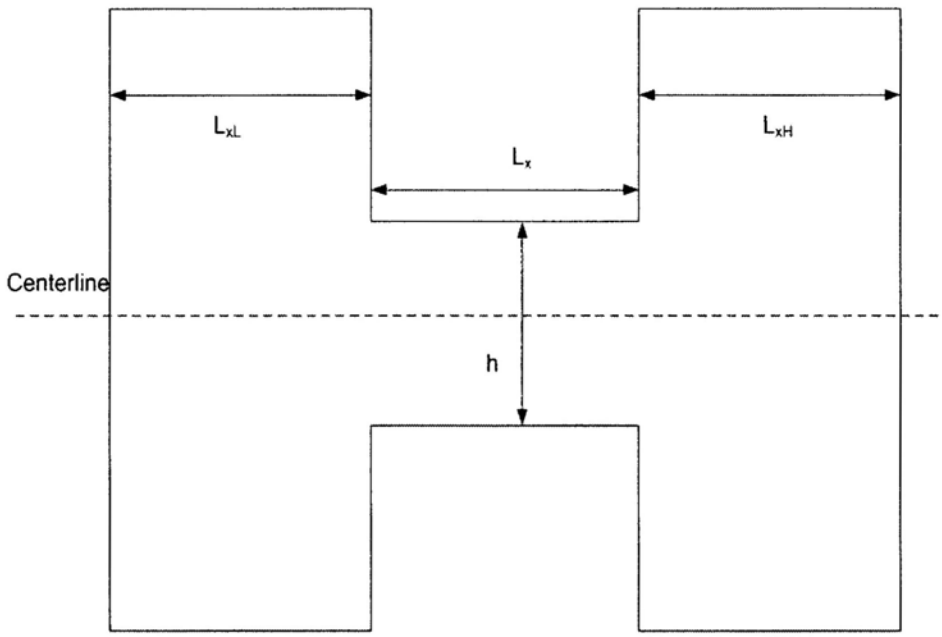

Figure 5.5: Scheme of one stage Knudsen compressor

To save computation time, the simulation grid was formed above the centerline. The setup of the simulation grid is shown if Fig. 6.6. This time the simulation domain is a closed system, the pressure boundary condition used in

chapter 4 is not applicable here. The flow regions adjacent to the simulated grid are solid wall with either specular or diffuse reflection except for the centerline, which was considered as a wall with fully specular reflection. There was no gas flow in or out of the simulation grid, so the number of simulated molecules was fixed. The shaded area is included in the simulation gird, but with zero simulated molecules in them since there is no flow through this region.

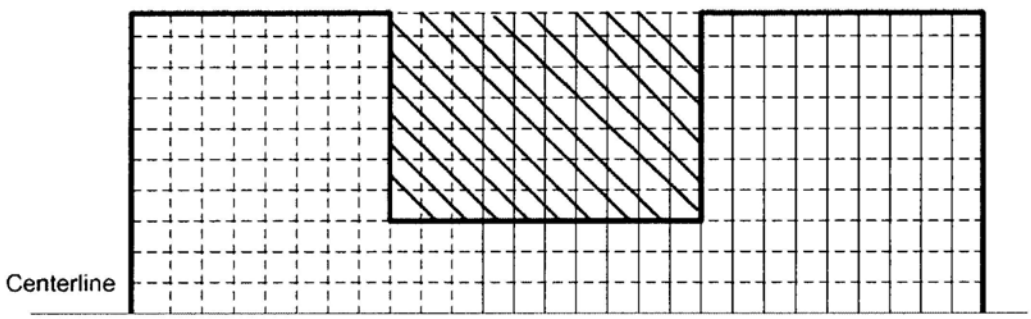

Figure 6.6: Cell setup

The two chambers have different temperatures, T_1 = 300K and T_2 = 600K, and a linear temperature gradient is set along the wall. The gas temperature is initialized to the same with its adjacent wall. The initial pressure of the whole region is 1 atm (i.e. 101.3 kPa). 200 cells were arranged in x direction and 100 cells were in y direction. The height of the channel h = 0.1 μm, the length of the channel was 1 μm, height of the chamber is 1 μm, the total length of the computation region is 6 μm. The ratio L_{xL}/L_{xH} has three different numbers as 1, 4 and 10 to represents different volume ratio.

From Fig. 6.7, we found the pressure of cool chamber decreases to 88 kPa and the hot chamber's pressure increases to 116 kPa, a temperature difference about 28 kPa was generated. Fig. 6.8 and Fig. 6.9 show the pressure profile of volume ratio 4 and 10. It is seen for volume ratio of 4, the pressure in the left chamber is about 83 kPa and in the right chamber is 113 kPa; for volume ratio of 10, the left chamber's pressure is even lower to 77 kPa and in right chamber's pressure is 103 kPa. In the real case, one side of the aerogel is evaporation chamber, while another side is open to the environment, so the volume ratio of 10 is closer to real.

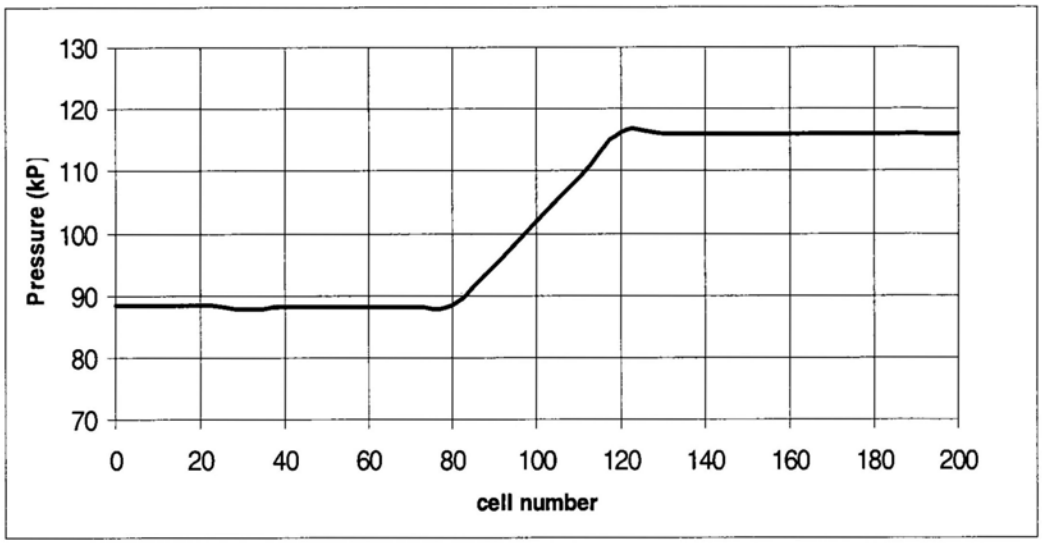

Figure 6.7: Pressure profile along the centerline of volume ratio is 1

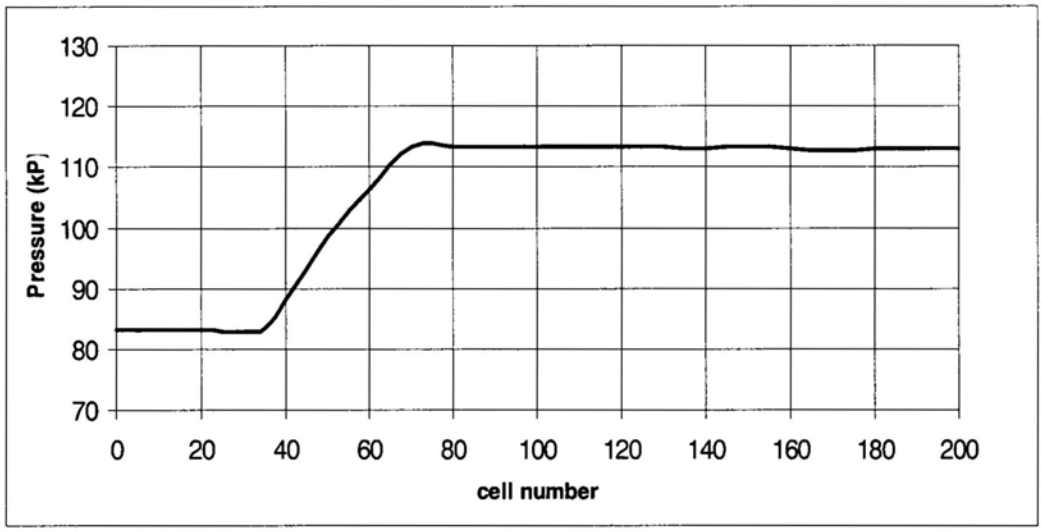

Figure 6.8: Pressure profile along the centerline of volume ratio is 4

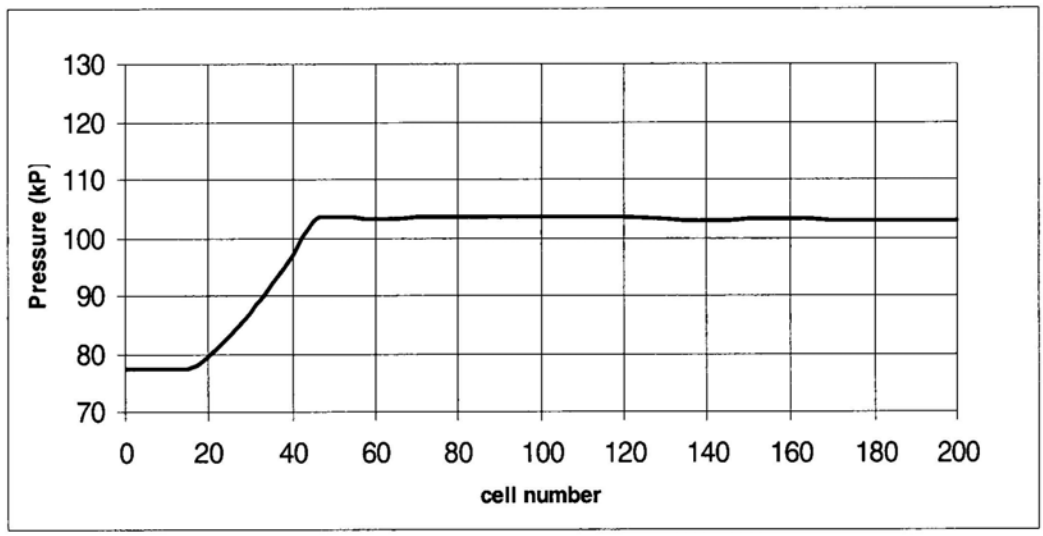

Figure 6.9: Pressure profile along the centerline of volume ratio is 10

The above results show the possibility of generating a vacuum with one stage Knudsen compressor under atmosphere condition. But as mentioned, the straight channel can not fully reveal the networking in aerogel membrane. So, in our second simulation model as shown in Fig. 6.10, three walls are added in the channel. It will be more close to real aerogel membrane.

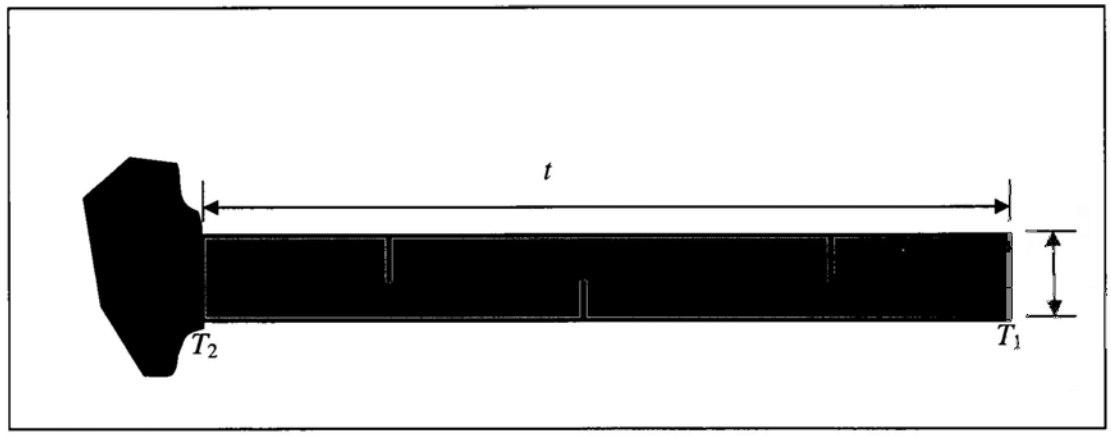

Figure 6.10: Micro channel in aerogel

In pervious simulation, we directly give a temperature difference ΔT = 300K. This is not ture, since the membrane is not an absolute thermal isolate material, there is a heat transfer process. As shown in Fig. 6.10, t is the thickness of aerogel layer, T_1 is temperature of the hot end (i.e. the temperature at the focus point), T_2 is the

temperature of the cool end, and T_3 is the temperature in the evaporation chamber. For given T_1 and T_3, the value of T_2 can be calculated from a simple heat transfer model. The heat transfer equation is:

$$h(T_2 - T_3) = \frac{d(T_1 - T_2)}{t} \qquad (6\text{-}3)$$

where, $d \approx 0.004$W/m.K is the heat conductivity coefficient of the aerogel, $h \approx 25$ W/m^2·K is the natural heat convention coefficient. During this simulation, it is assumed that T_1 = 600 K and T_3 = 300 K. With different thickness, we got different T_2 as shown in Table 6.1. It is found that for very thin membrane as t = 1 μm, the ΔT is only 2 K, it is not enough to drive the Knudsen effect and 1 μm thickness is also not mechanical real. In this case, our following simulation is based on t = 0.2 mm.

Table 6.1: Cold side temperature for different membrane thickness t

thickness	t=1μm	t=0.1mm	t=0.2mm	t=1mm
T_2	598K	484.6K	433.3K	341.4K

The total number of computational cell is 8000, the average number of simulated molecules per cell is 20, and thus the total number of simulated molecules in the domain is about 160000. Each calculation takes more than 4 hours to get convergence. When the convergence is reached, the difference of average hot connector section pressures from the previous two samples divided by that from the last sample is less than a specific small number (in these programs<10^{-3}). The calculated temperature and pressure distribution is shown in Fig. 6.11 and Fig. 6.12. From the figures, it is seen that a pressure difference about 10 kPa is generated. This also proves that at atmosphere pressure, the Knudsen effect can also works with nano scale channel aerogel. It in turns proves the possibility of using aerogel materials to make up a macroscopic Knudsen compressor for pumping.

Figure 6.11: The temperature distribution in aerogel's micro channel

Figure 6.12: The pressure distribution in the aerogel's micro channel

Table 6.2 contains more simulation results. We find for thick membrane which means very long channel length, the pressure difference is very small, this may caused by the large resistance in long tube. These results inform us that during real operation we must carefully choose the membrane thickness.

Table 6.2: Pressure difference for different channel size

size	0.1mm,100nm	0.2mm,100nm	0.2mm,200nm	0.3mm,100nm	1mm,100nm
ΔP	8kPa	12kPa	10kPa	8kPa	0

6.3.2 Strategy for controlling the pumping and heating

Given a certain amount of solar energy, E, in which a part, E_h, is used for heating the water and the rest, E_v, is used for Knudsen compressor to pumping; that is:

$$E = E_h + E_v \tag{6-4}$$

We wish to find the optimal division of E_h and E_v such that the fresh water productivity is maximized. The system's schematic is shown in Fig. 6.13, to establish the mathematical model, the following assumptions have been made for the solar desalination device: first, steady state conditions throughout the device; second, make up water flow rates into the system are constant.

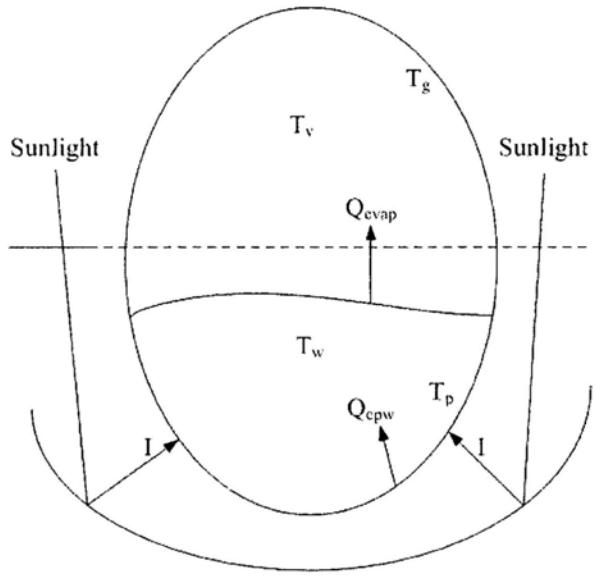

Figure 6.13: Schematic of lotus water device

The energy balance equations for different parts of the system are described as follows:

The energy equation of the lower shell of the evaporation chamber can be written as:

$$\partial I = Q_{cpw} \tag{6-5}$$

where, I is solar intensity. α is reflection coefficient of the reflective mirror in Fig. 6.4. The convection heat transfer from shell to water is $Q_{cpw} = h_{c,p-w}(T_p - T_w)A$, $h_{c,p-w}$ is the convection heat transfer coefficient, T_p and T_w are the shell temperature and water temperature respectively, A is the surface area, we set it as 1m^2. The radiation heat transfer from lower shell to upper condensation shell is neglected.

The energy equation for water is:

$$m_{in}C_wT_{in} + Q_{cpw} = Q_{evpa} + m_{out}C_wT_{out} \tag{6-6}$$

where, m_{in} and m_{out} is the mass flow rate of inlet and outlet water, C_w is the specific heat of water. T_{in} is set at 28 °C. The convection heat from water to air is neglected.

In the literature, many correlations can be found to calculated the evaporation heat flux. The evaporation heat flux into calm air is estimated by using the Ryan correlation [Yilmaz and Aybar, 1999]

$$Q_{evap} = 0.027\Delta T^{1/3} P_{sat}(1-\varphi) \tag{6-7}$$

where $\triangle T$ is the virtual temperature difference between water (T_w) and vapor region (T_m), P_{sat} is saturated pressure corresponding to T_m. φ, the relative humidity is

$$\varphi = \frac{P_v}{P_{sat}} \tag{6-8}$$

where P_v is partial pressure of vapor.

The energy equation for the condensation cover is:

$$Q_{cond} = Q_{cga} \tag{6-9}$$

where, The convection heat transfer from cover to air is $Q_{cga} = h_{c,g-a}(T_g - T_a)A$, T_g is the temperature of the condensation cover, T_a is the temperature of atmosphere. The radiation heat transfer from cover to air is neglected.

Similar with (6-7), the condensation heat flux is [Yilmaz and Aybar, 1999]

$$Q_{cond} = 85(T_m - T_g)\varphi \tag{6-10}$$

The mass balance for the device is:

$$m_{in} = m_{out} + m_{evap} \tag{6-11}$$

$$m_{evap} = m_{cond} \tag{6-12}$$

The evaporation mass flow and condensation mass flow are calculated by

$$m_{evap} = \frac{Q_{evap}}{\Delta H_v} \tag{6-13}$$

$$m_{evap} = \frac{Q_{cond}}{\Delta H_v} \tag{6-14}$$

where ΔH_v is the latent heat of vaporization.

Based on the simulation results of DSMC, we can calculate the the pumping effect of Knudsen compressor. The relationship between the input energy and the pressure of water vapor in the evaporation chamber is:

$$P_v = 4.636 \exp(-0.01199E_v) + 0.7437 \exp(0.0003226E_v) \quad (6\text{-}15)$$

The saturated vapor pressure, P_{sat}, which is a function of T_m. It can be calculated using an empirical equation [Cengel and Boles, 1994]:

$$P_{sat} = 9.53\times10^{-7}\times(T_m)^4 - 3.12\times10^{-5}\times(T_m)^3 + 3.45\times10^{-3}\times(T_m)^2 + 2.09\times10^{-2}\times(T_m) + 6.11\times10^{-1} \quad (6\text{-}16)$$

The above equations constitute the comprehensive model, based on which simulations can be carried out.

6.4 Results and Discussions

The parameters that are used in the simulation are given in Table 6.3.

Table 6.3: Simulation parameters

Paremeters	Symbol	Value
Inlet mass flow rate	m_{in} (kg/h)	3.6
Specific heat of water	C_w (J/kg K)	4148
Reflection coefficient	α	0.8
Latent heat of vaporization	ΔH_v (J/kg)	2300×10^3
Convection heat transfer coefficient	$h_{c,p\text{-}w}$ (W/m^2 °C)	400
Convection heat transfer coefficient	$h_{c,g\text{-}a}$ (W/m^2 °C)	40

The calculated temperatures against input solar energy are shown in Fig. 6.14. As expected, the correlation is almost linear. The higher the solar intensity, the higher the water and vapor temperatures. As an example, when I = 1000 W, T_s is about 360 K (87 °C) and the T_v = 310 K (37 °C).

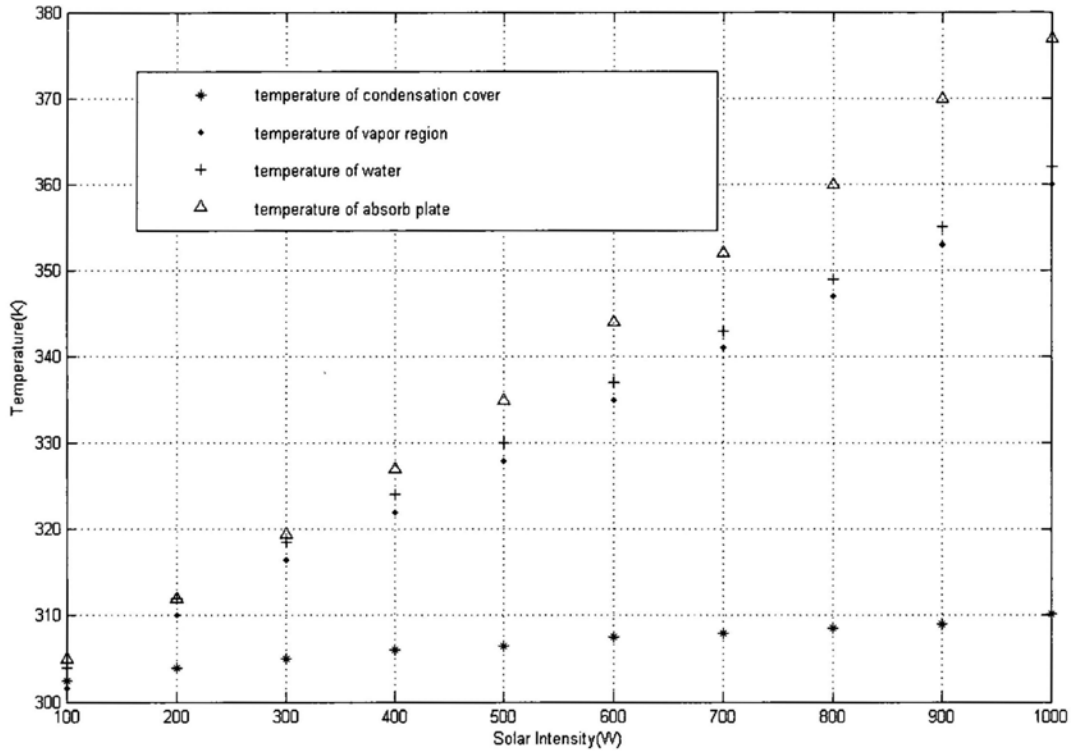

Figure 6.14: Temperature of water and vapor versus solar energy for heating

With the model presented in the previous section, Fig. 6.15 shows the evaporation rate as a function of water temperature, T_s, and the portion of the energy used for pumping, E_v. From the figure, it is seen that when the heating temperature is high (higher than 80 °C), vacuuming does less help. This is because the liquid molecule at the surface already gets sufficient energy to vaporize. Though, when the heating temperature is low, which is typical in the case of using low quality thermal energy such as solar energy, vacuuming is very much helpful. This is because the low pressure gives the liquid molecule less resistance. Though, as shown in the figure, continuous increase pumping energy (more than 20%) will not getting higher vacuuming degree and hence, will become less effective.

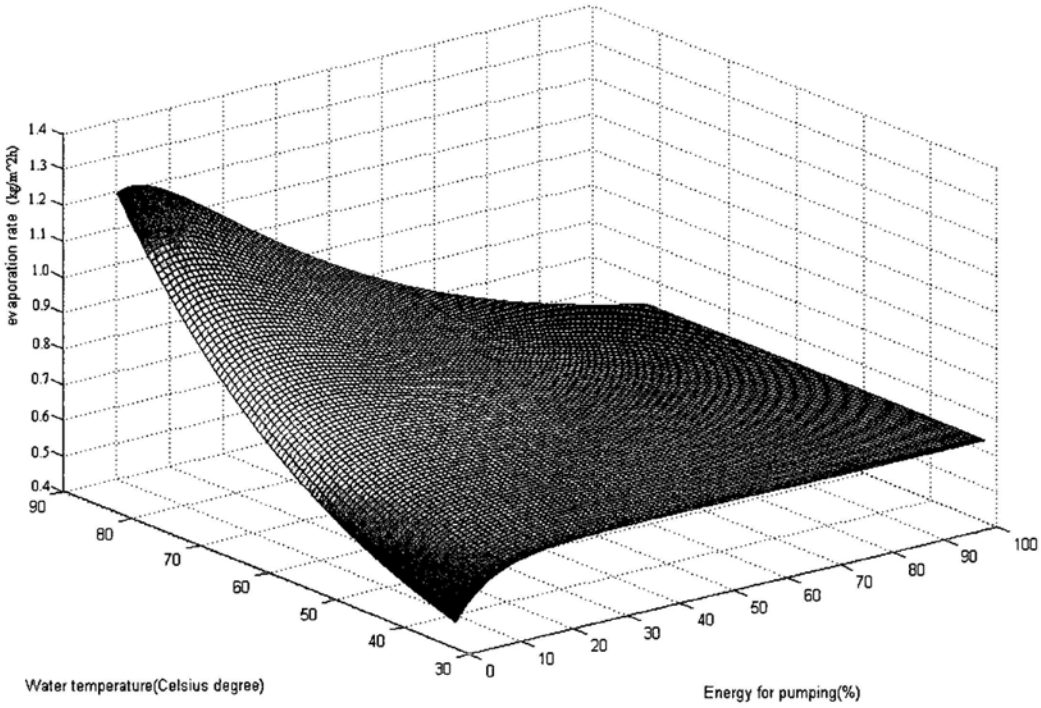

Figure 6.15: evaporation rate as a function of the water temperature, T_s, and the portion of the energy for pumping, E_v, for Solar radiation I= 1000W

More specifically, Table 6.4 shows the optimal evaporation rate under different temperature. From the table, the aforementioned trend is clear.

Table 6.4: Optimal working condition under different water temperature

Temperature (°C)	Optimal pumping energy (%)	Optimal evaporation rate (kg/m^{2}h)
40	22	0.54
50	19	0.66
60	12	0.81
70	9	1.04
80	4	1.20

Fig. 6.16 shows the solar intensity of a typical summer day in June in Northern Cyprus [Aybar, 2006]. Fig. 6.17 shows the evaporation rate of that day. From the figure, it is seen that, using the presented technology will result an

improvement of 30% than direct heating. The maximum evaporation rate for 1 hour in 1 m^2 area could reach 1.1 kg and the total evaporation rate for a day is about 5.4 $kg/day \cdot m^2$. This number is much greater than the simple distillation method.

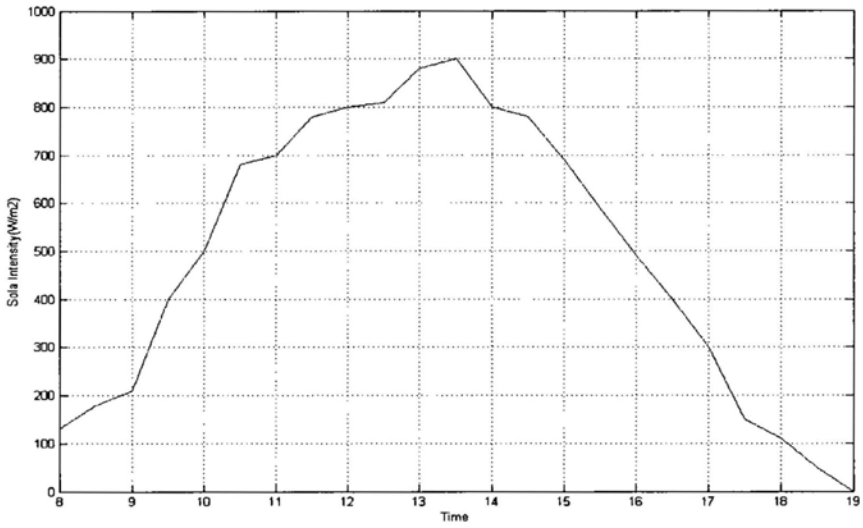

Figure 6.16: Solar intensity of a typical summer day

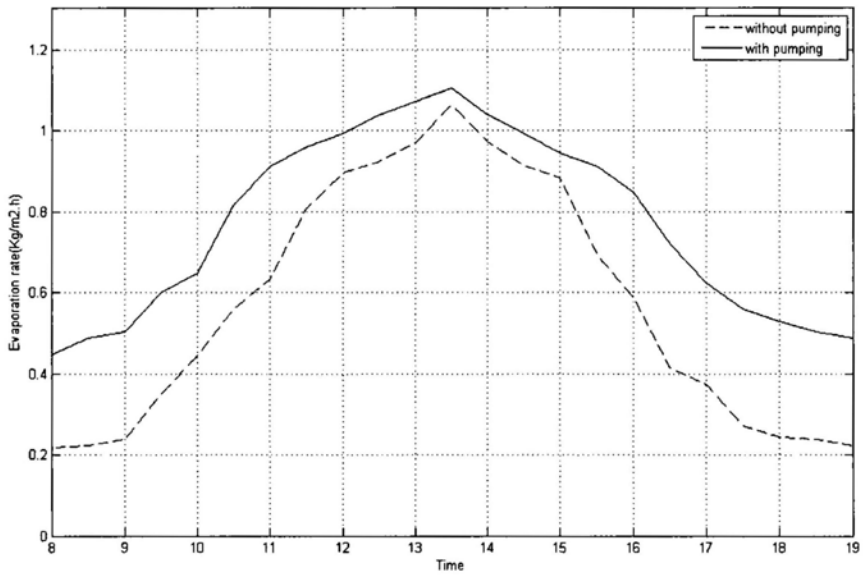

Figure 6.17: Fresh water production rate with and without the presented technology

6.5 Conclusions

This chapter presented a new method to increase the efficiency of solar thermal desalination. Based on the discussion above, following conclusions can be drawn.

(1) Based on DSMC, it is shown that with nano-channel aerogel Knudsen compressor can generate a vacuuming effect of 10 kPa under solar radiation and atmosphere pressure.

(2) Based on computer simulation. The presented new technology could generate more than 5 kg fresh water in 1 m^2 area per day, which is higher than simple distillation method.

(3) Besides the fresh water productivity, operating under low temperature is also thermodynamically efficient.

(4) It is not conflict with other technologies and can be integrated with other technologies such like multi-stages heat recovery, in this case a higher productivity could be expected.

(5) The presented system is simple and does not require additional energy input or other mechanical equipment. It is self-sustainable.

Chapter 7:
Conclusions

7.1 Contributions

This thesis explores new applications based on micro flow phenomenon. It consists of two parts: one is about energy and the other concerns water. Based on a combination of physical and mathematical modeling, computer simulations and experiment validation, several achievements are made. Specifically, three original contributions are made as summarized below:

- A new model for describing the mass transport in Direct Contact Membrane Distillation (DCMD) process is developed. Again, DSMC method is combined with traditional heat transfer model. It avoids the over simplification of the resistance mechanism in the conversional mass transfer model. The model helps us to better understanding the resistance mechanisms in DCMD process. An experiment is setup. The experiment results of a commercial PTFE membrane validate the accuracy of the model. Moreover, aerogel material is proposed for the DCMD process. Based on computer simulation, it is seen that the aerogel's high hydrophobic property; low heat conductivity and high porosity offer a good performance over the conventional PTFE material. The water flux for $1m^2$ membrane area is about 53 kg/h. Without heat recovery procedure, the daily distillated water productivity is 10.0 kg/day for 1 m^2 solar collector area.
- A new solar thermal energy harvesting method is proposed and studied. It is a new application of the so-called Knudsen compressor, which utilizes temperature difference to generate increased pressure and gas flow. A Direct Simulation Monte Carlo (DSMC) program is developed to simulate the performance of Knudsen compressor. The simulation results show that with aerogel material the Knudsen compressor can work efficiently under atmosphere pressure. Based on this principle a device is designed. The device has a simple structure with no moving parts. It is estimated the device has a conversion efficiency of 7.57% from thermal to kinetic energy.

- A new solar desalination device is designed and analyzed. Evolving from the aforementioned Knudsen compressor, DSMC result shows that with nano-channel aerogel material a vacuuming effect of 10 kPa under solar radiation and atmosphere pressure can be generated. By utilizing this effect, a new desalination device is proposed. Thermodynamic analysis shows the advantages of operating at low temperature. Based on computer simulation, the new device could generate about 5 kg fresh water per day with 1 m^2 solar collection area. This productivity is higher than the direct solar still by as much as 30%. The device is simple and does not require additional energy input and/or other mechanical equipment, such as pumps and valves. It can work with other technologies such as multi-stages heat recovery, to achieve higher productivity.

7.2 Future Work

This thesis presents several new ideas for solving the energy and water problems. These technologies have great potentials, but there are still some steps to go before it can be implemented for practical applications. The future research includes:

- The DCMD experiment system has been setup and tested for PTFE membrane. The performance of aerogel membrane should be investigated by experiment. It is noted that the aerogel material is fragile, a membrane with hundreds micro meters is hard to fabricate and package. Some researchers have tried to find the solution to this problem [Nilsen et al., 2001; Sherman et al., 2009]. In addition, to get more accuracy simulation results, the mathematical model should be refined to include the temperature distribution in the feed side and the permeate side, more detailed description of heat transfer coefficient, and so on.
- For the energy harvesting device. The experiment validation of single and multi stage Knudsen compressor is necessary. The experiment result could be used to verify the model and optimize the design. The desired experiment data include the pressures of both hot side and cold side chambers, the differential pressures across a single Knudsen compressor stage, and the temperatures of both the hot and cold sides. Based on the experiment data, optimization can be carried out to

achieve the maximum mass flow over a design pressure ratio $(\wp_N)_{DES}$ or the minimum cascade volume per unit mass.

- The final goal of the energy harvest device is to generate electricity. Thus, in addition to the multi-stages Knudsen compressor, the micro generator for converting the kinetic energy of gas flow to electric energy is also important. Kinetic energy can be converted into electricity using electromagnetic, piezoelectric or electrostatic transduction mechanisms. Further research may be carried out to build an actual prototype.
- A new desalination device has been proposed and analyzed. In the future, experimental validation is needed. Also, a dynamic model should be developed to describe the transitional performance of the system. Besides, there are many other parameters that affect the fresh water productivity, such as the shape of the evaporation chamber, the concentration rate of the reflection mirror, the saline water flow rate and so on. Further investigation of the influence of these parameters should be added. Moreover, recovery of the condensation heat should be considered to further improve the fresh water productivity.
- DSMC is very effective for simulating the gas flow in micro scale. In all the three aforementioned studies, the flow covers not only one flow regime or one phase. For example, in the case of Knudsen compressor, the flow in capillary section is transitional flow and in connector section it is continuum flow. In the case of DSMC process, the mass transport in membrane is a gas flow, and the kinetic in the liquid-vapor interface needs more detailed two phase description. Hence, it is necessary to implement multi domain coupling simulation, such as DSMC / continuum coupling and/or DSMC / Molecular Dynamics coupling. This kind of couplings is very important to the understanding of fluid flow in MEMS devices and hence, shall be investigated in details in the future.

Appendix
FORTRAN Program of DSMC

```
*  DSMC2.FOR
     PROGRAM DSMC2
     INCLUDE "PARAMETER.F"
     DOUBLE PRECISION COL(MNSP,MNSP),MOVT,NCOL,SELT,SEPT,
    &                                 CS(7,MNC,MNSP),LAMD
     DOUBLE PRECISION CSS(9,MNSE,MNSP)
     COMMON /MOLS2 / NM,PP(2,MNM),PV(3,MNM),IPL(MNM),IPS(MNM),IR(MNM)
     COMMON /MOLSR / PR(MNM)
     COMMON /CELL2 / CC(MNC),CG(6,MNC),IC(2,MNC,MNSG),ISC(MNSC),
    &          CCG(2,MNC,MNSG,MNSG),ISCG(2,MNSC,MNSG),IG(2,MNSG),
    &          NCX,NCY,IFCX,IFCY,CWRX,CWRY,APX,RPX,APY,RPY
   COMMON /GAS   / SP(5,MNSP),SPM(6,MNSP,MNSP),ISP(MNSP)
     COMMON /GASR  / SPR(3,MNSP,MNSP),ISPR(3,MNSP),CT(MNC)
     COMMON /SAMPS / CSS*
     COMMON /CONST / PI,SPI,BOLTZ
     WRITE (*,*) ' INPUT 0,1 FOR CONTINUING,NEW CALCULATION:- '
     READ (*,*) NQL
     WRITE (*,*) ' INPUT 0,1 FOR CONTINUING,NEW SAMPLE:- '
     READ (*,*) NQLS
     IF (NQL.EQ.1) THEN
      CALL INIT2
     ELSE
      WRITE (*,*) ' READ THE RESTART FILE'
      OPEN (4,FILE='DSMC2.RES',STATUS='OLD',FORM='UNFORMATTED')
      READ (4) ALPI,ALPN,ALPT,APX,APY,BFND,BME,BMEJ,BMR,BMRJ,BOLTZ,CB,
    &         CC,CCG,CG,CH,COL,CS,CSR,CSS,CT,CW,CWRX,CWRY,DTM,FNDJ,
    &         FNUM,FSPJ,FTMP,FVJ,FH,FW,IB,IC,IFCX,IFCY,IIS,IJET,IPL,
    &         IPS,IR,ISC,ISCG,ISG,ISP,ISPR,ISURF,LFLX,LFLY,LIMJ,LIMS,
    &         MOVT,NCOL,NCX,NCY,NIS,NM,NPS,NSCX,NSCY,NSMP,NPR,NPT,
    &         NSP,PI,PP,PR,PV,RPX,RPY,SELT,SEPT,SP,SPI,SPM,SPR,TIME,
    &         TIMI,TMPJ,TSURF,VFX,VFY,WJ
      CLOSE (4)
     END IF
     IF (NQLS.EQ.1) CALL SAMPI2
100  NPR=NPR+1
     IF (NPR.LE.NPS) CALL SAMPI2
     DO 200 JJJ=1,NSP
      DO 150 III=1,NIS
       TIME=TIME+DTM
       WRITE (*,99001) III,JJJ,NIS,NSP,NM,IDINT(NCOL)
99001    FORMAT (' DSMC2:- Move',2I5,' of',2I5,I8,' Mols',I14,' Colls')
       CALL MOVE2
       CALL INDEXM
       CALL COLLMR
150   CONTINUE
     CALL SAMPLE2
200  CONTINUE
     WRITE (*,*) ' WRITING RESTART AND OUTPUT FILES',NPR,'  OF ',NPT
     OPEN (4,FILE='DSMC2.RES',FORM='UNFORMATTED')
     WRITE (4) ALPI,ALPN,ALPT,APX,APY,BFND,BME,BMEJ,BMR,BMRJ,BOLTZ,CB,
    &         CC,CCG,CG,CH,COL,CS,CSR,CSS,CT,CW,CWRX,CWRY,DTM,FNDJ,
    &         FNUM,FSPJ,FTMP,FVJ,FH,FW,IB,IC,IFCX,IFCY,IIS,IJET,IPL,
    &         IPS,IR,ISC,ISCG,ISG,ISP,ISPR,ISURF,LFLX,LFLY,LIMJ,LIMS,
    &         MOVT,NCOL,NCX,NCY,NIS,NM,NPS,NSCX,NSCY,NSMP,NPR,NPT,NSP,
    &         PI,PP,PR,PV,RPX,RPY,SELT,SEPT,SP,SPI,SPM,SPR,TIME,TIMI,
    &         TMPJ,TSURF,VFX,VFY,WJ

     CLOSE (4)
```

```
      IF(REAL(NPR)/10.0 .EQ. NPR/10) CALL OUT2
      IF (NPR.LT.NPT) GO TO 100
      STOP
      END
*   INIT2.FOR
      SUBROUTINE INIT2
      INCLUDE "PARAMETER.F"
      DOUBLE PRECISION COL(MNSP,MNSP),MOVT,NCOL,SELT,SEPT,
     &                                 CS(7,MNC,MNSP),LAMD
      COMMON /MOLS2 / NM,PP(2,MNM),PV(3,MNM),IPL(MNM),IPS(MNM),IR(MNM)
      COMMON /MOLSR / PR(MNM)
      COMMON /CELL2 / CC(MNC),CG(6,MNC),IC(2,MNC,MNSG),ISC(MNSC),
     &          CCG(2,MNC,MNSG,MNSG),ISCG(2,MNSC,MNSG),IG(2,MNSG),
     &          NCX,NCY,IFCX,IFCY,CWRX,CWRY,APX,RPX,APY,RPY
      COMMON /GAS   / SP(5,MNSP),SPM(6,MNSP,MNSP),ISP(MNSP)
      COMMON /GASR  / SPR(3,MNSP,MNSP),ISPR(3,MNSP),CT(MNC)
            COMMON /CONST / PI,SPI,BOLTZ
      PI=3.141592654
      SPI=SQRT(PI)
      BOLTZ=1.380622E-23
      NFACE=13
      FND=0.
      FTMP=273.
      VFX=0.
      VFY=0.
      IFCX=0
      IFCY=0
      LFLX=0
      LFLY=0
            DO 101 N=1,NFACE
            ALPI(N)=-1.
101         CONTINUE
      DO 100 N=1,4
       IB(N)=3
       DO 50 L=1,MNSP
        ISP(L)=1
        FSP(L)=0.
        BME(N,L)=0.
        BMR(N,L)=0.
50     CONTINUE
100   CONTINUE
      DO 200 L=1,MNSP
       BMEJ(L)=0.
       BMRJ(L)=0.
200   CONTINU
      CALL DATA2
      IF (MNSP.EQ.1) ISPD=0
      DO 300 N=1,MNSP
       DO 250 M=1,MNSP
        IF ((ISPR(3,N).EQ.0).AND.(M.NE.N)) THEN
         SPR(1,N,M)=SPR(1,N,N)
         SPR(2,N,M)=SPR(2,N,N)
         SPR(3,N,M)=SPR(3,N,N)
        END IF
        IF ((ISPD.EQ.0).OR.(N.EQ.M)) THEN
         SPM(1,N,M)=0.25*PI*(SP(1,N)+SP(1,M))**2
         SPM(2,N,M)=0.5*(SP(2,N)+SP(2,M))
         SPM(3,N,M)=0.5*(SP(3,N)+SP(3,M))
         SPM(4,N,M)=0.5*(SP(4,N)+SP(4,M))
        ELSE
         SPM(1,N,M)=PI*SPM(1,N,M)**2
        END IF
        SPM(5,N,M)=(SP(5,N)/(SP(5,N)+SP(5,M)))*SP(5,M)
```

```
      SPM(6,N,M)=GAM(2.5-SPM(3,N,M))
250   CONTINUE
300  CONTINUE
    TIME=0.
    NM=0
    NPR=0
    NCOL=0
    MOVT=0.
    SELT=0.
    SEPT=0.
    DO 400 M=1,MNSP
     DO 350 N=1,MNSP
      COL(M,N)=0.
350   CONTINUE
400  CONTINUE
    FW=CB(2)-CB(1)
    FH=CB(4)-CB(3)
    CG(1,1)=CB(1)
    IF (IFCX.EQ.0) THEN
     CW=FW/NCX
    ELSE
     RPX=CWRX**(1./(NCX-1.))
     APX=(1.-RPX)/(1.-RPX**NCX)
    END IF
    CG(4,1)=CB(3)
    IF (IFCY.EQ.0) THEN
     CH=FH/NCY
    ELSE
     RPY=CWRY**(1./(NCY-1.))
     APY=(1.-RPY)/(1.-RPY**NCY)
    END IF
    DO 500 MY=1,NCY
     DO 450 MX=1,NCX
      M=(MY-1)*NCX+MX
      CT(M)=FTMP
      IF (MX.EQ.1) CG(1,M)=CG(1,1)
      IF (MX.GT.1) CG(1,M)=CG(2,M-1)
      IF (IFCX.EQ.0) THEN
       CG(2,M)=CG(1,M)+CW
      ELSE
       CG(2,M)=CG(1,M)+FW*APX*RPX**(MX-1)
      END IF
      CG(3,M)=CG(2,M)-CG(1,M)
      IF (MY.EQ.1) CG(4,M)=CG(4,1)
      IF (MY.GT.1.AND.MX.EQ.1) CG(4,M)=CG(5,M-1)
      IF (MY.GT.1.AND.MX.GT.1) CG(4,M)=CG(4,M-1)
      IF (IFCY.EQ.0) THEN
       CG(5,M)=CG(4,M)+CH
      ELSE
       CG(5,M)=CG(4,M)+FH*APY*RPY**(MY-1)
      END IF
      CG(6,M)=CG(5,M)-CG(4,M)
      CC(M)=CG(3,M)*CG(6,M)
      DO 420 L=1,MNSG
       DO 410 K=1,MNSG
        CCG(2,M,L,K)=RF(0)
        CCG(1,M,L,K)=SPM(1,1,1)*300.*SQRT(FTMP/300.)
410     CONTINUE
420    CONTINUE
450   CONTINUE
500  CONTINUE
    IF (IFCX.EQ.1) THEN
     APX=(1.-RPX)/APX
```

```
      RPX=LOG(RPX)
     END IF
     IF (IFCY.EQ.1) THEN
      APY=(1.-RPY)/APY
      RPY=LOG(RPY)
     END IF
     DO 600 N=1,MNC
      DO 550 M=1,NSCY
       DO 520 K=1,NSCX
        L=(N-1)*NSCX*NSCY+(M-1)*NSCX+K
        ISC(L)=N
520     CONTINUE
550    CONTINUE
600   CONTINUE
     IF (IIS.GT.0.AND.ISG.GT.0) THEN
      DO 650 L=1,MNSP
       REM=0
       IF (IIS.EQ.1) VMP=SQRT(2.*BOLTZ*FTMP/SP(5,L))
       DO 620 N=1,MNC
        IPROB=1
        IF (LFLX.NE.0) THEN
         NY=(N-1)/NCX+1
         NX=N-(NY-1)*NCX
         IF ((LFLX.GT.0.AND.LFLY.GT.0).AND.
     &        (NX.LT.LFLX.AND.NY.LT.LFLY)) IPROB=0
         IF ((LFLX.GT.0.AND.LFLY.LT.0).AND.
     &        (NX.LT.LFLX.AND.NY.GT.-LFLY)) IPROB=0
         IF ((LFLX.LT.0.AND.LFLY.GT.0).AND.
     &        (NX.GT.-LFLX.AND.NY.LT.LFLY)) IPROB=0
         IF ((LFLX.LT.0.AND.LFLY.LT.0).AND.
     &        (NX.GT.-LFLX.AND.NY.GT.-LFLY)) IPROB=0
        END IF
        IF (IPROB.EQ.1) THEN
         A=FND*CC(N)*FSP(L)/FNUM+REM
         IF (N.LT.MNC) THEN
          MM=A
          REM=(A-MM)
         ELSE
          MM=NINT(A)
         END IF
         IF (MM.GT.0) THEN
          DO 604 M=1,MM
           IF (NM.LT.MNM) THEN
            NM=NM+1
            IPS(NM)=L
            PP(1,NM)=CG(1,N)+RF(0)*(CG(2,N)-CG(1,N))
            NCOLM=(PP(1,NM)-CG(1,N))*(NSCX-.001)/CG(3,N)+1
            PP(2,NM)=CG(4,N)+RF(0)*(CG(5,N)-CG(4,N))
            NROW=(PP(2,NM)-CG(4,N))*(NSCY-.001)/CG(6,N)+1
            IPL(NM)=(N-1)*NSCX*NSCY+(NROW-1)*NSCX+NCOLM
            DO 602 K=1,3
             CALL RVELC(PV(K,NM),A,VMP)
602          CONTINUE
            PV(1,NM)=PV(1,NM)+VFX
            PV(2,NM)=PV(2,NM)+VFY
            IF (ISPR(1,L).GT.0) CALL SROT(PR(NM),FTMP,ISPR(1,L))
           END IF
604        CONTINUE
         END IF
        END IF
620     CONTINUE
650    CONTINUE
      WRITE (*,99001) NM
```

```
99001   FORMAT (' ',I6,' MOLECULES')
      END IF
      IF (IIS.GT.0) THEN
       DO 700 N=1,4
        IF (IB(N).EQ.1) THEN
         WRITE (*,*) 'side',N
         DO 660 L=1,MNSP
          VMP=SQRT(2.*BOLTZ*FTMP/SP(5,L))
          IF (N.EQ.1) SC=VFX/VMP
          IF (N.EQ.2) SC=-VFX/VMP
          IF (N.EQ.3) SC=VFY/VMP
          IF (N.EQ.4) SC=-VFY/VMP
          IF (ABS(SC).LT.10.1) A=(EXP(-SC*SC)+SPI*SC*(1.+ERF(SC)))
     &                          /(2.*SPI)
          IF (SC.GT.10.) A=SC
          IF (SC.LT.-10.) A=0.
          IF (N.EQ.1.OR.N.EQ.2) THEN
           BME(N,L)=FND*FSP(L)*A*VMP*DTM*FH/FNUM
          ELSE
           BME(N,L)=FND*FSP(L)*A*VMP*DTM*FW/FNUM
          END IF
          WRITE (*,*) ' species ',L,' entering mols ',BME(N,L)
660       CONTINUE
        END IF
700    CONTINUE
      END IF
      IF (IJET.GT.0) THEN
       DO 750 L=1,MNSP
        VMP=SQRT(2.*BOLTZ*TMPJ/SP(5,L))
        SC=FVJ/VMP
        IF (ABS(SC).LT.10.1) A=(EXP(-SC*SC)+SPI*SC*(1.+ERF(SC)))
     &                        /(2.*SPI)
        IF (SC.GT.10.) A=SC
        IF (SC.LT.-10.) A=0.
        J2=LIMJ(2)
        J3=LIMJ(3)
        IF (IJET.EQ.1.OR.IJET.EQ.2) THEN
         WJ=CG(2,J3)-CG(1,J2)
        ELSE
         WJ=CG(5,(J3-1)*NCX+1)-CG(4,(J2-1)*NCX+1)
        END IF
        BMEJ(L)=FNDJ*FSPJ(L)*A*VMP*DTM*WJ/FNUM
        WRITE (*,*) ' entering mols in jet ',BMEJ(L)
750    CONTINUE
      END IF
      RETURN
      END
*   MOVE2.FOR
      SUBROUTINE MOVE2
      INCLUDE "PARAMETER.F"
      DOUBLE PRECISION COL(MNSP,MNSP),MOVT,NCOL,SELT,SEPT,
     &                                 CS(7,MNC,MNSP),LAMD
      DOUBLE PRECISION CSS(9,MNSE,MNSP)
      COMMON /MOLS2 / NM,PP(2,MNM),PV(3,MNM),IPL(MNM),IPS(MNM),IR(MNM)
      COMMON /MOLSR / PR(MNM)
      COMMON /CELL2 / CC(MNC),CG(6,MNC),IC(2,MNC,MNSG),ISC(MNSC),
     &          CCG(2,MNC,MNSG,MNSG),ISCG(2,MNSC,MNSG),IG(2,MNSG),
     &          NCX,NCY,IFCX,IFCY,CWRX,CWRY,APX,RPX,APY,RPY
      COMMON /GAS   / SP(5,MNSP),SPM(6,MNSP,MNSP),ISP(MNSP)
      COMMON /GASR  / SPR(3,MNSP,MNSP),ISPR(3,MNSP),CT(MNC)
      COMMON /SAMPS / CSS
            IFT=-1
      N=0
```

```
100  N=N+1
          IF (N.LE.NM) THEN
     IF (IFT.LT.0) AT=DTM
     IF (IFT.GT.0) AT=RF(0)*DTM
150    MOVT=MOVT+1
     MSC=IPL(N)
     MC=ISC(MSC)
     XI=PP(1,N)
     IF ((XI+0.00001*CG(3,1)).LT.CB(1).OR.
    &   (XI-0.00001*CG(3,MNC)).GT.CB(2)) THEN
       WRITE (*,*) ' MOL ',N,' X COORD OUTSIDE FLOW ',XI
       CALL REMOVE(N)
       GO TO 100
     END IF
     YI=PP(2,N)
     IF ((YI+0.00001*CG(6,1)).LT.CB(3).OR.
    &   (YI-0.00001*CG(6,MNC)).GT.CB(4)) THEN
       WRITE (*,*) ' MOL ',N,' Y COORD OUTSIDE FLOW ',YI
       CALL REMOVE(N)
       GO TO 100
     END IF
     DX=PV(1,N)*AT
     DY=PV(2,N)*AT
     X=XI+DX
     Y=YI+DY
     DO 200 KS=1,NFACE
       IF (ISURF(KS).GT.0) THEN
         IF (ISURF(KS).EQ.1.OR.ISURF(KS).EQ.2) THEN
           L1=LIMS(KS,1)
           IF (L1.LE.NCY) THEN
             YS=CG(4,(L1-1)*NCX+1)
           ELSE
             YS=CB(4)
             L1=L1-1
           END IF
           IF ((ISURF(KS).EQ.1.AND.(YI.GT.YS.AND.Y.LT.YS)).OR.
    &          (ISURF(KS).EQ.2.AND.(YI.LT.YS.AND.Y.GT.YS))) THEN
             XC=XI+(YS-YI)*DX/DY
             IF (XC.LE.CB(1).AND.IB(1).EQ.2) THEN
               XC=2.*CB(1)-XC
               PV(1,N)=-PV(1,N)
             END IF
             IF (XC.GE.CB(2).AND.IB(2).EQ.2) THEN
               XC=2.*CB(2)-XC
               PV(1,N)=-PV(1,N)
             END IF
             L2=LIMS(KS,2)
             L3=LIMS(KS,3)
             XSU=CG(1,L2)
             XSD=CG(2,L3)
             IF (XC.GT.XSU.AND.XC.LT.XSD) THEN
               IF (IFCX.EQ.0) THEN
                 MC=(XC-CB(1))/CW+0.99999
               ELSE
                 XD=(XC-CB(1))/FW+1.E-6
                 MC=1.+(LOG(1.-XD*APX))/RPX
               END IF
               IF (MC.LT.1) MC=1
               IF (MC.GT.NCX) MC=NCX
               MCS=MC-(L2-1)
               IF (ISURF(KS).EQ.1) MC=MC+(L1-1)*NCX
               IF (ISURF(KS).EQ.2) MC=MC+(L1-2)*NCX
                                   IF(KS.GE.2)     THEN
```

```
                                        DO 34 NNN=1,KS-1
                                        MCS=MCS+LIMS(NNN,3)-LIMS(NNN,2)+1
34                                      CONTINUE
                                    END IF
          AT=AT*(Y-YS)/DY
          CALL REFLECT2(N,KS,MCS,XC,YS,MC)
          GO TO 150
         END IF
        END IF
       END IF
       IF (ISURF(KS).EQ.3.OR.ISURF(KS).EQ.4) THEN
        L1=LIMS(KS,1)
        IF (L1.LE.NCX) THEN
         XS=CG(1,L1)
        ELSE
         XS=CB(2)
         L1=L1-1
        END IF
        IF ((ISURF(KS).EQ.3.AND.(XI.GT.XS.AND.X.LT.XS)).OR.
     &      (ISURF(KS).EQ.4.AND.(XI.LT.XS.AND.X.GT.XS))) THEN
         YC=YI+(XS-XI)*DY/DX
         L2=LIMS(KS,2)
         L3=LIMS(KS,3)
         YSU=CG(4,(L2-1)*NCX+1)
         YSD=CG(5,(L3-1)*NCX+1)
         IF (YC.GT.YSU.AND.YC.LT.YSD) THEN
          IF (IFCY.EQ.0) THEN
           MC=(YC-CB(3))/CH+0.99999
          ELSE
           YD=(YC-CB(3))/FH+1.E-6
           MC=1.+(LOG(1.-YD*APY))/RPY
          END IF
          IF (MC.LT.1) MC=1
          IF (MC.GT.NCY) MC=NCY
          MCS=MC-(L2-1)
          IF (ISURF(KS).EQ.3) MC=(MC-1)*NCX+L1
          IF (ISURF(KS).EQ.4) MC=(MC-1)*NCX+L1-1
C           IF (KS.EQ.2) MCS=MCS+LIMS(1,3)-LIMS(1,2)+1
                                    IF(KS.GE.2)      THEN
                                        DO 33 NNN=1,KS-1
                                        MCS=MCS+LIMS(NNN,3)-LIMS(NNN,2)+1
33                                      CONTINUE
                                    END IF
          AT=AT*(XS-XI)/DX
          CALL REFLECT2(N,KS,MCS,XS,YC,MC)
          GO TO 150
         END IF
        END IF
       END IF
      END IF
200   CONTINUE
     IF (X.LT.CB(1).OR.X.GT.CB(2)) THEN
      IF (X.LT.CB(1)) K=1
      IF (X.GT.CB(2)) K=2
      IF (IB(K).EQ.2) THEN
       X=2.*CB(K)-X
       PV(1,N)=-PV(1,N)
      ELSE
       CALL REMOVE(N)
       GO TO 100
      END IF
     END IF
     IF (Y.LT.CB(3).OR.Y.GT.CB(4)) THEN
```

```
      IF (Y.LT.CB(3)) K=3
      IF (Y.GT.CB(4)) K=4
      IF (IB(K).EQ.2) THEN
       Y=2.*CB(K)-Y
       PV(2,N)=-PV(2,N)
      ELSE
       CALL REMOVE(N)
       GO TO 100
      END IF
     END IF
     IF (X.LT.CG(1,MC).OR.X.GT.CG(2,MC).OR.Y.LT.CG(4,MC).OR.
    &    Y.GT.CG(5,MC)) THEN
      IF (IFCX.EQ.0) THEN
       MCX=(X-CB(1))/CW+0.99999
      ELSE
       XD=(X-CB(1))/FW+1.E-6
       MCX=1.+(LOG(1.-XD*APX))/RPX
      END IF
      IF (MCX.LT.1) MCX=1
      IF (MCX.GT.NCX) MCX=NCX
      IF (IFCY.EQ.0) THEN
       MCY=(Y-CB(3))/CH+0.99999
      ELSE
       YD=(Y-CB(3))/FH+1.E-6
       MCY=1.+(LOG(1.-YD*APY))/RPY
      END IF
      IF (MCY.LT.1) MCY=1
      IF (MCY.GT.NCY) MCY=NCY
      MC=(MCY-1)*NCX+MCX
     END IF
     MSCX=((X-CG(1,MC))/CG(3,MC))*(NSCX-.001)+1
     MSCY=((Y-CG(4,MC))/CG(6,MC))*(NSCY-.001)+1
     MSC=(MSCY-1)*NSCX+MSCX+NSCX*NSCY*(MC-1)
     IF (MSC.LT.1) MSC=1
     IF (MSC.GT.MNSC) MSC=MNSC
     IPL(N)=MSC
     PP(1,N)=X
     PP(2,N)=Y
     GO TO 100
    ELSE IF (IFT.LT.0) THEN
     IFT=1
     CALL ENTER2
     N=N-1
     GO TO 100
    END IF
    RETURN
    END
*   ENTER2.FOR
    SUBROUTINE ENTER2
    INCLUDE "PARAMETER.F"
    DOUBLE PRECISION COL(MNSP,MNSP),MOVT,NCOL,SELT,SEPT,
    &                                 CS(7,MNC,MNSP),LAMD
    COMMON /MOLS2 / NM,PP(2,MNM),PV(3,MNM),IPL(MNM),IPS(MNM),IR(MNM)
    COMMON /MOLSR / PR(MNM)
    COMMON /CELL2 / CC(MNC),CG(6,MNC),IC(2,MNC,MNSG),ISC(MNSC),
    &          CCG(2,MNC,MNSG,MNSG),ISCG(2,MNSC,MNSG),IG(2,MNSG),
    &          NCX,NCY,IFCX,IFCY,CWRX,CWRY,APX,RPX,APY,RPY
    COMMON /GAS   / SP(5,MNSP),SPM(6,MNSP,MNSP),ISP(MNSP)
    COMMON /GASR  / SPR(3,MNSP,MNSP),ISPR(3,MNSP),CT(MNC)
    COMMON /CONST / PI,SPI,BOLTZ
          DOUBLE PRECISION VEL(3),SMU(3),SVEL(3,MNC),SN,SM,SMCC,SRDF,SRE,TT,
    &          TROT,DBOLTZ,SS(9)
    DBOLTZ=BOLTZ
```

```
      DO 100 N=1,4
    IF (IB(N).EQ.1) THEN
     IF (N.LT.3) NCS=NCY
     IF (N.GT.2) NCS=NCX
     DO 20 NC=1,NCS
      IF (LFLX.NE.0) THEN
       IF (N.EQ.1) THEN
        IF (LFLY.GT.0.AND.LFLX.GT.0.AND.NC.LT.LFLY) GO TO 20
        IF (LFLY.LT.0.AND.LFLX.GT.0.AND.NC.GT.LFLY) GO TO 20
       END IF
       IF (N.EQ.2) THEN
        IF (LFLY.GT.0.AND.LFLX.LT.0.AND.NC.LT.LFLY) GO TO 20
        IF (LFLY.LT.0.AND.LFLX.LT.0.AND.NC.GT.LFLY) GO TO 20
       END IF
       IF (N.EQ.3) THEN
        IF (LFLX.GT.0.AND.LFLY.GT.0.AND.NC.LT.LFLX) GO TO 20
        IF (LFLX.LT.0.AND.LFLY.GT.0.AND.NC.GT.LFLX) GO TO 20
       END IF
       IF (N.EQ.4) THEN
        IF (LFLX.GT.0.AND.LFLY.LT.0.AND.NC.LT.LFLX) GO TO 20
        IF (LFLX.LT.0.AND.LFLY.LT.0.AND.NC.GT.LFLX) GO TO 20
       END IF
      END IF
         IF (N.EQ.1) NCR=1+(NC-1)*NCX
         IF (N.EQ.2) NCR=NC*NCX
         IF (N.EQ.3) NCR=NC
         IF (N.EQ.4) NCR=NC+(NCY-1)*NCX
         IF(NSMP.GT.0.AND.NPR.GT.1) THEN
         A=FNUM/(CC(NCR)*NSMP)
    SN=0.
    SM=0.
    DO 250 K=1,3
     SMU(K)=0.
250   CONTINUE
    SMCC=0.
    SRE=0.
    SRDF=0.
    DO 300 L=1,MNSP
     SN=SN+CS(1,NCR,L)
     SM=SM+SP(5,L)*CS(1,NCR,L)
     DO 260 K=1,3
      SMU(K)=SMU(K)+SP(5,L)*CS(K+1,NCR,L)
260    CONTINUE
     SMCC=SMCC+(CS(5,NCR,L)+CS(6,NCR,L)+CS(7,NCR,L))*SP(5,L)
     SRE=SRE+CSR(NCR,L)
     SRDF=SRDF+ISPR(1,L)*CS(1,NCR,L)
     SUU=SUU+SP(5,L)*CS(5,NCR,L)
300   CONTINUE
    DENN=SN*A
    DEN=DENN*SM/SN
    DO 350 K=1,3
     VEL(K)=SMU(K)/SM
     SVEL(K,NCR)=VEL(K)
350   CONTINUE
    UU=VEL(1)**2+VEL(2)**2+VEL(3)**2
    TT=(SMCC-SM*UU)/(3.D00*DBOLTZ*SN)
    IF (SRDF.GT.1.E-6) TROT=(2.D00/DBOLTZ)*SRE/SRDF
    TEMP=(3.D00*TT+(SRDF/SN)*TROT)/(3.+SRDF/SN)
    PRESSURE=DENN*BOLTZ*TEMP
         GAMA=(5.+ISPR(1,1))/(3.+ISPR(1,1))
    AA=SQRT(GAMA*BOLTZ*TEMP/SP(5,1))
         IF (N.EQ.1) THEN
         VFX=(PIN-PRESSURE)/(DEN*AA)
```

```
            VFY=0
            FTMP=TMPIN
            FND=PIN/BOLTZ/FTMP
            END IF
            IF (N.EQ.2) THEN
            DENO=DEN+(PRESSURE-POUT)/(AA**2)
            VFX=(PRESSURE-POUT)/(DEN*AA)
            VFY=VEL(2)
            FTMP=PRESSURE/(DENO*BOLTZ/SP(5,1))
            FND=DENO/SP(5,1)
            END IF
          END IF
            DO 10 L=1,MNSP
             VMP=SQRT(2.*BOLTZ*FTMP/SP(5,L))
             IF (N.LT.3) A=BME(N,L)*CG(6,(NC-1)*NCX+1)/FH+BMR(N,L)
             IF (N.GT.2) A=BME(N,L)*CG(3,NC)/FW+BMR(N,L)
             M=A
             BMR(N,L)=A-M
             IF (M.GT.0) THEN
              IF (N.EQ.1.OR.N.EQ.2) THEN
               IF (ABS(VFX).GT.1.E-6) THEN
                IF (N.EQ.1) SC=VFX/VMP
                IF (N.EQ.2) SC=-VFX/VMP
               END IF
              END IF
              IF (N.EQ.3.OR.N.EQ.4) THEN
               IF (ABS(VFY).GT.1.E-6) THEN
                IF (N.EQ.3) SC=VFY/VMP
                IF (N.EQ.4) SC=-VFY/VMP
               END IF
              END IF
              FS1=SC+SQRT(SC*SC+2.)
              FS2=0.5*(1.+SC*(2.*SC-FS1))
              DO 4 K=1,M
               IF (NM.LT.MNM) THEN
                NM=NM+1
                IF ((N.LT.3.AND.ABS(VFX).GT.1.E-6).OR.
     &              (N.GT.2.AND.ABS(VFY).GT.1.E-6)) THEN
                 QA=3.
                 IF (SC.LT.-3.) QA=ABS(SC)+1.
2                 U=-QA+2.*QA*RF(0)
                 UN=U+SC
                 IF (UN.LT.0.) GO TO 2
                 A=(2.*UN/FS1)*EXP(FS2-U*U)
                 IF (A.LT.RF(0)) GO TO 2
                 IF (N.EQ.1) PV(1,NM)=UN*VMP
                 IF (N.EQ.2) PV(1,NM)=-UN*VMP
                 IF (N.EQ.3) PV(2,NM)=UN*VMP
                 IF (N.EQ.4) PV(2,NM)=-UN*VMP
                ELSE
                 IF (N.EQ.1) PV(1,NM)=SQRT(-LOG(RF(0)))*VMP
                 IF (N.EQ.2) PV(1,NM)=-SQRT(-LOG(RF(0)))*VMP
                 IF (N.EQ.3) PV(2,NM)=SQRT(-LOG(RF(0)))*VMP
                 IF (N.EQ.4) PV(2,NM)=-SQRT(-LOG(RF(0)))*VMP
                END IF
                IF (N.LT.3) THEN
                 CALL RVELC(PV(2,NM),PV(3,NM),VMP)
                 PV(2,NM)=PV(2,NM)+VFY
                END IF
                IF (N.GT.2) THEN
                 CALL RVELC(PV(1,NM),PV(3,NM),VMP)
                 PV(1,NM)=PV(1,NM)+VFX
                END IF
```

```
              IF (ISPR(1,L).GT.0) CALL SROT(PR(NM),FTMP,ISPR(1,L))
              IF (N.EQ.1) PP(1,NM)=CB(1)+0.001*CG(3,1)
              IF (N.EQ.2) PP(1,NM)=CB(2)-0.001*CG(3,MNC)
              IF (N.EQ.3) PP(2,NM)=CB(3)+0.001*CG(6,1)
              IF (N.EQ.4) PP(2,NM)=CB(4)-0.001*CG(6,MNC)
              IPS(NM)=L
              IF (N.LT.3) THEN
                IF (N.EQ.1) MC=(NC-1)*NCX+1
                IF (N.EQ.2) MC=NC*NCX
                PP(2,NM)=CG(4,MC)+RF(0)*CG(6,MC)
              END IF
              IF (N.GT.2) THEN
                IF (N.EQ.3) MC=NC
                IF (N.EQ.4) MC=(NCY-1)*NCX+NC
                PP(1,NM)=CG(1,MC)+RF(0)*CG(3,MC)
              END IF
              MSCX=((PP(1,NM)-CG(1,MC))/CG(3,MC))*(NSCX-.001)+1
              MSCY=((PP(2,NM)-CG(4,MC))/CG(6,MC))*(NSCY-.001)+1
              MSC=(MSCY-1)*NSCX+MSCX+NSCX*NSCY*(MC-1)
              IF (MSC.LT.1) MSC=1
              IF (MSC.GT.MNSC) MSC=MNSC
              IPL(NM)=MSC
            ELSE
              WRITE (*,*)
     &' WARNING: EXCESS MOLECULE LIMIT - RESTART WITH AN INCREASED FNUM'
            END IF
4           CONTINUE
          END IF
10        CONTINUE
20      CONTINUE
      END IF
100   CONTINUE
      IF (IJET.GT.0) THEN
        NCS=LIMJ(3)-LIMJ(2)+1
        DO 150 NC=1,NCS
          DO 120 L=1,MNSP
            VMP=SQRT(2.*BOLTZ*TMPJ/SP(5,L))
            NCL=NC+LIMJ(2)-1
            IF (IJET.LT.3) A=BMEJ(L)*CG(3,NCL)/WJ+BMRJ(L)
            IF (IJET.GT.2) A=BMEJ(L)*CG(6,(NCL-1)*NCX+1)/WJ+BMRJ(L)
            M=A
            BMRJ(L)=A-M
            IF (M.GT.0) THEN
              IF (ABS(FVJ).GT.1.E-6) SC=FVJ/VMP
              FS1=SC+SQRT(SC*SC+2.)
              FS2=0.5*(1.+SC*(2.*SC-FS1))
              DO 105 K=1,M
                IF (NM.LT.MNM) THEN
                  NM=NM+1
                  IF (ABS(FVJ).GT.1.E-6) THEN
                    QA=3.
                    IF (SC.LT.-3.) QA=ABS(SC)+1.
102                   U=-QA+2.*QA*RF(0)
                    UN=U+SC
                    IF (UN.LT.0.) GO TO 102
                    A=(2.*UN/FS1)*EXP(FS2-U*U)
                    IF (A.LT.RF(0)) GO TO 102
                    IF (IJET.EQ.1) PV(2,NM)=UN*VMP
                    IF (IJET.EQ.2) PV(2,NM)=-UN*VMP
                    IF (IJET.EQ.3) PV(1,NM)=UN*VMP
                    IF (IJET.EQ.4) PV(1,NM)=-UN*VMP
                  ELSE
                    IF (IJET.EQ.1) PV(2,NM)=SQRT(-LOG(RF(0)))*VMP
```

```
            IF (IJET.EQ.2) PV(2,NM)=-SQRT(-LOG(RF(0)))*VMP
            IF (IJET.EQ.3) PV(1,NM)=SQRT(-LOG(RF(0)))*VMP
            IF (IJET.EQ.4) PV(1,NM)=-SQRT(-LOG(RF(0)))*VMP
           END IF
           IF (IJET.LT.3) CALL RVELC(PV(1,NM),PV(3,NM),VMP)
           IF (IJET.GT.2) CALL RVELC(PV(2,NM),PV(3,NM),VMP)
           IF (ISPR(1,L).GT.0) CALL SROT(PR(NM),TMPJ,ISPR(1,L))
           IF (IJET.LT.3) THEN
            MC=(LIMJ(1)-1)*NCX+LIMJ(2)-1+NC
            YJ=CG(4,MC)
            IF (IJET.EQ.2) MC=MC-NCX
           END IF
           IF (IJET.GT.2) THEN
            MC=LIMJ(1)+(LIMJ(2)-1)*NCX+(NC-1)*NCX
            XJ=CG(1,MC)
            IF (IJET.EQ.4) MC=MC-1
           END IF
           IF (IJET.EQ.1) PP(2,NM)=YJ+0.001*CG(6,MC)
           IF (IJET.EQ.2) PP(2,NM)=YJ-0.001*CG(6,MC)
           IF (IJET.EQ.3) PP(1,NM)=XJ+0.001*CG(3,MC)
           IF (IJET.EQ.4) PP(1,NM)=XJ-0.001*CG(3,MC)
           IPS(NM)=L
           IF (IJET.LT.3) PP(1,NM)=CG(1,MC)+RF(0)*CG(3,MC)
           IF (IJET.GT.2) PP(2,NM)=CG(4,MC)+RF(0)*CG(6,MC)
           MSCX=((PP(1,NM)-CG(1,MC))/CG(3,MC))*(NSCX-.001)+1
           MSCY=((PP(2,NM)-CG(4,MC))/CG(6,MC))*(NSCY-.001)+1
           MSC=(MSCY-1)*NSCX+MSCX+NSCX*NSCY*(MC-1)
           IF (MSC.LT.1) MSC=1
           IF (MSC.GT.MNSC) MSC=MNSC
           IPL(NM)=MSC
          ELSE
           WRITE (*,*)
  &' WARNING: EXCESS MOLECULE LIMIT - RESTART WITH AN INCREASED FNUM'
          END IF
105        CONTINUE
        END IF
120     CONTINUE
150    CONTINUE
    END IF
    RETURN
    END
*   REFLECT2.FOR
    SUBROUTINE REFLECT2(N,KS,K,XC,YC,MC)
    INCLUDE "PARAMETER.F"
    DOUBLE PRECISION COL(MNSP,MNSP),MOVT,NCOL,SELT,SEPT,
   &                                 CS(7,MNC,MNSP),LAMD
    DOUBLE PRECISION CSS(9,MNSE,MNSP)
    COMMON /MOLS2 / NM,PP(2,MNM),PV(3,MNM),IPL(MNM),IPS(MNM),IR(MNM)
    COMMON /MOLSR / PR(MNM)
    COMMON /CELL2 / CC(MNC),CG(6,MNC),IC(2,MNC,MNSG),ISC(MNSC),
   &          CCG(2,MNC,MNSG,MNSG),ISCG(2,MNSC,MNSG),IG(2,MNSG),
   &          NCX,NCY,IFCX,IFCY,CWRX,CWRY,APX,RPX,APY,RPY
    COMMON /GAS   / SP(5,MNSP),SPM(6,MNSP,MNSP),ISP(MNSP)
    COMMON /GASR  / SPR(3,MNSP,MNSP),ISPR(3,MNSP),CT(MNC)
    COMMON /SAMPS / CSS
    COMMON /CONST / PI,SPI,BOLTZ
        L=IPS(N)
    CSS(1,K,L)=CSS(1,K,L)+1.
    IF (ISURF(KS).EQ.1) THEN
     CSS(2,K,L)=CSS(2,K,L)-SP(5,L)*PV(2,N)
     CSS(4,K,L)=CSS(4,K,L)+SP(5,L)*PV(1,N)
    END IF
    IF (ISURF(KS).EQ.2) THEN
```

```
      CSS(2,K,L)=CSS(2,K,L)+SP(5,L)*PV(2,N)
      CSS(4,K,L)=CSS(4,K,L)+SP(5,L)*PV(1,N)
    END IF
    IF (ISURF(KS).EQ.3) THEN
      CSS(2,K,L)=CSS(2,K,L)-SP(5,L)*PV(1,N)
      CSS(4,K,L)=CSS(4,K,L)+SP(5,L)*PV(2,N)
    END IF
    IF (ISURF(KS).EQ.4) THEN
      CSS(2,K,L)=CSS(2,K,L)+SP(5,L)*PV(1,N)
      CSS(4,K,L)=CSS(4,K,L)+SP(5,L)*PV(2,N)
    END IF
    CSS(5,K,L)=CSS(5,K,L)+0.5*SP(5,L)
   &          *(PV(1,N)**2+PV(2,N)**2+PV(3,N)**2)
    CSS(7,K,L)=CSS(7,K,L)+PR(N)
    IF (TSURF(KS).LT.0.) THEN
      IF (ISURF(KS).EQ.1.OR.ISURF(KS).EQ.2) PV(2,N)=-PV(2,N)
      IF (ISURF(KS).EQ.3.OR.ISURF(KS).EQ.4) PV(1,N)=-PV(1,N)
    ELSE IF (ALPI(KS).LT.0.) THEN
      VMP=SQRT(2.*BOLTZ*TSURF(KS)/SP(5,L))
      IF (ISURF(KS).EQ.1) THEN
        PV(2,N)=SQRT(-LOG(RF(0)))*VMP
        CALL RVELC(PV(1,N),PV(3,N),VMP)
      END IF
      IF (ISURF(KS).EQ.2) THEN
        PV(2,N)=-SQRT(-LOG(RF(0)))*VMP
        CALL RVELC(PV(1,N),PV(3,N),VMP)
      END IF
      IF (ISURF(KS).EQ.3) THEN
        PV(1,N)=SQRT(-LOG(RF(0)))*VMP
        CALL RVELC(PV(2,N),PV(3,N),VMP)
      END IF
      IF (ISURF(KS).EQ.4) THEN
        PV(1,N)=-SQRT(-LOG(RF(0)))*VMP
        CALL RVELC(PV(2,N),PV(3,N),VMP)
      END IF
      IF (ISPR(1,L).GT.0) CALL SROT(PR(N),TSURF(KS),ISPR(1,L))
    ELSE IF (ALPI(KS).GE.0) THEN
      VMP=SQRT(2.*BOLTZ*TSURF(KS)/SP(5,L))
      IF (ISURF(KS).EQ.1.OR.ISURF(KS).EQ.2) THEN
        IF (ISURF(KS).EQ.1) VNI=-PV(2,N)/VMP
        IF (ISURF(KS).EQ.2) VNI=PV(2,N)/VMP
        UPI=PV(1,N)/VMP
      END IF
      IF (ISURF(KS).EQ.3.OR.ISURF(KS).EQ.4) THEN
        IF (ISURF(KS).EQ.3) VNI=-PV(1,N)/VMP
        IF (ISURF(KS).EQ.4) VNI=PV(1,N)/VMP
        UPI=PV(2,N)/VMP
      END IF
      WPI=PV(3,N)/VMP
      ANG=ATAN2(WPI,UPI)
      VPI=SQRT(UPI*UPI+WPI*WPI)
      ALPHAN=ALPN(KS)
      R=SQRT(-ALPHAN*LOG(RF(0)))
      TH=2.*PI*RF(0)
      UM=SQRT(1.-ALPHAN)*VNI
      VN=SQRT(R*R+UM*UM+2.*R*UM*COS(TH))
      ALPHAT=ALPT(KS)*(2.-ALPT(KS))
      R=SQRT(-ALPHAT*LOG(RF(0)))
      TH=2.*PI*RF(0)
      UM=SQRT(1.-ALPHAT)*VPI
      VP=UM+R*COS(TH)
      WP=R*SIN(TH)
      IF (ISURF(KS).EQ.1.OR.ISURF(KS).EQ.2) THEN
```

```
      IF (ISURF(KS).EQ.1) PV(2,N)=VN*VMP
      IF (ISURF(KS).EQ.2) PV(2,N)=-VN*VMP
      PV(1,N)=(VP*COS(ANG)-WP*SIN(ANG))*VMP
     END IF
     IF (ISURF(KS).EQ.3.OR.ISURF(KS).EQ.4) THEN
      IF (ISURF(KS).EQ.3) PV(1,N)=VN*VMP
      IF (ISURF(KS).EQ.4) PV(1,N)=-VN*VMP
      PV(2,N)=(VP*COS(ANG)-WP*SIN(ANG))*VMP
     END IF
     PV(3,N)=(VP*SIN(ANG)+WP*COS(ANG))*VMP
     IF (ISPR(1,L).GT.0) THEN
                 ALPHAI=ALPI(KS)
                 OM=SQRT(PR(N)*(1.-ALPHAI)/(BOLTZ*TSURF(KS)))
      IF (ISPR(1,L).EQ.2) THEN
                  R=SQRT(-ALPHAI*LOG(RF(0)))
       CTH=COS(2.*PI*RF(0))
      ELSE
10      X=4.*RF(0)
       A=2.7182818*X*X*EXP(-X*X)
       IF (A.LT.RF(0)) GO TO 10
       R=SQRT(ALPHAI)*X
       CTH=2.*RF(0)-1.
      END IF
      PR(N)=BOLTZ*TSURF(KS)*(R*R+OM*OM+2.*R*OM*CTH)
     END IF
    END IF
    IF (ISURF(KS).EQ.1) THEN
     PP(1,N)=XC
     PP(2,N)=YC+0.001*CG(6,MC)
    END IF
    IF (ISURF(KS).EQ.2) THEN
     PP(1,N)=XC
     PP(2,N)=YC-0.001*CG(6,MC)
    END IF
    IF (ISURF(KS).EQ.3) THEN
     PP(1,N)=XC+0.001*CG(3,MC)
     PP(2,N)=YC
    END IF
    IF (ISURF(KS).EQ.4) THEN
     PP(1,N)=XC-0.001*CG(3,MC)
     PP(2,N)=YC
    END IF
    IPL(N)=(MC-1)*NSCX*NSCY+1
    IF (ISURF(KS).EQ.1) CSS(3,K,L)=CSS(3,K,L)+SP(5,L)*PV(2,N)
    IF (ISURF(KS).EQ.2) CSS(3,K,L)=CSS(3,K,L)-SP(5,L)*PV(2,N)
    IF (ISURF(KS).EQ.3) CSS(3,K,L)=CSS(3,K,L)+SP(5,L)*PV(1,N)
    IF (ISURF(KS).EQ.4) CSS(3,K,L)=CSS(3,K,L)-SP(5,L)*PV(1,N)
    IF (ISURF(KS).EQ.1) CSS(9,K,L)=CSS(9,K,L)-SP(5,L)*PV(1,N)
    IF (ISURF(KS).EQ.2) CSS(9,K,L)=CSS(9,K,L)-SP(5,L)*PV(1,N)
    IF (ISURF(KS).EQ.3) CSS(9,K,L)=CSS(9,K,L)-SP(5,L)*PV(2,N)
    IF (ISURF(KS).EQ.4) CSS(9,K,L)=CSS(9,K,L)-SP(5,L)*PV(2,N)
    CSS(6,K,L)=CSS(6,K,L)-0.5*SP(5,L)
   &         *(PV(1,N)**2+PV(2,N)**2+PV(3,N)**2)
    CSS(8,K,L)=CSS(8,K,L)-PR(N)
    RETURN
    END
*   REMOVE.FOR
    SUBROUTINE REMOVE(N)
    INCLUDE "PARAMETER.F"
    COMMON /MOLS2 / NM,PP(2,MNM),PV(3,MNM),IPL(MNM),IPS(MNM),IR(MNM)
    COMMON /MOLSR / PR(MNM)
    PP(1,N)=PP(1,NM)
    PP(2,N)=PP(2,NM)
```

```
      DO 100 M=1,3
       PV(M,N)=PV(M,NM)
100   CONTINUE
      PR(N)=PR(NM)
      IPL(N)=IPL(NM)
      IPS(N)=IPS(NM)
      NM=NM-1
      N=N-1
      RETURN
      END
*     SAMPI2.FOR
      SUBROUTINE SAMPI2
      INCLUDE "PARAMETER.F"
      DOUBLE PRECISION COL(MNSP,MNSP),MOVT,NCOL,SELT,SEPT,
     &                                 CS(7,MNC,MNSP),LAMD
      DOUBLE PRECISION CSS(9,MNSE,MNSP)
      COMMON /SAMPS / CSS
      NSMP=0
      TIMI=TIME
      DO 200 L=1,MNSP
       DO 50 N=1,MNC
        CS(1,N,L)=1.E-6
        DO 20 M=2,7
         CS(M,N,L)=0.
20      CONTINUE
        CSR(N,L)=0.
50     CONTINUE
       DO 100 N=1,MNSE
        CSS(1,N,L)=1.E-6
        DO 60 M=2,9
         CSS(M,N,L)=0.
60      CONTINUE
100    CONTINUE
200   CONTINUE
      RETURN
      END
*     SAMPLE2.FOR
      SUBROUTINE SAMPLE2
      INCLUDE "PARAMETER.F"
      DOUBLE PRECISION COL(MNSP,MNSP),MOVT,NCOL,SELT,SEPT,
     &                                 CS(7,MNC,MNSP),LAMD
      COMMON /MOLS2 / NM,PP(2,MNM),PV(3,MNM),IPL(MNM),IPS(MNM),IR(MNM)
      COMMON /MOLSR / PR(MNM)
      COMMON /CELL2 / CC(MNC),CG(6,MNC),IC(2,MNC,MNSG),ISC(MNSC),
     &          CCG(2,MNC,MNSG,MNSG),ISCG(2,MNSC,MNSG),IG(2,MNSG),
     &          NCX,NCY,IFCX,IFCY,CWRX,CWRY,APX,RPX,APY,RPY
      NSMP=NSMP+1
      DO 100 NN=1,MNSG
       DO 50 N=1,MNC
        L=IC(2,N,NN)
        IF (L.GT.0) THEN
         DO 10 J=1,L
          K=IC(1,N,NN)+J
          M=IR(K)
          I=IPS(M)
          CS(1,N,I)=CS(1,N,I)+1
          DO 5 LL=1,3
           CS(LL+1,N,I)=CS(LL+1,N,I)+PV(LL,M)
           CS(LL+4,N,I)=CS(LL+4,N,I)+PV(LL,M)**2
5         CONTINUE
          CSR(N,I)=CSR(N,I)+PR(M)
10       CONTINUE
        END IF
```

```
50    CONTINUE
100  CONTINUE
     RETURN
     END
*  OUT2.FOR
     SUBROUTINE OUT2
     INCLUDE "PARAMETER.F"
     DOUBLE PRECISION COL(MNSP,MNSP),MOVT,NCOL,SELT,SEPT,
    &                                 CS(7,MNC,MNSP),LAMD
     DOUBLE PRECISION CSS(9,MNSE,MNSP)
     COMMON /MOLS2 / NM,PP(2,MNM),PV(3,MNM),IPL(MNM),IPS(MNM),IR(MNM)
     COMMON /MOLSR / PR(MNM)
     COMMON /CELL2 / CC(MNC),CG(6,MNC),IC(2,MNC,MNSG),ISC(MNSC),
    &          CCG(2,MNC,MNSG,MNSG),ISCG(2,MNSC,MNSG),IG(2,MNSG),
    &          NCX,NCY,IFCX,IFCY,CWRX,CWRY,APX,RPX,APY,RPY
     COMMON /GAS   / SP(5,MNSP),SPM(6,MNSP,MNSP),ISP(MNSP)
     COMMON /GASR  / SPR(3,MNSP,MNSP),ISPR(3,MNSP),CT(MNC)
     COMMON /SAMPS / CSS
     COMMON /CONST / PI,SPI,BOLTZ
     DOUBLE PRECISION VEL(3),SMU(3),SVEL(3,MNC),SN,SM,SMCC,SRDF,SRE,TT,
    &          TROT,DBOLTZ,SS(9)
     DBOLTZ=BOLTZ
     OPEN (4,FILE='DSMC2.OUT',FORM='FORMATTED')
     WRITE (4,*) ' FLOW SAMPLED FROM TIME ',TIMI,' TO TIME ',TIME
     WRITE (4,*) ' COLLISIONS:-'
     WRITE (4,99001) ((IDINT(COL(M,L)),M=1,MNSP),L=1,MNSP)
99001 FORMAT (5I12)
     WRITE (4,*) ' TOTAL NUMBER OF SAMPLES ',NSMP
     WRITE (4,*) NM,' MOLECULES'
     WRITE (4,*) MOVT,' TOTAL MOLECULAR MOVES'
     IF (NCOL.GT.0) THEN
      WRITE (4,*) INT(SELT),' SELECTIONS ',INT(NCOL),
    &       ' COLLISION EVENTS, RATIO  ',REAL(NCOL/SELT)
      IF (NCOL.GT.0) WRITE (4,*) ' MEAN COLLISION SEPARATION ',
    &                  REAL(SEPT/NCOL)
     END IF
     WRITE (4,*)
     DO 100 KS=1,NFACE
      IF (ISURF(KS).GT.0) THEN
       WRITE (4,*) ' SURFACE ',KS
       WRITE (4,*)
       NEL=LIMS(KS,3)-LIMS(KS,2)+1
       IF (KS.EQ.1) THEN
        NEL1=1
        NEL2=NEL
       ELSE
        NEL1=LIMS(1,3)-LIMS(1,2)+2
        NEL2=NEL1+NEL-1
       END IF
       A=FNUM/(TIME-TIMI)
       WRITE (4,*)
    &'  X COORD    Y COORD     SAMPLE  FRACTION SPECIES 1,  SPECIES2
    &....'
       DO 20 K=NEL1,NEL2
        IF (ISURF(KS).LT.3) THEN
         IF (LIMS(KS,1).LE.NCY) THEN
          NC=(LIMS(KS,1)-1)*NCX+1
          Y=CG(4,NC)
         ELSE
          Y=CB(4)
         END IF
         NC=LIMS(KS,2)+K-NEL1
         X=0.5*(CG(1,NC)+CG(2,NC))
```

```
        END IF
        IF (ISURF(KS).GT.2) THEN
         IF (LIMS(KS,1).LE.NCX) THEN
          X=CG(1,LIMS(KS,1))
         ELSE
          X=CB(2)
         END IF
         NC=(LIMS(KS,2)+K-NEL1-1)*NCX+1
         Y=0.5*(CG(4,NC)+CG(5,NC))
        END IF
        SS(1)=0.
        DO 10 L=1,MNSP
         SS(1)=SS(1)+CSS(1,K,L)
10       CONTINUE
        WRITE (4,99002) X,Y,SS(1),(CSS(1,K,L)/SS(1),L=1,MNSP)
99002     FORMAT (2F12.5,F12.1,6F12.6)
20      CONTINUE
       WRITE (4,*)
   &' X COORD   Y COORD   NUM FLUX  INC PRESS  REFL PRESS   INCS
   &H STR  REFL SH STR INC TR EN  REFL TR EN  INC ROT EN  REFL ROTEN
   &NET HEAT FLUX'
      DO 60 K=NEL1,NEL2
       IF (ISURF(KS).LT.3) THEN
        IF (LIMS(KS,1).LE.NCY) THEN
         NC=(LIMS(KS,1)-1)*NCX+1
         Y=CG(4,NC)
        ELSE
         Y=CB(4)
        END IF
        NC=LIMS(KS,2)+K-NEL1
        X=0.5*(CG(1,NC)+CG(2,NC))
        AR=CG(3,NC)
       END IF
       IF (ISURF(KS).GT.2) THEN
        IF (LIMS(KS,1).LE.NCX) THEN
         X=CG(1,LIMS(KS,1))
        ELSE
         X=CB(2)
        END IF
        NC=(LIMS(KS,2)+K-NEL1-1)*NCX+1
        Y=0.5*(CG(4,NC)+CG(5,NC))
        AR=CG(6,NC)
       END IF
       DO 30 N=1,9
        SS(N)=0.
        DO 25 L=1,MNSP
         SS(N)=SS(N)+CSS(N,K,L)
25       CONTINUE
30      CONTINUE
       DO 40 N=1,9
        SS(N)=SS(N)*A/AR
40      CONTINUE
       WRITE (4,99003) X,Y,(SS(N),N=1,4),SS(9),SS(5),SS(6),SS(7),
   &              SS(8),SS(5)+SS(6)+SS(7)+SS(8)
99003    FORMAT (14E12.5)
60     CONTINUE
     END IF
100  CONTINUE
    WRITE (4,*) ' FLOWFIELD PROPERTIES '
    WRITE (4,*) 'SAMPLES'
    WRITE (4,*) ' CELL    N SP 1   N SP 2    ETC '
    DO 200 N=1,MNC
     XC=0.5*(CG(1,N)+CG(2,N))
```

```
      YC=0.5*(CG(4,N)+CG(5,N))
      WRITE (4,99004) XC,YC,(IDINT(CS(1,N,L)),L=1,MNSP)
200   CONTINUE
99004 FORMAT (' ',2F9.4,5I9)
     OPEN(24,FILE='TECDA1.DAT')
          OPEN(25,FILE='SP1.DAT')
     OPEN(26,FILE='SP2.DAT')
          WRITE(24,*)       'VARIABLES="X","Y","U","V","TEMP","PRES"'
          WRITE(24,*)       'ZONE F=POINT, I=',NCX, ',J=',NCY
          WRITE(25,*)       'VARIABLES="X","Y","DEN1"'
          WRITE(25,*)       'ZONE F=POINT, I=',NCX, ',J=',NCY
     WRITE(26,*)  'VARIABLES="X","Y","DEN2"'
          WRITE(26,*)       'ZONE F=POINT, I=',NCX, ',J=',NCY
          WRITE (4,*) ' FLOWFIELD PROPERTIES'
     WRITE (4,*)
    &' CELL   X COORD   Y COORD    DENSITY    TR TEMP   ROT TEMP   OVT
    &EMP    U        V        W'
     DO 400 N=1,MNC
      A=FNUM/(CC(N)*NSMP)
      SN=0.
      SM=0.
      DO 250 K=1,3
       SMU(K)=0.
250    CONTINUE
      SMCC=0.
      SRE=0.
      SRDF=0.
      DO 300 L=1,MNSP
       SN=SN+CS(1,N,L)
       SM=SM+SP(5,L)*CS(1,N,L)
       DO 260 K=1,3
        SMU(K)=SMU(K)+SP(5,L)*CS(K+1,N,L)
260     CONTINUE
       SMCC=SMCC+(CS(5,N,L)+CS(6,N,L)+CS(7,N,L))*SP(5,L)
       SRE=SRE+CSR(N,L)
       SRDF=SRDF+ISPR(1,L)*CS(1,N,L)
       SUU=SUU+SP(5,L)*CS(5,N,L)
300    CONTINUE
      DENN=SN*A
      DEN=DENN*SM/SN
      DO 350 K=1,3
       VEL(K)=SMU(K)/SM
       SVEL(K,N)=VEL(K)
350    CONTINUE
      UU=VEL(1)**2+VEL(2)**2+VEL(3)**2
      TT=(SMCC-SM*UU)/(3.D00*DBOLTZ*SN)
      IF (SRDF.GT.1.E-6) TROT=(2.D00/DBOLTZ)*SRE/SRDF
      TEMP=(3.D00*TT+(SRDF/SN)*TROT)/(3.+SRDF/SN)
           PRESSURE=DENN*BOLTZ*TEMP
      CT(N)=TEMP
      XC=0.5*(CG(1,N)+CG(2,N))
      YC=0.5*(CG(4,N)+CG(5,N))
      WRITE (4,99005) N,XC,YC,DEN,TT,TROT,TEMP,VEL(1),VEL(2),VEL(3)
99005  FORMAT (' ',I5,2F10.4,1P,E12.4,0P,6F10.4,2E12.4)
           WRITE(24,*)       XC,YC,VEL(1),VEL(2),TEMP,PRESSURE
400   CONTINUE
           CLOSE(24)
     WRITE (4,*)
     DO 500 L=1,MNSP
      WRITE (4,*) ' SPECIES ',L
      WRITE (4,*)
    &' CELL   X COORD   Y COORD   N DENS    DENSITY    TTX      TTY
    &     T     TZ    TR TEMP   ROT TEMP    TEMP   U DIF VEL V DIF VEL
```

```
   & W DIF VEL '
     DO 450 N=1,MNC
       A=FNUM/(CC(N)*NSMP)
       DENN=CS(1,N,L)*A
       DEN=SP(5,L)*DENN
       DO 420 K=1,3
         VEL(K)=CS(K+1,N,L)/CS(1,N,L)
*--VEL defines the average velocity of the species L molecules
420      CONTINUE
       UU=VEL(1)**2+VEL(2)**2+VEL(3)**2
       TTX=(SP(5,L)/DBOLTZ)*(CS(5,N,L)/CS(1,N,L)-VEL(1)**2)
       TTY=(SP(5,L)/DBOLTZ)*(CS(6,N,L)/CS(1,N,L)-VEL(2)**2)
       TTZ=(SP(5,L)/DBOLTZ)*(CS(7,N,L)/CS(1,N,L)-VEL(3)**2)
       TT=(SP(5,L)/(3.D00*DBOLTZ))
   &      *((CS(5,N,L)+CS(6,N,L)+CS(7,N,L))/CS(1,N,L)-UU)

       IF (ISPR(1,L).GT.0) THEN
         TROT=2.D00*CSR(N,L)/(ISPR(1,L)*DBOLTZ*CS(1,N,L))
       ELSE
         TROT=0.
       END IF
       TEMP=(3.D00*TT+ISPR(1,L)*TROT)/(3.+ISPR(1,L))
       DO 440 K=1,3
         VEL(K)=VEL(K)-SVEL(K,N)
440      CONTINUE
       XC=0.5*(CG(1,N)+CG(2,N))
       YC=0.5*(CG(4,N)+CG(5,N))
       WRITE (4,99006) N,XC,YC,DENN,DEN,TTX,TTY,TTZ,TT,TROT,TEMP,
   &                   VEL(1),VEL(2),VEL(3)
99006    FORMAT (' ',I5,2F9.4,1P,2E12.4,0P,9F10.4)
    IF (L.EQ.1) THEN
           WRITE(25,*)       XC,YC,DEN
           ELSE
           WRITE(26,*) XC,YC,DEN
           END IF
450    CONTINUE
500  CONTINUE
    CLOSE(25)
           CLOSE(26)
    CLOSE (4)
C---FLOWRATE
           OPEN (27,FILE='FLOWRATE.TXT')
           WRITE (27,*) ' FLOWFIELD PROPERTIES'
    FLOWRATE=0.
    DO 401 N=1,NCY
     NCR=100+(N-1)*NCX
           A=FNUM/(CC(NCR)*NSMP)
     SN=0.
     SM=0.
     DO 251 K=1,3
      SMU(K)=0.
251    CONTINUE
     SMCC=0.
     SRE=0.
     SRDF=0.
     DO 301 L=1,MNSP
      SN=SN+CS(1,NCR,L)
      SM=SM+SP(5,L)*CS(1,NCR,L)
      DO 261 K=1,3
       SMU(K)=SMU(K)+SP(5,L)*CS(K+1,NCR,L)
261     CONTINUE
      SMCC=SMCC+(CS(5,NCR,L)+CS(6,NCR,L)+CS(7,NCR,L))*SP(5,L)
      SRE=SRE+CSR(NCR,L)
```

```
      SRDF=SRDF+ISPR(1,L)*CS(1,NCR,L)
      SUU=SUU+SP(5,L)*CS(5,NCR,L)
301   CONTINUE
     DENN=SN*A
     DEN=DENN*SM/SN
     DO 351 K=1,3
      VEL(K)=SMU(K)/SM
      SVEL(K,NCR)=VEL(K)
351   CONTINUE
     UU=VEL(1)**2+VEL(2)**2+VEL(3)**2
     TT=(SMCC-SM*UU)/(3.D00*DBOLTZ*SN)
     IF (SRDF.GT.1.E-6) TROT=(2.D00/DBOLTZ)*SRE/SRDF
     TEMP=(3.D00*TT+(SRDF/SN)*TROT)/(3.+SRDF/SN)
          PRESSURE=DENN*BOLTZ*TEMP
     WRITE(27,*) DEN,VEL(1),PRESSURE
          FLOWRATE=FLOWRATE+DEN*VEL(1)
401  CONTINUE
    WRITE(27,*)  FLOWRATE
         CLOSE(27)
    RETURN
    END
*   SROT.FOR
    SUBROUTINE SROT(PR,TEMP,IDF)
    COMMON /CONST / PI,SPI,BOLTZ
    IF (IDF.EQ.2) THEN
     PR=-LOG(RF(0))*BOLTZ*TEMP
    ELSE
     A=0.5*IDF-1.
50    ERM=RF(0)*10.
     B=((ERM/A)**A)*EXP(A-ERM)
     IF (B.LT.RF(0)) GO TO 50
     PR=ERM*BOLTZ*TEMP
    END IF
    RETURN
    END
*   ERF.FOR
    FUNCTION ERF(S)
    B=ABS(S)
    IF (B.GT.4.) THEN
     D=1.
    ELSE
     C=EXP(-B*B)
     T=1./(1.+0.3275911*B)
     D=1.-(0.254829592*T-0.284496736*T*T+1.421413741*T*T*T-
   &   1.453152027*T*T*T*T+1.061405429*T*T*T*T*T)*C
    END IF
    IF (S.LT.0.) D=-D
    ERF=D
    RETURN
    END
*   INDEXM.FOR
    SUBROUTINE INDEXM
    INCLUDE "PARAMETER.F"
    COMMON /MOLS2 / NM,PP(2,MNM),PV(3,MNM),IPL(MNM),IPS(MNM),IR(MNM)
    COMMON /CELL2 / CC(MNC),CG(6,MNC),IC(2,MNC,MNSG),ISC(MNSC),
   &            CCG(2,MNC,MNSG,MNSG),ISCG(2,MNSC,MNSG),IG(2,MNSG),
   &            NCX,NCY,IFCX,IFCY,CWRX,CWRY,APX,RPX,APY,RPY
    COMMON /GAS   / SP(5,MNSP),SPM(6,MNSP,MNSP),ISP(MNSP)
    DO 200 MM=1,MNSG
     IG(2,MM)=0
     DO 50 NN=1,MNC
      IC(2,NN,MM)=0
50    CONTINUE
```

```
      DO 100 NN=1,MNSC
       ISCG(2,NN,MM)=0
100    CONTINUE
200   CONTINUE
      DO 300 N=1,NM
       LS=IPS(N)
       MG=ISP(LS)
       IG(2,MG)=IG(2,MG)+1
       MSC=IPL(N)
       ISCG(2,MSC,MG)=ISCG(2,MSC,MG)+1
       MC=ISC(MSC)
       IC(2,MC,MG)=IC(2,MC,MG)+1
300   CONTINUE
      M=0
      DO 400 L=1,MNSG
       IG(1,L)=M
       M=M+IG(2,L)
400   CONTINUE
      DO 600 L=1,MNSG
       M=IG(1,L)
       DO 450 N=1,MNC
        IC(1,N,L)=M
        M=M+IC(2,N,L)
450    CONTINUE
       M=IG(1,L)
       DO 500 N=1,MNSC
        ISCG(1,N,L)=M
        M=M+ISCG(2,N,L)
        ISCG(2,N,L)=0
500    CONTINUE
600   CONTINUE
      DO 700 N=1,NM
       LS=IPS(N)
       MG=ISP(LS)
       MSC=IPL(N)
       ISCG(2,MSC,MG)=ISCG(2,MSC,MG)+1
       K=ISCG(1,MSC,MG)+ISCG(2,MSC,MG)
       IR(K)=N
700   CONTINUE
      RETURN
      END
*     SELECT.FOR
      SUBROUTINE SELECT
      INCLUDE "PARAMETER.F"
      COMMON /MOLS2 / NM,PP(2,MNM),PV(3,MNM),IPL(MNM),IPS(MNM),IR(MNM)
      COMMON /CELL2 / CC(MNC),CG(6,MNC),IC(2,MNC,MNSG),ISC(MNSC),
     &                CCG(2,MNC,MNSG,MNSG),ISCG(2,MNSC,MNSG),IG(2,MNSG),
     &                NCX,NCY,IFCX,IFCY,CWRX,CWRY,APX,RPX,APY,RPY
      COMMON /GAS   / SP(5,MNSP),SPM(6,MNSP,MNSP),ISP(MNSP)
      COMMON /CONST / PI,SPI,BOLTZ
      COMMON /ELAST / VRC(3),VRR,VR,L,M,LS,MS,CVR,MM,NN,N
      K=INT(RF(0)*(IC(2,N,NN)-0.001))+IC(1,N,NN)+1
      L=IR(K)
100   MSC=IPL(L)
      IF ((NN.EQ.MM.AND.ISCG(2,MSC,MM).EQ.1).OR.
     &   (NN.NE.MM.AND.ISCG(2,MSC,MM).EQ.0)) THEN
       NST=1
       NSG=1
150     INC=NSG*NST
       NSG=-NSG
       NST=NST+1
       MSC=MSC+INC
       IF (MSC.LT.1.OR.MSC.GT.MNSC) GO TO 150
```

```
      IF (ISC(MSC).NE.N.OR.ISCG(2,MSC,MM).LT.1) GO TO 150
     END IF
     K=INT(RF(0)*(ISCG(2,MSC,MM)-0.001))+ISCG(1,MSC,MM)+1
     M=IR(K)
     IF (L.EQ.M) GO TO 100
     DO 200 K=1,3
      VRC(K)=PV(K,L)-PV(K,M)
200  CONTINUE
     VRR=VRC(1)**2+VRC(2)**2+VRC(3)**2
     VR=SQRT(VRR)
     LS=IPS(L)
     MS=IPS(M)
     CVR=VR*SPM(1,LS,MS)*((2.*BOLTZ*SPM(2,LS,MS)/(SPM(5,LS,MS)*VRR))
    &    **(SPM(3,LS,MS)-0.5))/SPM(6,LS,MS)
     RETURN
     END
*    ELASTIC.FOR
     SUBROUTINE ELASTIC
     INCLUDE "PARAMETER.F"
     COMMON /MOLS2 / NM,PP(2,MNM),PV(3,MNM),IPL(MNM),IPS(MNM),IR(MNM)
     COMMON /GAS   / SP(5,MNSP),SPM(6,MNSP,MNSP),ISP(MNSP)
     COMMON /CONST / PI,SPI,BOLTZ
     COMMON /ELAST / VRC(3),VRR,VR,L,M,LS,MS,CVR,MM,NN,N
     DIMENSION VRCP(3),VCCM(3)
     RML=SPM(5,LS,MS)/SP(5,MS)
     RMM=SPM(5,LS,MS)/SP(5,LS)
     DO 100 K=1,3
      VCCM(K)=RML*PV(K,L)+RMM*PV(K,M)
100  CONTINUE
     IF (ABS(SPM(4,LS,MS)-1.).LT.1.E-3) THEN
      B=2.*RF(0)-1.
      A=SQRT(1.-B*B)
      VRCP(1)=B*VR
      C=2.*PI*RF(0)
      VRCP(2)=A*COS(C)*VR
      VRCP(3)=A*SIN(C)*VR
     ELSE
      B=2.*(RF(0)**SPM(4,LS,MS))-1.
      A=SQRT(1.-B*B)
      C=2.*PI*RF(0)
      OC=COS(C)
      SC=SIN(C)
      D=SQRT(VRC(2)**2+VRC(3)**2)
      IF (D.GT.1.E-6) THEN
       VRCP(1)=B*VRC(1)+A*SC*D
       VRCP(2)=B*VRC(2)+A*(VR*VRC(3)*OC-VRC(1)*VRC(2)*SC)/D
       VRCP(3)=B*VRC(3)-A*(VR*VRC(2)*OC+VRC(1)*VRC(3)*SC)/D
      ELSE
       VRCP(1)=B*VRC(1)
       VRCP(2)=A*OC*VRC(1)
       VRCP(3)=A*SC*VRC(1)
      END IF
     END IF
     DO 200 K=1,3
      PV(K,L)=VCCM(K)+VRCP(K)*RMM
      PV(K,M)=VCCM(K)-VRCP(K)*RML
200  CONTINUE
     RETURN
     END
*    RVELC.FOR
     SUBROUTINE RVELC(U,V,VMP)
          A=SQRT(-LOG(RF(0)))
     B=6.283185308*RF(0)
```

```
      U=A*SIN(B)*VMP
      V=A*COS(B)*VMP
      RETURN
      END
*     GAM.FOR
      FUNCTION GAM(X)
      A=1.
      Y=X
      IF (Y.LT.1.) THEN
       A=A/Y
      ELSE
50      Y=Y-1
       IF (Y.GE.1.) THEN
        A=A*Y
        GO TO 50
       END IF
      END IF
      GAM=A*(1.-0.5748646*Y+0.9512363*Y**2-0.6998588*Y**3+
     &    0.4245549*Y**4-0.1010678*Y**5)
      RETURN
      END
*     COLLMR.FOR
      SUBROUTINE COLLMR
      INCLUDE "PARAMETER.F"
      DOUBLE PRECISION COL(MNSP,MNSP),MOVT,NCOL,SELT,SEPT,
     &                                 CS(7,MNC,MNSP),LAMD
      COMMON /MOLS2 / NM,PP(2,MNM),PV(3,MNM),IPL(MNM),IPS(MNM),IR(MNM)
      COMMON /MOLSR / PR(MNM)
      COMMON /CELL2 / CC(MNC),CG(6,MNC),IC(2,MNC,MNSG),ISC(MNSC),
     &          CCG(2,MNC,MNSG,MNSG),ISCG(2,MNSC,MNSG),IG(2,MNSG),
     &          NCX,NCY,IFCX,IFCY,CWRX,CWRY,APX,RPX,APY,RPY
      COMMON /GAS   / SP(5,MNSP),SPM(6,MNSP,MNSP),ISP(MNSP)
      COMMON /GASR  / SPR(3,MNSP,MNSP),ISPR(3,MNSP),CT(MNC)
      COMMON /CONST / PI,SPI,BOLTZ
      COMMON /ELAST / VRC(3),VRR,VR,L,M,LS,MS,CVR,MM,NN,N
*--VRC(3) are the pre-collision components of the relative velocity
      DO 100 N=1,MNC
*--consider collisions in cell N
       DO 50 NN=1,MNSG
        DO 20 MM=1,MNSG
         SN=0.
         DO 10 K=1,MNSP
          IF (ISP(K).EQ.MM) SN=SN+CS(1,N,K)
10        CONTINUE
         IF (SN.GT.1.) THEN
          AVN=SN/FLOAT(NSMP)
         ELSE
          AVN=IC(2,N,MM)
         END IF
         ASEL=0.5*IC(2,N,NN)*AVN*FNUM*CCG(1,N,NN,MM)*DTM/CC(N)
     &        +CCG(2,N,NN,MM)
         NSEL=ASEL
         CCG(2,N,NN,MM)=ASEL-NSEL
         IF (NSEL.GT.0) THEN
          IF (((NN.NE.MM).AND.(IC(2,N,NN).LT.1.OR.IC(2,N,MM).LT.1))
     &         .OR.((NN.EQ.MM).AND.(IC(2,N,NN).LT.2))) THEN
           CCG(2,N,NN,MM)=CCG(2,N,NN,MM)+NSEL
          ELSE
           CVM=CCG(1,N,NN,MM)
           SELT=SELT+NSEL
           DO 12 ISEL=1,NSEL
            CALL SELECT
            IF (CVR.GT.CVM) CVM=CVR
```

```
            IF (RF(0).LT.CVR/CCG(1,N,NN,MM)) THEN
              NCOL=NCOL+1
              SEPT=SEPT+
     &             SQRT((PP(1,L)-PP(1,M))**2+(PP(2,L)-PP(2,M))**2)
              COL(LS,MS)=COL(LS,MS)+1.D00
              COL(MS,LS)=COL(MS,LS)+1.D00
              IF (ISPR(1,LS).GT.0.OR.ISPR(1,MS).GT.0) CALL INELR
              CALL ELASTIC
            END IF
12          CONTINUE
           CCG(1,N,NN,MM)=CVM
          END IF
        END IF
20      CONTINUE
50    CONTINUE
100   CONTINUE
      RETURN
      END
*   INELR.FOR
      SUBROUTINE INELR
      INCLUDE "PARAMETER.F"
      COMMON /MOLSR / PR(MNM)
      COMMON /GAS   / SP(5,MNSP),SPM(6,MNSP,MNSP),ISP(MNSP)
      COMMON /GASR  / SPR(3,MNSP,MNSP),ISPR(3,MNSP),CT(MNC)
      COMMON /ELAST / VRC(3),VRR,VR,L,M,LS,MS,CVR,MM,NN,N
      DIMENSION IR(2)
      ETI=0.5*SPM(5,LS,MS)*VRR
      ECI=0.
      ECF=0.
      ECC=ETI
      XIB=2.5-SPM(3,LS,MS)
      IRT=0
      DO 100 NSPP=1,2
       IF (NSPP.EQ.1) THEN
         K=L
         KS=LS
         JS=MS
       ELSE
         K=M
         KS=MS
         JS=LS
       END IF
       IR(NSPP)=0
       IF (ISPR(1,KS).GT.0) THEN
         IF (ISPR(2,KS).EQ.0) THEN
           ATK=1./SPR(1,KS,JS)
         ELSE
           ATK=1./(SPR(1,KS,JS)+SPR(2,KS,JS)*CT(N)+SPR(3,KS,JS)*CT(N)
     &           **2)
         END IF
         IF (ATK.GT.RF(0)) THEN
           IRT=1
           IR(NSPP)=1
           ECC=ECC+PR(K)
           ECI=ECI+PR(K)
           XIB=XIB+0.5*ISPR(1,KS)
         END IF
       END IF
100   CONTINUE
      IF (IRT.EQ.1) THEN
       DO 150 NSPP=1,2
         IF (IR(NSPP).EQ.1) THEN
           IF (NSPP.EQ.1) THEN
```

```
          K=L
          KS=LS
        ELSE
          K=M
          KS=MS
        END IF
        XIB=XIB-0.5*ISPR(1,KS)
        IF (ISPR(1,KS).EQ.2) THEN
          ERM=1.-RF(0)**(1./XIB)
        ELSE
          XIA=0.5*ISPR(1,KS)
          CALL LBS(XIA-1.,XIB-1.,ERM)
        END IF
        PR(K)=ERM*ECC
        ECC=ECC-PR(K)
        ECF=ECF+PR(K)
      END IF
150   CONTINUE
    ETF=ETI+ECI-ECF
    A=SQRT(2.*ETF/SPM(5,LS,MS))
    IF (ABS(SPM(4,LS,MS)-1.).LT.1.E-3) THEN
      VR=A
    ELSE
      DO 160 K=1,3
        VRC(K)=VRC(K)*A/VR
160     CONTINUE
      VR=A
    END IF
  END IF
  RETURN
  END
*  LBS.FOR
  SUBROUTINE LBS(XMA,XMB,ERM
100  ERM=RF(0)
  IF (XMA.LT.1.E-6.OR.XMB.LT.1.E-6) THEN
    IF (XMA.LT.1.E-6.AND.XMB.LT.1.E-6) RETURN
    IF (XMA.LT.1.E-6) P=(1.-ERM)**XMB
    IF (XMB.LT.1.E-6) P=(1.-ERM)**XMA
  ELSE
    P=(((XMA+XMB)*ERM/XMA)**XMA)*(((XMA+XMB)*(1.-ERM)/XMB)**XMB)
  END IF
  IF (P.LT.RF(0)) GO TO 100
  RETURN
  END
*  RF.FOR
  FUNCTION RF(IDUM)
  SAVE MA,INEXT,INEXTP
  PARAMETER (MBIG=1000000000,MSEED=161803398,MZ=0,FAC=1.E-9)
  DIMENSION MA(55)
  DATA IFF/0/
  IF (IDUM.LT.0.OR.IFF.EQ.0) THEN
    IFF=1
    MJ=MSEED-IABS(IDUM)
    MJ=MOD(MJ,MBIG)
    MA(55)=MJ
    MK=1
    DO 50 I=1,54
      II=MOD(21*I,55)
      MA(II)=MK
      MK=MJ-MK
      IF (MK.LT.MZ) MK=MK+MBIG
      MJ=MA(II)
50    CONTINUE
```

```
      DO 100 K=1,4
        DO 60 I=1,55
          MA(I)=MA(I)-MA(1+MOD(I+30,55))
          IF (MA(I).LT.MZ) MA(I)=MA(I)+MBIG
60      CONTINUE
100   CONTINUE
      INEXT=0
      INEXTP=31
    END IF
200   INEXT=INEXT+1
    IF (INEXT.EQ.56) INEXT=1
    INEXTP=INEXTP+1
    IF (INEXTP.EQ.56) INEXTP=1
    MJ=MA(INEXT)-MA(INEXTP)
    IF (MJ.LT.MZ) MJ=MJ+MBIG
    MA(INEXT)=MJ
    RF=MJ*FAC
    IF (RF.GT.1.E-8.AND.RF.LT.0.99999999) RETURN
    GO TO 200
    END
*   DATA2.FOR
    SUBROUTINE DATA2
    INCLUDE "PARAMETER.F"
    DOUBLE PRECISION COL(MNSP,MNSP),MOVT,NCOL,SELT,SEPT,
    &                                 CS(7,MNC,MNSP),LAMD
    COMMON /GAS   / SP(5,MNSP),SPM(6,MNSP,MNSP),ISP(MNSP)
    COMMON /GASR  / SPR(3,MNSP,MNSP),ISPR(3,MNSP),CT(MNC)
    COMMON /CELL2 / CC(MNC),CG(6,MNC),IC(2,MNC,MNSG),ISC(MNSC),
    &          CCG(2,MNC,MNSG,MNSG),ISCG(2,MNSC,MNSG),IG(2,MNSG),
    &          NCX,NCY,IFCX,IFCY,CWRX,CWRY,APX,RPX,APY,RPY
        COMMON /CONST / PI,SPI,BOLTZ
    NCX=100
    NCY=10
    NSCX=2
    NSCY=2
    IFCX=0
    IFCY=0
    IIS=1
    ISG=1
    TMPIN=300.
        PIN=101325.
        POUT=30132.5
    FND=PIN/BOLTZ/FTMP
    VFX=0.
    VFY=0.
    FSP(1)=0.1
    FSP(2)=0.9
    CB(1)=0.0
    CB(2)=5E-7
    CB(3)=0.
    CB(4)=5E-8
    FNUM=FND*CB(2)*CB(4)/MNM
    IB(1)=1
    IB(2)=1
    IB(3)=2
    IB(4)=2
        ISURF(4)=2
        ISURF(5)=2
        ISURF(6)=2
        ISURF(7)=2
        ISURF(8)=2
        ISURF(9)=2
        ISURF(10)=2
```

```
      ISURF(11)=2
      ISURF(12)=2
      ISURF(13)=2
LIMS(4,1)=NCY+1
LIMS(4,2)=1
LIMS(4,3)=10
LIMS(5,1)=NCY+1
LIMS(5,2)=10
LIMS(5,3)=20
LIMS(6,1)=11
LIMS(6,2)=20
LIMS(6,3)=30
LIMS(7,1)=NCY+1
LIMS(7,2)=30
LIMS(7,3)=40
LIMS(8,1)=11
LIMS(8,2)=40
LIMS(8,3)=50
LIMS(9,1)=11
LIMS(9,2)=50
LIMS(9,3)=60
LIMS(10,1)=11
LIMS(10,2)=60
LIMS(10,3)=70
LIMS(11,1)=11
LIMS(11,2)=70
LIMS(11,3)=80
LIMS(12,1)=11
LIMS(12,2)=80
LIMS(12,3)=90
LIMS(13,1)=11
LIMS(13,2)=90
LIMS(13,3)=100
TSURF(4)=333.
TSURF(5)=330.
TSURF(6)=327.
TSURF(7)=323.
TSURF(8)=320.
TSURF(9)=317.
TSURF(10)=313.
TSURF(11)=309.
TSURF(12)=306.
TSURF(13)=303.
IJET=0
SP(1,1)=4.17E-10
SP(2,1)=273.
SP(3,1)=0.74
SP(4,1)=1.0
SP(5,1)=4.65E-26
      SP(1,2)=2.8E-10
SP(2,2)=273.
SP(3,2)=0.74
SP(4,2)=1.0
SP(5,2)=2.99E-26
ISPR(1,1)=2
ISPR(1,2)=2
SPR(1,1,1)=5.
SPR(1,1,2)=5.
      SPR(1,2,2)=5.
SPR(1,2,2)=5.
ISPR(2,1)=0
ISPR(2,2)=0
ISP(1)=1
```

```
      LAMD=1./PI/SP(1,1)**2/FND/SQRT(2.)
      DTM=0.2*(CB(2)-CB(1))/NCX
      DTM=DTM/SQRT(2*BOLTZ*FTMP/SP(5,1))
NIS=2
NSP=10
NPS=30
NPT=10000
RETURN
END
```

Bibliography

[1]. Arkilic, E.B., "Measurement of the Mass Flow and Tangential Momentum Accommodation Coefficient in Silicon Micromachined Channels", Ph.D Thesis, Cambridge, MIT, 1997.

[2]. Allen, M.P. and Tildesley, D.J., Computer Simulation of Liquid, Oxford Uinversity Press, 1987.

[3]. Alexander, F.J. and Garcia, A.L., "The direct simulation Monte Carlo method", *Computers in Physics*, Vol.11, pp: 588-93, 1997.

[4]. Alexander, F.J., Garcia, A.L., and Alder, B.J., "Cell size dependence of transport coefficients in stochastic particle algorithm", *Phys. Fluids,* Vol.10, pp:1540-1542, 1998.

[5]. Anderson, S.I., Kjellander, N. and Rodesjo, B., "Design and field tests of a new membrane distillation desalination process", *Desalination*, Vol.56, pp.345–354, 1985.

[6]. Al-Obaidania, S., Curcio, E., Macedoniob, F. Profio, G.D., Al-Hinai, H. and Drioli, E., "Potential of membrane distillation in seawater desalination: Thermal efficiency, sensitivity study and cost estimation", *Journal of Membrane Science,* Vol.323, pp: 85–98, 2008.

[7]. Ajona, J.I., "ACE-20 Spanish parabolic trough collector", *Proceedings of 6th International Symposium on Solar Thermal Concentrating Technologies*, vol.I, 1992.

[8]. Al-Karaghouli, A.A. and Alnaser, W.E., "Performance of single and double basin solar stills", *Applied Energy*, Vol.78, pp: 347-354, 2004.

[9]. Aybar, H.Ş., "Mathematical modeling of an inclined solar water distillation system", *Desalination*, Vol.190, pp: 63–70, 2006.

[10]. Bier, C. and Plantikow, U., "Solar powered desalination by membrane distillation", *IDA World Congress on Desalination and Water Science*, UAE: Abu Dhabi, pp: 397–410. 1995.

[11]. Bird, G.A., *Molecular Gas Dynamics and the Direct Simulation of Gas Flows*, New York: Oxford University, 1994.

[12]. Bird, G.A., "Direct simulation of the Boltzmann equation", *Physics of Fluids*, Vol.13, pp: 2676, 1970.

[13]. Bayt, R.L., "Analysis, Fabrication and Testing of a MEMS-based Micropropulsion System", Ph.D Thesis. Cambridge, MIT, 1999.

[14]. Bhatnagar, P., Gross, E. and Krook, K., "A Model for collision processes in gasses", *Physical Review*, Vol. 94, pp: 511-524, 1954.

[15]. Beskok, A., "Simulation and Models for Gas Flows in Microgeometries", Ph.D Thesis, Princeton University, 1996.

[16]. Beskok, A., Karniadakis, G.E. and Trimmer, W., "Rarefaction and Compressibility Effects in Gas Microflows", *Journal of Fluids Engineering*, Vol. 118, pp: 448-456, 1996.

[17]. Banat, F.A. and Simandl, J., "Theoretical and experimental study in membrane distillation", *Desalination*, Vol.95, pp: 39–52, 1994.

[18]. Banat, F.A. and Simandl, J., "Desalination by membrane distillation : a parametric study", *Separation science and technology*, Vol.33, pp: 201-226, 1998.

[19]. Badran, A.A., Al-Hallaq, A.A., Salman, I.A.E. and Odat, M.Z., "A solar still augmented a flat-plate collector", *Desalination*, Vol.172, pp: 227-234, 2005.

[20]. Badran, O.O. and Al-Tahaineh, H.A, "The effect of coupling a flat-plate collector on the solar still productivity", *Desalination*, Vol.183, pp: 137-142, 2005.

[21]. Cercignani, C., *The Boltzmann Equation and its Applications*, New York: Springer, 1988.

[22]. Cesare, S., *Survey of energy resources 2001 — solar energy*, London: World Energy Council, 2001.

[23]. Cengel, Y.A., and Boles M.A., *Thermodynamics, an Engineering Approach*, 2nd Ed., McGraw-Hill Inc., 1994.

[24]. Duan, S.H., Ito, A. and Ohkawa, A., "Removal of trichloroethylene from water by aeration, pervaporation and membrane distillation", *Journal of Chemical Engineer Japan*, Vol.34, pp: 1069–1073, 2001.

[25]. Delyannis, E. and Belessiotis, V., "A historical overview of renewable energies", *Proceedings of Mediterranean Conference on Renewable Energy Sources for Water Production*, Greece: Santorini, pp: 13–17, 1996.

[26]. El-Bahi, A. and Inan, D., "A Solar Still With Minimum Inclination, Coupled to an Outside Condenser", *Desalination*, Vol.123, pp: 79–83, 1999.

[27]. El-Bourawi, M.S., Ding, Z., Maa, R. and Khayet, M., "A framework for better understanding membrane distillation separation process", *Journal of Membrane Science*, Vol.285, pp: 4–29, 2006.

[28]. El-Sebaii, A.A., "Thermal performance of a triple-basin solar still", *Desalination*, Vol.174, pp: 23-37, 2005.

[29]. Feynman, R.P., "There's Plenty of Room at the Bottom", *Miniaturization*. Gilbert H.D. (Ed.), New York: Reinhold Publishing, pp: 282-296, 1961.

[30]. Frisch, U., Hasslacher, H. and Pomeau, Y., "Lattice-gas automata for the Navier-Stokes equation", *Physical Review Letter*, Vol.56, pp:1505-1508, 1986.

[31]. Findley, M.E., "Vaporization through porous membranes", *Industrial Engineering Chemistry Process Design and Development*, Vol.6, pp: 226–230, 1967.

[32]. Fan, J. and Shen, C., "Statistical simulation of low-speed rarefied gas flows", *Journal of Computational Physics*, Vol.167, pp: 393-412, 2001.

[33]. Fath, E.S.H., "Solar distillation: a promising alternative for water provision with free energy, simple technology and a clean environment", *Desalination*, Vol.116, pp: 45–56, 1998.

[34]. Gad-el-Hak, M., "The Fluid Mechanics of Microdevices—The Freeman Scholar Lecture", *Journal of Fluid Engineering*, Vol.121, pp: 5-33, 1999.

[35]. Guo, Z.Y. and Li, Z.X., "Size effect on microscale single-phase flow and heat transfer", *International Journal of Heat and Mass Transfer*, Vol.46, pp:149-159, 2003.

[36]. Gore, D.W., "Gore-Tex membrane distillation", *Proceedings of the 10th Annual Convention of the Water Supply Improvement Association,* USA: Hononulu, 1982.

[37]. Graeter, F., Duerrbeck M. and Rheinlaender J., "Multi-effect still for hybrid solar/fossil desalination of sea and brackish water", *Desalination*, Vol.138, pp: 111–119, 2001.

[38]. García-Rodríguez, L., "Renewable energy applications in desalination: state of the art", *Solar Energy*, Vol.75, pp: 381–393, 2003.

[39]. Gracia-Rodriguez, L., Palmero-Marrero A. and Comez-Camacho C., "Comparison of solar thermal technologies for applications in seawater desalination", *Desalination*, Vol.142, pp:135–142, 2002.

[40]. Garica, A.L. and Wagner, W., "Time step truncation error in direct simulation Monte Carlo", *Phys. Fluids*, Vol.12, pp:2621-2633, 2000.

[41]. Goosens, M.F.A., Sablani, S.S., Shayya, W.H., Paton, C. and Al-Hinai, H., "Thermodynamic and Economic Considerations in Solar desalination," *Desalination*, Vol.129, pp:63–89, 2000.

[42]. Ho, C.M. and Tai, Y.C., "Micro-Electro-Mechanical-Systems (MEMS) and Fluid Flows", *Annul Review of Fluid Mechanics*, Vol.30, pp: 579-612, 1998.

[43]. Hussain, A. (Ed.), *Integrated Power and Desalination Plants*, Oxford: Eolss Publishers Co. Ltd., 2003.

[44]. Hadjiconstantinou, N.G., Simek, O., "Constant-Wall-Temperature Nusselt Number in Micro and Nano-Channels", *Journal of Heat Transfer*, Vol.124, pp: 356-364, 2002.

[45]. Hadjiconstantinou, N.G. and Simek, O., "Constant-Wall-Temperature Nusselt Number in Micro and Nano-Channels", *Journal of Heat Transfer*, Vol.124, pp: 356-364, 2002.

[46]. Hermann, M., Koschikowski, J. and Rommel, M., "Corrosion-free solar collectors for thermally driven seawater desalination", *Proceedings of EuroSun 2000 Conference,* , Denmark: Copenhagen, 2000.

[47]. Hua, D.W., Anderson, J., Di-Gregorio, J., Smith, D.M. and Beaucage, G., "Structural analysis of silica aerogels", *Journal of Non-Crystalline Solids*, Vol.186, pp: 142-148, 1995.

[48]. Hash, D., Hassan, H., "Two-dimensional coupling issues of hybrid DSMC/Navier-Stokes solvers", *AIAA*, 2507, 1997.

[49]. Hong, H., Jin, H., Ji, J., Wang, Z. and Cai, R., "Solar thermal power cycle with integration of methanol decomposition and middle-temperature solar thermal energy", *Solar Energy*, Vol.78, pp: 49–58, 2005.

[50]. Imdakm, A.O. and Matsuura, T., "A Monte Carlo simulation model for membrane distillation processes: direct contact (MD)", *Journal of Membrane Science*, Vol.237, pp: 51–59, 2004.

[51]. Ilgaz, M. and Celenligil, M.C., "DSMC Simulations of Low-Density Choked Flows in Parallel-Plate Channels", *In: AIP Conference Proceedings*, Vol.1, pp:831-840, 2003.

[52]. Jones, F.E., Evaporation of Water, Lewis Published Inc., 1992.

[53]. Koplik, J. and Banavar, J.R., "Continuum Reductions from Molecular Hydrodynamics", *Annual Review of Fluid Mechanics*, Vol. 27, pp: 257-292, 1995.

[54]. Kennard, E.H., *Kinetic Theory of Gases*, McGraw-hill, 1938.

[55]. Koschikowski, J., Wieghaus, M. and Rommel, M., "Solar thermal-driven desalination plants based on membrane distillation", *Desalination,* Vol.156, pp: 295–304, 2003.

[56]. Khayet, M., Godino, M.P. and Mengual, J.I., "Theory and experiments on sweeping gas membrane distillation", *Journal of Membrane Science*, Vol.165, pp: 261–272, 2000.

[57]. Khayet, M., Godino, M.P. and Mengual, J.I., "Possibility of nuclear desalination through various membrane distillation configurations: a comparative study", *International Journal of Nuclear Desalination*, Vol.1, pp: 30–46, 2003.

[58]. Khayet, M. and Matsuura, T., "Pervaporation and Vacuum Membrane Distillation Processes: Modeling and Experiments", *American Institute of Chemical Engineers Journal*, Vol.50, pp: 1697-1712, 2004.

[59]. Khayet, M., Imdakm, A.O. and Matsuura, T., "Monte Carlo simulation and experimental heat and mass transfer in direct contact membrane distillation", *International Journal of Heat and Mass Transfer*, Vol.53, pp: 1249–1259, 2010.

[60]. Kalogirou, S., "Seawater desalination using renewable energy sources", *Progress on Energy Combustion Science*, Vol.31, pp: 242–281, 2005.

[61]. Knudsen, M., "Eine Revision der Gleichgewichtsbedinggung der Gase. Thermische Molekularstromung", *Annual Physik*, Vol.31, pp: 205-229, 1910.

[62]. Karniadiakis, G.E. and Beskok, A., *Micro Flows: Fundamentals and Simulation*, New York: Springer, pp: 145, 2002.

[63]. Koura, K. and Matsumoto, H., "Variable soft sphere molecular model for inverse-power-low or Lennard-Jones potential", *Physics of Fluids*, Vol.3, pp: 2459-2465, 1991.

[64]. Koura, K. and Matsumoto, H., "Variable soft sphere molecular model for air species", *Physics of Fluids*, Vol.4, pp: 1083-1085, 1992.

[65]. Kunc, J.A., Hash, D.B. and Hassan, H.A., "The GHS interaction model for strong attractive potentials", *Physics of Fluids*, Vol.7, pp: 1173-1175, 1995.

[66]. Kronenberg, G. and Lokiec, F., "Low-temperature distillation processes in single- and dual-purpose plants", *Desalination*, Vol.136, pp: 189–197, 2001.

[67]. Lim, C.Y., Shu, C., Niu, X.D. and Chew, Y.T., "Application of lattice Boltzmann method to simulate microchannel flows", *Physics of Fluids*, Vol.14, pp: 2299-2308, 2003.

[68]. Liou, W.W. and Fang, Y., "Heat Transfer in Microchannel Devices Using DSMC", *Journal of Micro Electro and Mechanics System*, Vol.10, pp: 274-279, 2001.

[69]. Lawson, K.W. and Lloyd, D.R., "Membrane distillation", *Journal of Membrane Science*, Vol.124, pp: 1–25, 1997.

[70]. Lord, R.G., "Application of the C-L scattering kernel to DSMC calculation", Beylich A.E. (Ed.), *Rarefied Gas Dynamics*, VCH, pp:1427-1433, 1991.

[71]. Luft, W., "Five solar-energy desalination systems", *International Journal of Solar Energy*, Vol.1, pp:21–32, 1982.

[72]. Lee, W.Y., Wong, M. and Zohar, Y. "Flow Separation in Constriction Microchannels", *Proceeding of IEEE MEMS'01*, pp: 495-498, 2001.

[73]. Lee, S.Y.K., Wong, M. and Zohar, Y., "Pressure Losses in Microchannels with Bends", *Proceeding of IEEE MEMS'01*, pp: 491-494, 2001.

[74]. Leitner, G. F., "Is there a water crisis?", *International Desalination and Water Reuse Quarterly*, Vol.7, pp: 10-21, 1998.

[75]. Maxwell, J.C., *Philosophical Transactions of the Royal Society,* London. Vol.1, Appendix, 1878.

[76]. McNamara, G.R. and Zanetti, G., "Use of the Boltzmann Equation to Simulate Lattice-gas Automata", *Physical Review Letters*, Vol.61, pp:2332, 1988.

[77]. Meninger, S., Mur-Miranda, J.O. and Amirtharajah, R., "Vibration-to-electric Energy Conversion", *IEEE Transactions on very large scale integration (VLSI) system*, Vol.9, pp: pp: 64-76, 2001.

[78]. Minaev, S.S. and Fursenko, R.V., "Estimates of efficiency of a small-size thermoelectric channel in terms of conversion of heat produced by gas combustion to electric power", *Combustion Explosion and Shock Waves*, Vol.43, pp: 384-390, 2007.

[79]. Mengual, J.I. and Pena, L., "Membrane distillation", *Colloid Interface Science,* Vol.1, pp: 17–29,1997.

[80]. Mink, G., Aboabbous, M.M. and Karmazsin, E., "Design parameters, performance testing and analysis of a double-glazed, Air blown solar still with heat recycling", *Solar Energy*, Vol.62, pp: 309–317, 1998.

[81]. Mathioulakis, E., Belessiotis, V. and Delyannis, E., "Desalination by using alternative energy: Review and state-of-the-art", *Desalination*, Vol.203, pp: 346–365, 2007.

[82]. Meninger, S., Mur-Miranda, J.O. and Amirtharajah, R., "Vibration-to-electric Energy Conversion", *IEEE Transaction on VLSI System*, Vol.9, pp: 64-76, 2001.

[83]. Nordsieck, A. and Hicks, B.L., "Monte Carlo evaluation of the Boltzmann collision integral", *Rarefied gas dynamics,* Brundin C.L. (Ed.), New York: Academic Press, pp : 675-710, 1967.

[84]. Minaev, S.S. and Fursenko, R.V., "Estimates of efficiency of a small-size thermoelectric channel in terms of conversion of heat produced by gas combustion to electric power", *Combustion Explosion and Shock Waves*, Vol.43, pp: 384-390, 2007.

[85]. Muntz, E.P., Sone, Y., Aoki, K., Vargo, S.E. and Young, M., "Performance Analysis and Optimization Considerations for a Knudsen Compressor in Transitional Flow", *Journal of Vacuum Science and Technology A*, Vol.1, pp: 214, 2002.

[86]. Muntz, E.P. and Vargo, S.E. "Micro Scale Vacuum Pumps", *The MEMS Handbook*, Gad-el-Hak, G. (ed.), CRC Press, 29_1-29_28, 2002.

[87]. Nie, X., Doolen, G.D. and Chen, S., "Lattice-Boltzmann Simulations of Fluid Flows in MEMS", *Journal of Statistical Physics*, Vol.107, pp: 279-289, 2002.

[88]. Nilsen, E., Rigacci, A., Einarsrud, M.A., and Pajonk, G.M., "Strengthening of Silica Gels and Aerogels by Washing and Aging Processes", *Journal of Non-Crystalline Solids*, Vol. 285, pp: 1-7, 2001.

[89]. Oregan, B. and Gratzel, M., "Low-cost, High-efficiency Solar-Cell Based on Dye-Sensitized Colloidal Tio2 Films", *Nature*, Vol.353, pp: 737-740, 1991.

[90]. Oliver, M., "Solar energy: A new day dawning?: Silicon Valley sunrise", *Nature*, Vol.443, pp: 19-22, 2006.

[91]. Oran, E.S., Oh, C.K. and Cybyk, B.Z., "Direct Simulation Monte Carlo: Recent Advances and Applications", *Annual Review of Fluid Mechanics*, Vol.30, pp: 403-441, 1998.

[92]. Pong, K.C., Ho, C.M., Liu, J.Q., and Tai, Y.C., "Nonlinear Pressure Distribution in Uniform Microchannels", *Application of Microfabrication to Fluid Mechanics*, Vol.197, pp: 51-56, 1994.

[93]. Phattaranawik, J. and Jiraratananon, R., "Direct contact membrane distillation: effect of mass transfer on heat transfer", *Journal of Membrane Science*, Vol.188, pp: 137–143, 2001.

[94]. Phattaranawik, J., Jiraratananon, R., Fane, A.G., "Heat transport and membrane distillation coefficients in direct contact membrane distillation", *Journal of Membrane Science*, Vol.212, pp: 177–193, 2003.

[95]. Pham-Van-Diep, G., Keeley, P., Muntz, E.P. and Weaver, D.P., "A Micromechanical Knudsen Compressor", *Rarefied gas dynamics: 19th International Symposium*, Oxford University Press, UK: Oxford, pp: 715–721, 1995.

[96]. Reimers, C.E., Tender, L.M., Fertig, S. and Wang, W., "Harvesting energy from the marine sediment-water interface", *Environmental Science & Technology*, Vol.35, pp: 192-195, 2001.

[97]. Rommel, M., Hermann, M. and Koschikowski, J., "The SODESA project: development of solar collectors with corrosion-free absorbers and first results of the desalination pilot plant", *Proceedings of Mediterranean Conference on Policies and Strategies for Desalination and Renewable Energies*, Greece: Santorini, 2000.

[98]. Rheinlaender, J. and Graeter, F., "Technologies for desalination of typically 10 m^3 of water per day", *Desalination*, Vol.139, pp: 393–397, 2001.

[99]. Reynolds, O., *Philosophical Transactions of the Royal Society,* London, Series B, Vol.170, pp: 727, 1879.

[100]. Reid, R.C., Prausnitz, J.M. and Sherwood, T.K.. *The properties of Gases and Liquids*, 3rd Edn., New York: McGraw-Hill, 1997.

[101]. Schaaf, S. and Chambre, P., *Flow of Rarefied Gases*, Princeton: Princeton University Press, 1961.

[102]. Shen, C., Tian, D.B., Xie, C. and Fan, J., "Examination of the LBM in Simulation of Microchannel Flow in Transitional Regime", *The First International Conference on Microchannels and Minichannels*, New York: Rochester, pp: 405-410, 2003.

[103]. Shen, J., "DSMC Method and The Calculation of Rarefied Gas Flow", *Advances in Mechanics*, Vol.26, pp:1-13, 1996.

[104]. Shen, J., *Rarefied Gas Dynamics*, Beijing: National Defense Industry Publication, 2003.

[105]. Sun, Q. and Boyd, I.D., "A direct simulation method for subsonic, microscale gas flows", *Journal Computational Physics*, Vol.179, pp: 400-425, 2002.

[106]. Sebald, G., Lefeuvre, E. and Guyornar, D, "Pyroelectric energy conversion: Optimization principles", *IEEE Transactions on Ultrasonic Ferroelectrics and Frequency Control,* Vol.55, pp: 538-551, 2008.

[107]. Schofield, R.W. and Fane, A.G. and Fell, C.J.D, "Heat and mass transfer in membrane distillation", *Journal of Membrane Science*, Vol.33, pp: 299–313, 1987.

[108]. Schofield, R.W., Fane, A.G. and Fell, C.J.D., "Gas and vapor transport through microporous membranes, I, Knudson Poiseuille transition", *Journal of Membrane Science*, Vol.53, pp: 159–171, 1990.

[109]. Schofield, R.W., Fane, A.G. and Fell, C.J.D., "Gas and vapor transport through microporous membranes, II, Membrane distillation", *Journal Membrane Science*, Vol. 53, pp: 173–185, 1990.

[110]. Sone, Y. and Itakura, E., "Analysis of Poiseuille and Thermal Transpiration Flow for Arbitrary Knudsen Numbers by a Modified Knudsen Number Expansion Method and Their Database", *Journal of Vacuum Society Japan*, Vol.38, pp: 92-94, 1990. (translated from Japanese)

[111]. Sone, Y., Waniguchi, Y. and Aoki, K., "One-way flow of a rarefied gas induced in a channel with periodic temperature distribution", *Physics of Fluids*, Vol.8, pp: 2227, 1996.

[112]. Sone, Y., Ohwada, T. and Aoki, K., "Temperature jump and Knudsen layer in a rarefied gas over a plane wall: Numerical analysis of the linearized Boltzmann equation for hard-sphere molecules", *Physics of Fluids A*, Vol.1, pp: 363, 1989.

[113]. Sherman M.A., Anderson A.M. and Carroll M.K., *Modifying the Mechanical Strength of Aerogels*, technical report, Union college, 2009.

[114]. Tsien, H.S., "Superaerodynamics, mechanics of rarefied gases", *Journal of Aeonautical Science*, Vol.13, pp: 653-664, 1946.

[115]. Tang, G.H., Tao, W.Q. and He, Y.L., "Gas Flow Study in MEMS Using Lattice Boltzmann Method", *The First International Conference on Microchannels and Minichannels*. New York: Rochester , pp: 389-395, 2003.

[116]. Tanaka, T., Yamashita, A. and Watanabe, K., *Proceeding of International Solar Energy Congress*, England: Brighton, Vol.2, pp. 1087, 1981.

[117]. Thirugnanasambandam, M., Iniyan, S. and Goic, R, "A review of solar thermal technologies", *Renewable and Sustainable Energy Reviews,* Vol.14, pp: 312–322, 2010.

[118]. Vargo, S.E., Muntz, E.P., Shiflett, G.R. and Tang, W.C., "Knudsen compressor as a micro and macroscale vacuum pump without moving parts or fluids", *Journal of Vacuum Science and Technology A*, Vol.17, pp: 2308-2313, 1999.

[119]. Vargo, S.E. and Muntz, E.P., "Initial Results From the First MEMS Fabricated Thermal Transpiration-Driven Vacuum Pump", In: Bartel T.J., Gallis M.A. (Eds.), *22nd International Symposium on Rarefied Gas Dynamics*, American Institute of Physics, Australia: Sydney, pp: 467-473, 2000.

[120]. Vargo, S.E., *The Development of the MEMS Knudsen Compressor as a Low Power Vacuum Pump for Portable and In Situ Instruments*, Los Angeles, CA: University of Southern California, 2000.

[121]. Voropoulos, K., Mathioulakis, E. and Belessiotis, V., "A hybrid solar desalination and water heating system", *Desalination*, Vol.164, pp: 189–195, 2004.

[122]. Wagner, W., "A convergence proof for Bird's direct simulation Monte Carlo method for the Boltzmann equation", *Journal of Statistical Physics*, Vol.66, pp: 1011-1044, 1992.

[123]. Woo, B.C. and Lee, H.W., "Relation between electric power and temperature difference for thermoelectric generator", *International Journal of Modern Physics B,* Vol.17, pp: 1421-1426, 2003.

[124]. Weast, R.C., Astle, M.J. and Beyer, W.H., *CRC Handbook of Chemistry and Physics*, 64th Edition. CRC Press, 1984.

[125]. Wang, M.R., Wang, J.C. and Li, Z.X., "Pressure boundary condition of DSMC", *Chinese Journal of Computational Physics* , Vol.2, pp: 48~52, 2004.

[126]. Yen, S.M., "Monte Carlo solutions of nonlinear Boltzmann equation for problems of heat transfer in rarefied gases", *International Journal of Heat and Mass Transfer,* Vol.14, pp: 1865-1869, 1970.

[127]. Yamashita, O., Odahara, H. and Satou, K., "Energy conversion efficiency of a thermoelectric generator under the periodically alternating temperature gradients", *Journal of Applied Physics*, Vol.101, number: 023704, 2007.

[128]. Yilmaz, T.P. and Aybar, H.S., "Evaluation of the correlations for predicting evaporative loss from water body", *ASHRAE Transactions*, Vol.105, pp: 185–190, 1999.

[129]. Yamada N., Hoshi A. and Ikegami, Y., "Performance simulation of solar-boosted ocean thermal energy conversion plant", *Renewable Energy*, Vol.34, pp: 1752–1758, 2009.

[130]. Zhang, P. and Du, R., "A New Energy Harvesting Method Based on Knudsen Compressor", *6th International Symposium on Multiphase Flow, Heat Mass Transfer and Energy Conversion*, China: Xi'an, Paper No.: MF-04, 2009.

[131]. Zhang, P. and Du, R., "Design and Analysis of a New Energy Harvesting Device Based on Knudsen Effect", *2009 Clean Technology Conference*, U.S.A: Houston , 2009.

[132]. Zhang, J.H., Dow, N., Duke, M., Ostarcevic, E., Li, J.D. and Stephen, G., "Identification of material and physical features of membrane distillation membranes for high performance desalination", *Journal of Membrane Science*, Vol.349, pp: 295–303, 2010.

[133]. Zaki, G., Radhwan, A. and Balbeid, A., "Analysis of assisted coupled solar stills", *Solar Energy*, Vol.51, pp: 277–288, 1993.

[134]. Zhou, X.P., Yang, J.K., Xiao, Bo and Hou, G.X., "Simulation of a pilot solar chimney thermal power generating equipment", *Renewable Energy*, Vol.32, pp: 1637-1644, 2007.

[135]. Zarza, E., Rojas, M.E., Gonza´ lez, L., Caballero, J.M. and Rueda, F., "INDITEP: the first precommercial DSG solar power plant", *Solar Energy* Vol.80, pp: 1270–1276, 2006.